

AALBORG UNIVERSITY ESBJERG

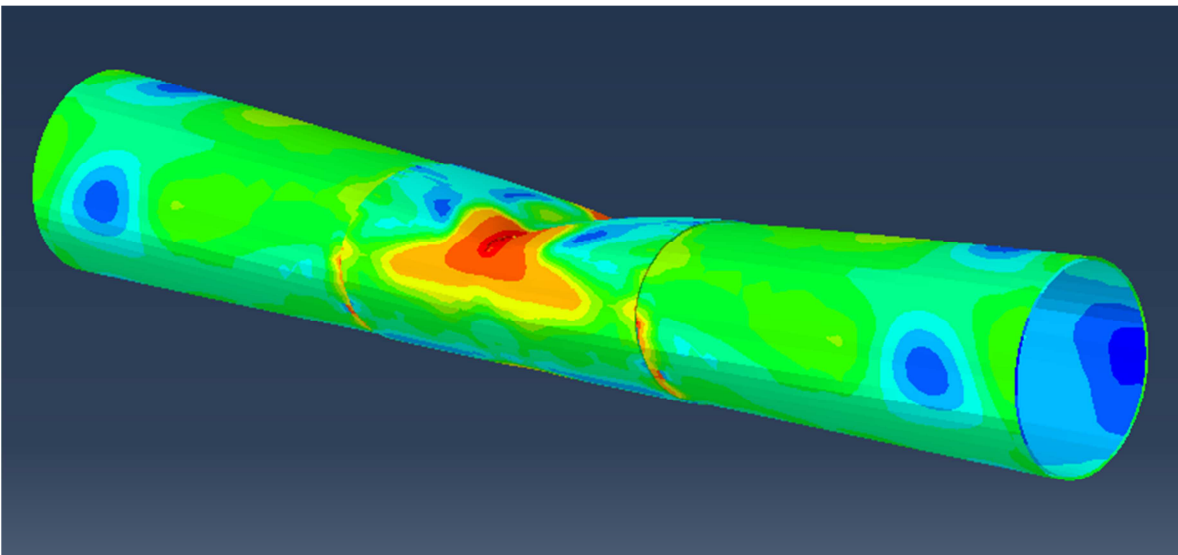
Finite Element Simulations of Trawl Gear Impact with Clad and Lined Pipelines

Master Thesis

In Corporation with DNV

Søren Mathiassen

Spring 2013



Title Sheet

Project title: Finite Element Simulations of Trawl Gear Impact with Clad and Lined Pipelines

Place: Aalborg University Esbjerg

Time period: 01.02.2013-20.06.2013

Author: Søren Mathiassen

Group number: BM4-4

Degree: Master Thesis in Mechanical Engineering

Pages: 87

Appendixes: 3

Attachments: 1

Advisor: Professor Lars Damkilde, Aalborg University Esbjerg

Acknowledgements: Professor Lars Damkilde, Aalborg University Esbjerg, for general guidance through the entire project period

M.Sc. Harald Wathne, DNV Høvik, for the proposal of the project and for guidance during the start-up phase of the project

M.Sc. Jesper Stavnsgaard Pedersen, DNV Esbjerg, for continuous guidance in the daily project work

M.Sc. Johannes Winther, DNV Esbjerg, for guidance when needed

Department 774, DNV Esbjerg, for providing software, laptop and general assistance through the project work

Abstract

With an increasing demand of subsea pipelines with high corrosion resistance such as clad and lined pipelines, the offshore industry has increased the focus on design of these types of pipes. Thus, a DNV guideline on how to treat clad and lined pipes is currently under development, but trawl gear impact has not been assessed. Consequently, it is proposed to do this master thesis to study the differences in clad and lined pipes compared with bare carbon steel pipes, by utilizing finite element analyses to simulate the trawl gear impact scenario. Furthermore, it is proposed to perform a parameter study with different diameters and D/t relations, with D being the pipe outer diameter and t the wall thickness.

The existing recommended practice DNV-RP-F111 covers trawl gear impact calculations with bare steel pipes. Thus, the analytical solutions of this recommended practice is studied to gain knowledge on the basic aspects of trawl gear impact. The analytical solutions are based on the assumption that all impact energy is absorbed locally, i.e. no global deformation of the pipeline is present. Various types of trawl gear are described but it is concluded that the clump weight contains the highest amount of kinetic energy, i.e. 47589 J corresponding to a velocity and mass of 2.8 m/s and 12140 kg respectively. The acceptance criteria of trawl gear impact is based on an estimate of the permanent indentation of the pipe.

By studying the composition of clad and lined pipes it is clear that the difference between the two pipes is the bonding, as clad pipes are metallurgical bonded and lined pipes are mechanical bonded between the corrosion resistant alloy CRA and the outer steel pipe. Thus, clad pipes are modelled with full contact between CRA and backing steel, while the lined pipe model contains contact defined by tangential friction and residual stresses to bond the CRA and backing steel. The materials selected for all analyses in this project are DNV SMYS 415 and Alloy 316L for backing and CRA respectively.

As the Abaqus finite element software is used for all simulations in this project a study is made to assess the possibilities available. The use of Abaqus/Explicit limits the available element selection to mainly first order elements with the possibility of enhancing with incompatible modes to improve bending behaviour. Generally, there are no limitations of applicable material models as Abaqus allows for the stress-strain relation to be typed in as table data. Thus, the Ramberg-Osgood material model is selected to represent both materials as it is fitted to the yield strength and ultimate tensile strength, specified in the standards. Furthermore, strain rate dependency is represented by the Cowper-Symonds relation and implemented in Abaqus by the scaling function. Finally, ductile damage and failure are defined to induce a limit to the straining capacity of the material corresponding to the minimum elongation specified by the standards.

The implementation of the above mentioned material definitions in Abaqus are verified by simple tensile tests, which additionally are used to calibrate the material models to fit the engineering stresses and strains and elongation as specified by the standards. Furthermore, simple bend tests are carried out to study the bending behaviour of the first order elements

available in Abaqus/Explicit. Generally, the incompatible element performs better, but as later impact simulations shows the incompatible element performs poorly while undergoing large deformations.

As the trawl gear impact model is double symmetric only $\frac{1}{4}$ of the geometry is modelled. Furthermore, the pipes are modelled with a combination of shell and solid elements, i.e. with solid elements at and around the impact area. The model is verified by comparing with test results performed by H. Wathne et al., ref. /2/. A convergence study is carried out but full convergence is failed as the solution shows deviations at the last reasonable mesh refinement, i.e. a mesh size of 2 mm x 2 mm which results in a calculation time of over eight hours. As a large number of analyses are needed to perform the requested parameter study, possible optimization options are studied to reduce calculation time. The option selected is to reduce the number of variables in the model, i.e. number of DOFs, partly by reducing the solid section to only represent half the circumference and partly by using a coarser mesh for the shell elements. The result is a slight but acceptable change in the contact force-displacement relationship, while the calculation times are reduced to 1-2 hours dependent on the pipe dimensions.

Finally, the trawl gear impact simulations are carried out with pipe diameters of 12", 16" and 24" with D/t relations of 15, 20, 25, 30 and 40. The simulations are performed with bare steel, clad and lined pipes, giving a total of 45 analyses. The main observations made from the analyses are listed below:

- All pipes generally shows smaller plastic deformation than estimated by DNV-RP-F111, except the bare steel pipes with $D/t=40$.
- The plastic deformations of both clad and lined pipes are smaller than for the bare steel pipes. Generally, clad pipes show the smallest plastic deformations.
- The plastic deformations are highly dependent of the diameter, but the diameter is not included in the analytical solution.
- Moderate delamination is observed for most lined pipes, except for the 12" $D/t=40$ lined pipe which shows severe delamination of approximately 3 mm at three different locations.
- Tests shows that internal pressure in lined pipes reduces the delamination significantly, but contact is not fully re-established between liner and outer pipe.

The results of the analyses should not be taken as fully trustworthy mainly due to limitations in meshing the geometry, but they bring a good insight into the differences between conventional steel pipes and clad or lined pipes when subjected to trawl gear impact.

Resumé

Med et øget behov for undervands rørledninger med rustbeskyttende egenskaber, som for eksempel beklædte og forede rør, har offshore industrien rettet større fokus mod designet af disse rør. DNV er derfor i gang med at udvikle en design guide omhandlende beklædte og forede rør, men konsekvenserne af stød fra trawlingudstyr på disse rør er endnu ikke undersøgt. Derfor er det af DNV foreslået at analysere disse rør under stødlaster fra fisketrawl ved anvendelse af FE-analyser. Endvidere ønskes det fra DNV at udføre et parameter studie med forskellige diametre og D/t forhold, hvor D er diameteren og t vægtykkelsen på røret.

DNV har udviklet en anbefalet retningslinje i form af DNV-RP-F111, som dækker stødlaster fra trawludstyr på rørledninger af almindeligt kulstofstål. De analytiske løsninger i denne analyseres med henblik på at give et generelt indblik i mekanismerne bag trawl stødlaster. Her konkluderes det bl.a. at den største kinetiske energi kommer fra en såkaldt klumpvægt, som har en masse på 12140 kg og en hastighed på 2.8 m/s. Endvidere konkluderes det at godkendelseskriteriet for trawl stødlaster er baseret på den permanente deformation af rørvæggen.

Ved at studere sammensætningen af disse beklædte og forede rør konkluderes det at den grundlæggende forskel er at beklædte rør har en metallurgisk binding med det ydre rør, mens forede rør har en mekanisk binding som er defineret af en friktionskoefficient og restspændinger fra fabrikationen. Materialerne vælges som DNV SMYS 415 og Alloy 316L for hhv. ydre rør og indre belægning.

FE programmet Abaqus anvendes til alle simuleringerne og materialemodellerne repræsenteres af Ramberg-Osgood relationen. Tøjningsrater implementeres ved Cowper-Symonds relationen og en begrænsning af bæreevnen for materialerne defineres ved duktile bruddefinitioner i Abaqus. Materialemodellerne tilpasses de i standarderne specificerede minimumskrav og implementeringen verificeres gennem simple trækprøvesimuleringer.

Anvendelsen af Abaqus/Explicit medfører visse begrænsninger da udvalget af elementer med enkelte undtagelser er begrænset til første ordens elementer. Elementerne testes under ren bøjning og det konkluderes at de præsteret tilfredsstillende mht. deformationer men med begrænsninger i spændingsberegningerne.

Modellen for simulering af trawl stødlasterne opbygges med dobbelt symmetri og en kombination af skal- og solidelementer. Modellen verificeres ved sammenligning med testresultater og resultatet er tilfredsstillende trods små afvigelser. Endvidere udføres et konvergensstudie men uden en egentlig konvergeret løsning. Dette skyldes beregningstiden som når op på over otte timer for en reduktion i meshstørrelse fra 3 mm til 2 mm, og dermed antages denne meshstørrelse som værende konvergeret. Da det ønskede parameterstudie indebærer et større antal analyser, reduceres beregningstiden, dels ved at reducere den solide del til kun at repræsentere halvdelen af tværsnittet og dels ved at øge

meshstørrelsen for skalelementerne. Dermed reduceres beregningstiden til mellem 1-2 timer afhængig af geometrien.

Parameterstudiet indebærer analyser af rør med diametre i 12", 16" og 24" med D/t forhold på 15, 20, 25, 30 og 40. Udover de balagte og forede rør, analyseres også rå stålrør. Dette gøres med henblik på at kunne sammenligne resultaterne uden at skulle tage hensyn til afvigelser grundet den reducerede model. Konklusionerne på analyser er som følger:

- Alle de analyserede rørdimensioner viser en mindre deformation end estimeret af løsningerne i DNV-RP-F111, på nær de rå stålrør med $D/t=40$.
- De plastiske deformationer for både beklædte og forede rør er mindre end for de rå stålrør. De beklædte rør viser generelt de mindste deformationer.
- De plastiske deformationer varierer signifikant med diameteren, men diameteren er ikke medtaget i de analytiske løsninger i DNV-RP-F111.
- De fleste forede rør viser delaminering mellem foring og ydre rør, specielt 12" røret med $D/t=40$ hvor delamineringen når op på ca. 3 mm flere steder.
- Tests viser at indvendigt tryk reducerer delamineringen, dog uden at reetablere fuld kontakt.

Generelt skal resultaterne ikke tolkes som den enlige sandhed, men de giver et godt billede af betydningen af hhv. beklædte og forede rør, og hvilke problemer disse rørtyper medfører.

Forewords

This master thesis in mechanical engineering is developed by Søren Mathiassen, group BM4-4, at Aalborg University Esbjerg, in corporation with DNV. The original thesis proposal is developed by Harald Wathne, DNV Høvik, and the extent of the thesis is further developed in corporation with Harald Wathne and Professor Lars Damkilde at Aalborg University Esbjerg.

A new guideline on how to treat clad and lined pipelines is currently under development by DNV, but denting by trawl gear impact with these types of pipelines has not been assessed yet. Thus, this master thesis proposal was made to simulate these impact scenarios by utilizing finite element simulations.

The reasons for selecting this proposal as a master thesis are the interest for finite element simulations and dynamics, plus the fact that future work at DNV involves pipelines in general.

All references found at the back of this report and are referred to by ref. /x/, with x being the reference number. All figures and tables without a reference are produced by author.

Søren Mathiassen

Contents

Title Sheet.....	I
Abstract.....	II
Resumé	IV
Forewords	VI
Contents	VIII
1. Introduction	1
1.1. Project Scope	2
1.2. Approach.....	2
1.3. Codes and Standards	3
1.4. Abbreviations	4
2. Types of Trawl Gear and Impact Calculations According to DNV-RP-F111	5
2.1. Types of Trawl Gear	5
2.2. Trawl Gear-Pipeline Interaction	8
2.3. Impact Calculations According to DNV-RP-F111	9
2.4. Conclusions.....	16
3. Clad and Lined Steel Pipes.....	17
3.1. General.....	17
3.2. Clad Steel Pipes	18
3.3. Lined Steel Pipes	18
3.4. Materials	20
3.5. Conclusions.....	21
4. The Abaqus Software	22
4.1. Abaqus/Explicit	22
4.2. Material Modelling in Abaqus	23
4.3. Constraints Options Available in Abaqus.....	29
4.4. Conclusions.....	30
5. The Ramberg-Osgood Material Model.....	31
6. Simple Verification Examples.....	33
6.1. Material Model Verification and Calibration	33
6.2. Element Performance during Bending.....	41
6.3. Verification of the Shell-to-Solid Coupling Constraint.....	45
6.4. Conclusions.....	46

7.	Model Calibration, Verification and Optimization.....	48
7.1.	General Modelling Considerations	48
7.2.	Model Verification.....	50
7.3.	Pre-study of Bare Carbon Steel Pipe	52
7.4.	Conclusions.....	60
8.	Implementation of Clad and Liner in the FE-model.....	62
8.1.	Clad Pipe Modelling Considerations	62
8.2.	Lined Pipe Modelling Considerations	63
8.3.	Conclusions.....	65
9.	Trawl Gear Impact Simulations: Parameter Study, Evaluations of Analytical Solutions From DNV-RP-F111 and General Observations	66
9.1.	Parameter Study: The Influence of Clad and Liner on the Permanent Indentation of Different Pipe Dimensions	66
9.2.	Evaluation of DNV-RP-F111 Analytical Solution	69
9.3.	Studying Contact Force-Displacement Curves	74
9.4.	General Observations.....	76
9.5.	Conclusions.....	78
10.	Additional Studies of Lined Pipes	80
10.1.	Delamination of Liner and Backing Material	80
10.2.	The Influence of Internal Pressure on Delamination and Plastic Deformation..	82
10.3.	The Influence of Lined Pipe Residual Stresses	83
10.4.	Conclusions	83
11.	Conclusions	84
11.1.	Material Modelling Conclusions.....	84
11.2.	Pipe Modelling Conclusions	85
11.3.	Conclusions on the Results	86
	References	87

Appendix and Attachments

Appendix 1	DNV-RP-F111 Advanced Approach
Appendix 2	Impact Analysis with Incompatible Elements
Appendix 3	Contact Force-Displacement Curves
Attachment 1	Project Description

1. Introduction

Transportation of oil, gas and water supply between platforms and to shore is done by means of subsea pipelines. Figure 1 gives an overview of the Mærsk Oil and Gas installations in the Danish sector with a selection of the pipelines connecting them.

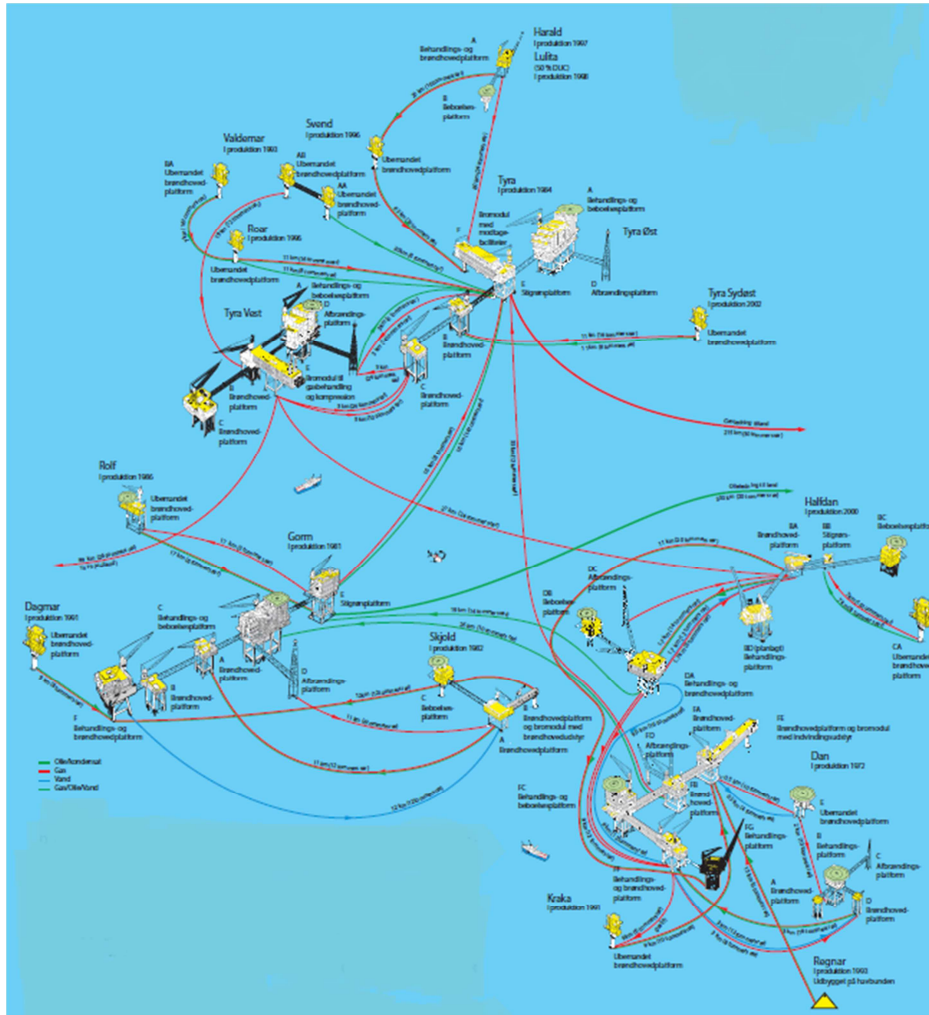


Figure 1: Mærsk Oil and Gas installations in the Danish offshore sector with a selection of the connecting pipelines ref. /3/.

A pipeline is either trenched, rock dumped or lying loose on the seabed, depending on the water depth, environmental conditions, seabed characteristics etc., but in the North Sea most pipelines are trenched. Trenching as well as rock dumping is expensive, but alternatively the pipeline is lying loose on the seabed, exposed to collisions with trawl fishing gear. Likewise, when a trenched pipeline is subject to scour, free spans can occur which also causes a hazard for both fishermen and the integrity of the pipeline.

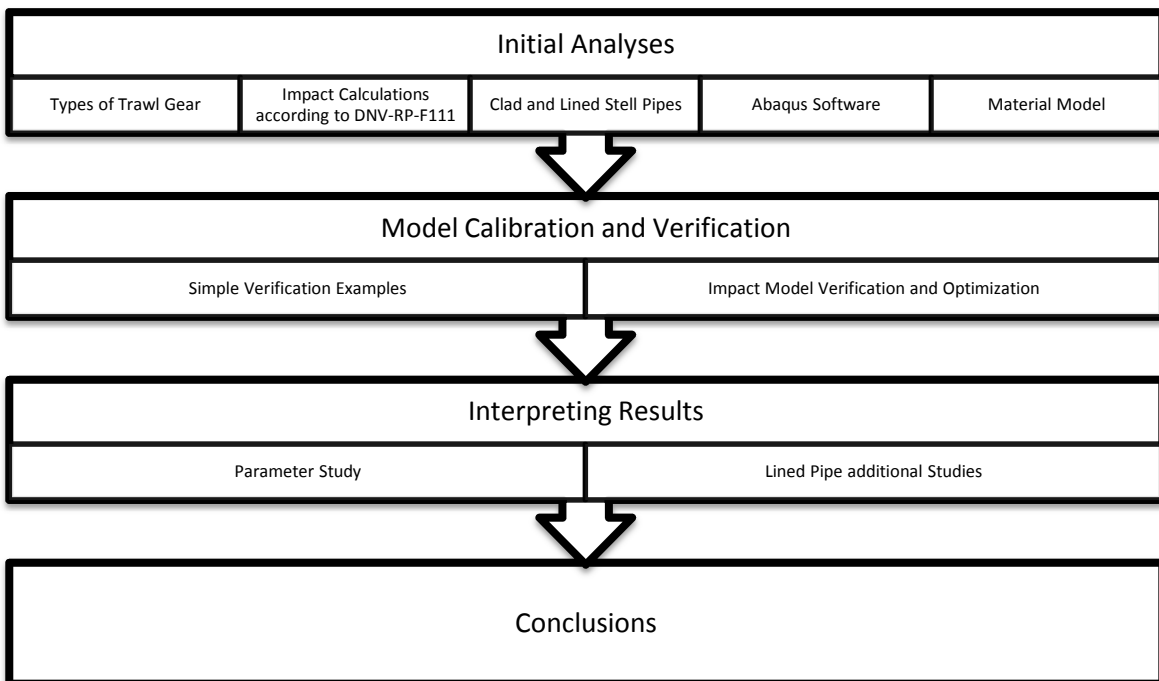
1.1. Project Scope

DNV has developed a method for assessing the damage from trawl gear impact on subsea pipelines, given in the recommended practice DNV-RP-F111, ref. /1/. This method covers conventional steel pipelines, but not clad or lined pipelines with an internal layer of corrosion resistant alloy CRA; see section 3 for further descriptions of clad and lined pipes. Thus, DNV has proposed to investigate the behaviour of clad and lined pipelines when subjected to trawl gear impact. The official project description is attached to this report; see Attachment 1. The aim is to investigate the differences in pipes with clad and liner by using FE-analyses to simulate the impact of trawl fishing gear.

The project scope is further developed during mail correspondence with Harald Wathne from DNV Høvik in Norway. Generally, the aim is to gain knowledge on how to treat clad and lined pipelines in the future with respect to trawl gear impact. A design guideline for clad and lined pipelines is currently under development but trawl gear impact has not been assessed. Thus, it is proposed to do a parameter study of pipes with different diameters and D/t relations subjected to trawl gear impact, with D being the pipe outer diameter and t the wall thickness. The proposed pipe dimensions are diameters in the range of 12”-24” with D/t relations of 15-40. Furthermore, additional studies of lined pipes are proposed to investigate possible delamination between liner and outer pipe, and if delamination is present, could internal pressure straighten the liner and re-establish contact.

1.2. Approach

The approach to this project is to perform initial analyses to form the basis of the FE-simulations. Generally, the project is divided into four main phases as illustrated below and described further in this section.



Generally, the **initial analyses** are carried out to gain knowledge regarding subjects relevant to this project. As this project deals with trawl gear impact simulations a study is made to determine the types of trawl gear used and the corresponding design parameters as specified by DNV-RP-F111, ref. /1/. Additionally, the existing solutions of trawl gear impact with bare steel pipes are studied as they will be used as benchmarking when interpreting results. Furthermore, clad and lined pipes are studied to gain knowledge of the composition and mechanical properties, including fabrication methods and commonly used materials. The FE software used in this project is Abaqus, wherefore a study is made to explore the possibilities in the program regarding the modelling of clad and lined pipes, including the material modelling which will be a main aspect of this project.

The **model calibration and verification** part is generally divided into two parts. The first part involves simple geometries to verify the general usage of Abaqus regarding material modelling, element selection and other relevant features. Additionally, the simple tensile test simulations are used to calibrate the material models. The second part involves the composition of the trawl gear impact model which is verified by comparing with test results.

The **interpreting results** part involves the actual studies as proposed in the project scope, including a parameter study and additional studies of lined pipes. When possible, results are compared with existing solutions as proposed by DNV-RP-F111.

Finally, general **conclusions** are made to summarize the knowledge gained through the project.

Generally, the approach is to gain conservative results without being over-conservative. The most distinct example is the material properties which are based on the minimum specified requirements from the relevant standards as this approach insures general applicability of the results.

1.3. Codes and Standards

The following codes and standards are used throughout the project:

DNV-OS-F101	Offshore Pipeline Systems, August 2012, ref. /4/.
DNV-RP-F110	Global Buckling of Submarine Pipelines, October 2007, ref. /5/.
DNV-RP-F111	Interference between Trawl Gear and Pipelines, October 2012, ref. /1/.
API 5LD	Specification for CRA Clad or Lined Steel Pipe, March 2009, ref. /6/.
ASME B36.10M-2004	Welded and Seamless Wrought Steel Pipe, October 2004, ref. /7/.
ASTM A240/A240M – 12a	Standard Specification for Chromium and Chromium-Nickel Stainless Steel Plate, Sheet, and Strip for Pressure Vessels and for General Applications, February 2013, ref. /8/.

1.4. Abbreviations

The following abbreviations are used in this project:

API	American Petroleum Institute
ASME	American Society of Mechanical Engineers
ASTM	American Society for Testing and Materials
CAE	Complete Abaqus Environment
CAPEX	Capital Expenses
CFD	Computational Fluid Dynamics
CRA	Corrosion Resistant Alloy
DEH	Direct Electrical Heating
DNV	Det Norske Veritas
DOF	Degree of Freedom
FE	Finite Element
FLD	Forming Limit Diagram
FLSD	Forming Limit Stress Diagram
MSFLD	Müshenborn-Sonne Forming Limit Diagram
OPEX	Operating Expenses
OS	Offshore Standard
RP	Recommended Practice
SMTS	Specified Minimum Tensile Strength
SMYS	Specified Minimum Yield Strength
SS	Stainless Steel
TFP	Tight Fit Pipe

2. Types of Trawl Gear and Impact Calculations According to DNV-RP-F111

To give a brief introduction to the trawl fishing gear used in the North Sea and the Norwegian Sea, this section describes the different types of trawl gear and applications as outlined in DNV-RP-F111, ref. /1/. Furthermore, the simplified analytical solutions represented by DNV-RP-F111 are described, including the acceptance criteria for permanent indentation of the pipeline.

2.1. Types of Trawl Gear

The following describes the different types of trawl gear used in the North Sea and the Norwegian Sea according to DNV-RP-F111, ref. /1/. Trawl gear used in the North Sea and the Norwegian Sea is divided into three main categories:

- Otter trawls
- Beam trawls
- Twin trawls

2.1.1. Otter Trawls and Trawl Boards

Typical types of otter trawling ships are:

- Consumption trawlers
- Industrial trawlers
- Prawn trawlers

Consumption trawlers have the largest equipment, and prawn trawlers operate in deeper waters and close to the coast. Otter trawls uses trawl boards to hold the trawl net open by hydrodynamic forces as illustrated in Figure 2. The trawl boards are dragged along the seabed and are likely to cause damage when crossing an exposed pipeline. The maximum mass of a trawl board is 4500-5000 kg, depending on the fishing method.

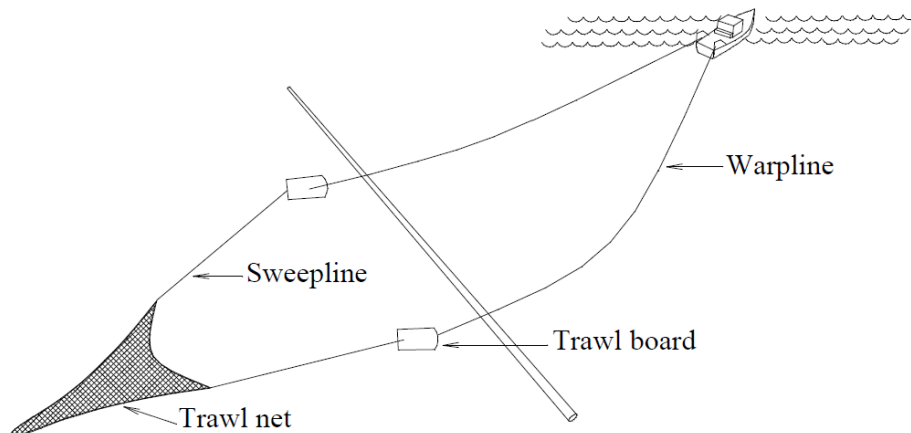


Figure 2: Otter trawl gear crossing a pipeline, ref. /1/.

It is mainly the type and quantity of fish that governs the type and size of the trawl board. Two major types of trawl boards are used in the North Sea and the Norwegian Sea, namely the V-shaped board and the polyvalent/rectangular board as illustrated in Figure 3. The polyvalent boards are found to give the highest loads in case of interaction with a pipeline.

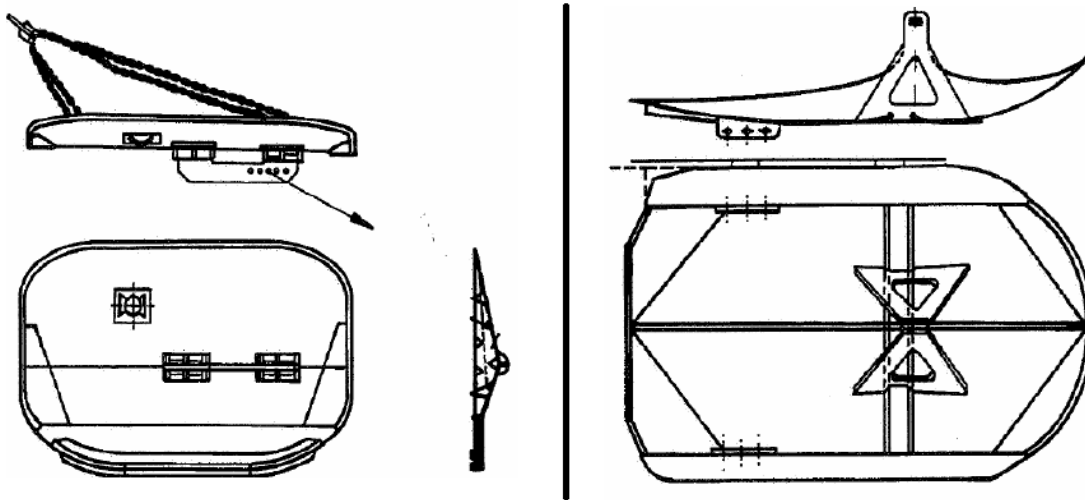


Figure 3: The two major types of trawl boards, with the V-shaped board (left) and the polyvalent board (right), ref. /1/.

2.1.2. Beam Trawls

Beam trawls are kept open by a transverse beam as illustrated in Figure 4. The beam shoes at the ends of the beam often have sharp edges which can cause severe damage to the pipeline. The maximum mass of a beam is 5500 kg.

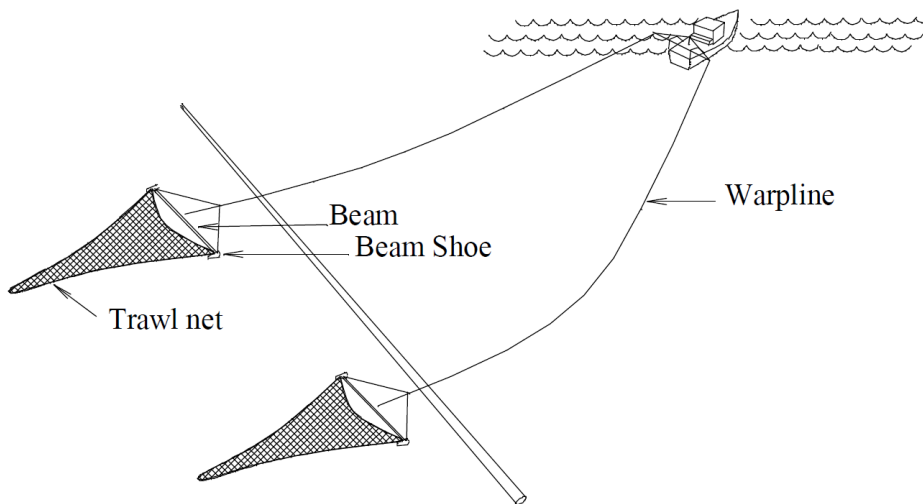


Figure 4: Beam trawl gear crossing a pipeline, ref. /1/.

The geometry of a typical beam trawl shoe is illustrated in Figure 5. Beam trawls are mainly used in sandy shallower waters like the southern parts of the North Sea.

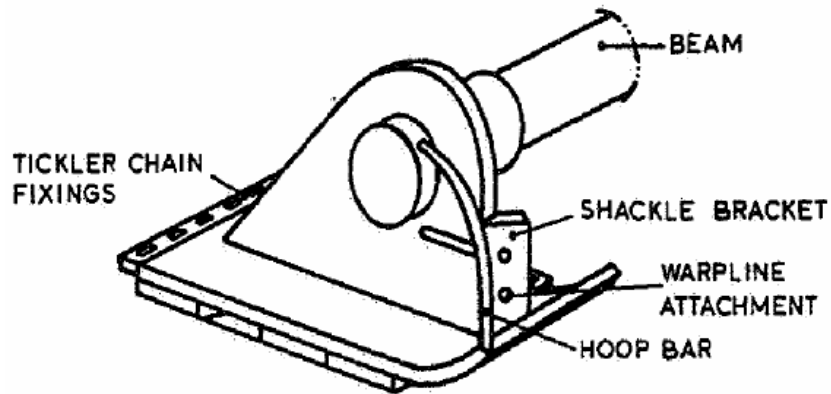


Figure 5: Typical geometry of a beam trawl shoe, ref. /1/.

2.1.3. Twin Trawls and Clump Weights

Twin trawls uses a combination of trawl boards and clump weight as illustrated in Figure 6. Clump weights vary in shapes and sizes, but the maximum mass is taken as 9000 kg.

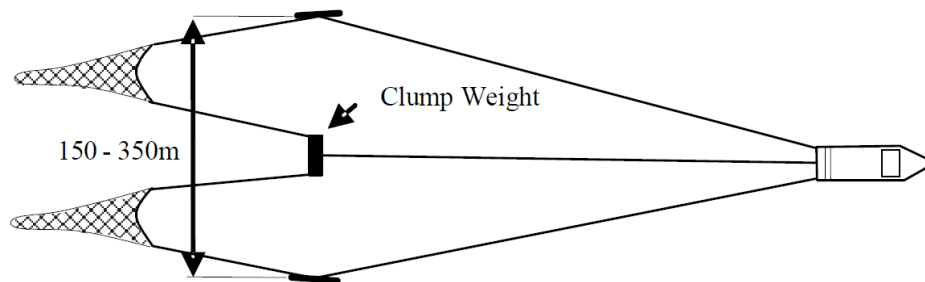


Figure 6: Twin trawl gear, ref. /1/.

Two types of commonly used clump weights are illustrated in Figure 7.

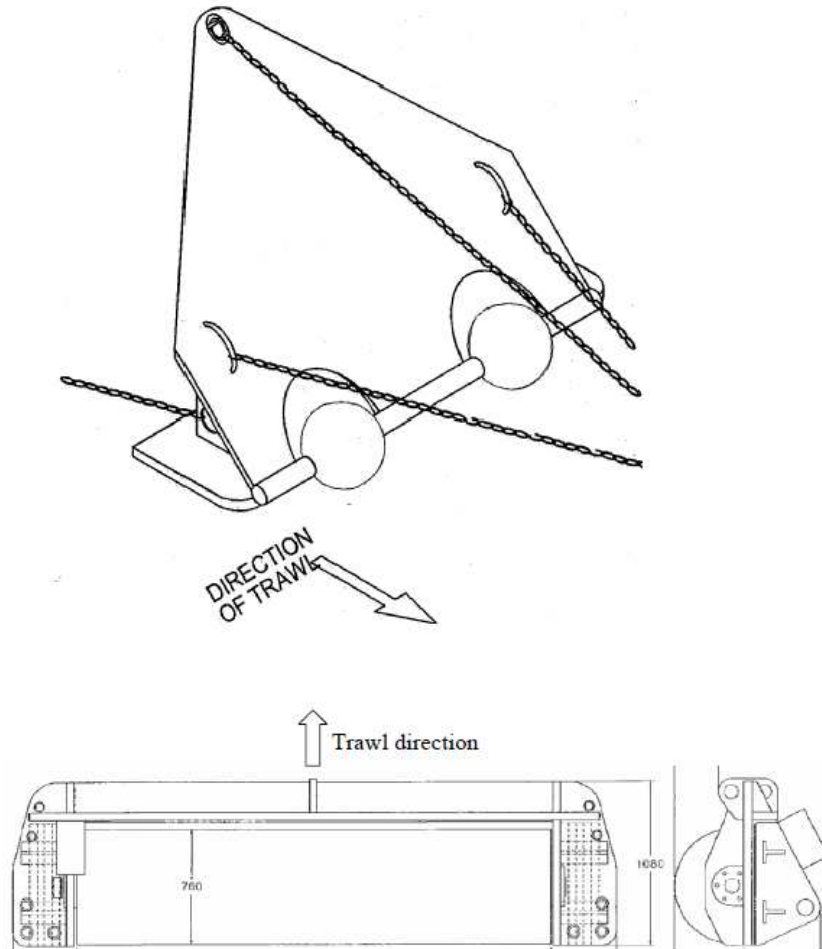


Figure 7: Two commonly used clump weights, the Bobbin type (top) and the Roller type (bottom).

2.1.4. Summary

The type of trawl gear used depends on the location, size of the fishing vessel and fishing method. Trawl gear is continuously developing and when assessing a specific location the newest information regarding fishing methods and trawl gear must be collected and used in the assessment.

2.2. Trawl Gear-Pipeline Interaction

When trawl gear is towed across a pipeline the interaction is divided into three possible phases according to DNV-RP-F111, ref. /1/:

- Impact
- Pull-over
- Hooking

Impact is when the trawl gear hits the pipeline and transfers the kinetic energy to the pipeline. Since the impact phase lasts a relatively short period of time, most of the energy is absorbed through local deformations of the pipe shell.

The **pull-over** phase is when the trawl gear is pulled over the pipeline by tension in the warpline. This phase covers a larger period of time, resulting in a more global response of the pipeline.

In extreme cases the trawl gear can get stuck under the pipeline, which results in loads as large as the breaking strength of the warpline. Free spanning pipelines increase the risk of this scenario, also referred to as **hooking**.

The scope of this project is to investigate trawl gear impact on clad and lined pipelines. Thus, the following section describes the analytical solutions to the impact phase as proposed by DNV-RP-F111.

2.3. Impact Calculations According to DNV-RP-F111

DNV has developed a method for assessing the damage from trawl gear impact on conventional subsea pipelines. More specific, two methods are described in DNV-RP-F111, ref. /1/:

- A simplified conservative method covering bare steel pipelines and pipelines with a thin layer of corrosion coating or concrete coating.
- An advanced method to assess pipelines not covered by the simplified approach; see Appendix 1.

2.3.1. General

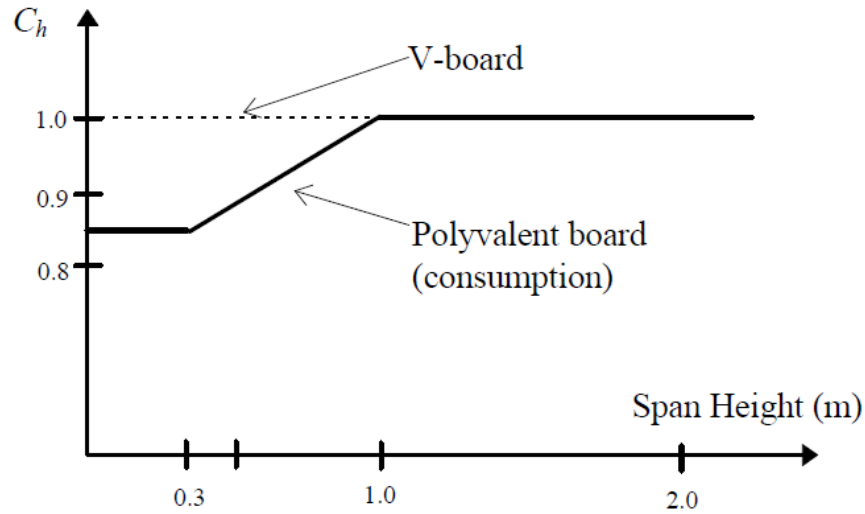
The contact force is associated with the transfer of kinetic energy from the trawl gear to the pipe, coating and surrounding soil. In general, the time of impact is so short that all energy is absorbed locally, but for pipelines with smaller cross sections the energy is also absorbed through global deformations.

In general, the impact energy depends on the effective mass and the effective velocity of the trawl gear in question. The total effective mass is the sum of the steel mass of the trawl gear and the associated hydrodynamic added mass of the entrained water. The effective velocity is the component of the towing velocity normal to the pipeline. In lack of detailed information of the design parameters, the conservative values in Table 1 are applicable.

Table 1: Design parameters for trawl gear impact, ref. /1/.

Parameters		Consumption		Industrial	Beam	Clump weight
Shape of board		Polyvalent & rectangular	V-board			
Direction of impact φ	deg	45	18	0	0	0
Effective impact velocity:	m/s	$2.8 C_h$	$2.8 C_h$	$1.8 C_h$	3.4	2.8
Steel mass: m_t	kg	4500	4500	5000	5500	9000
In plane stiffness: k_t	MN/m	500	500	500		4200
Bending board stiffness: k_b	MN/m	10	10	10		
Hydrodynamic added mass: m_a	kg	$2.14 m_t$	$1.60 m_t$	$2.90 m_t$ $2.14 m_t$	1500	3140

If free spans are present the impact velocity is possibly reduced with the C_h coefficient according to Figure 8. The in-plane stiffness of a clump weight is conservatively based on the stiffness of the corner plate of a Roller type clump weight; see Figure 7.


Figure 8: Reduction of impact velocity factor C_h as a function of span height, ref. /1/.

By studying the conservative design parameters in Table 1 it is clear that the beam trawl operates with the highest velocity, while the clump weight carries the largest mass.

2.3.2. Simplified Approach

A conservative model, to estimate trawl gear contact force and expected dent, is developed assuming that all the kinetic energy is absorbed through local deformations. To account for energy absorbed through global deformations and pipe-soil interaction, correction factors R_{fs} and R_{fa} are given in Figure 9.

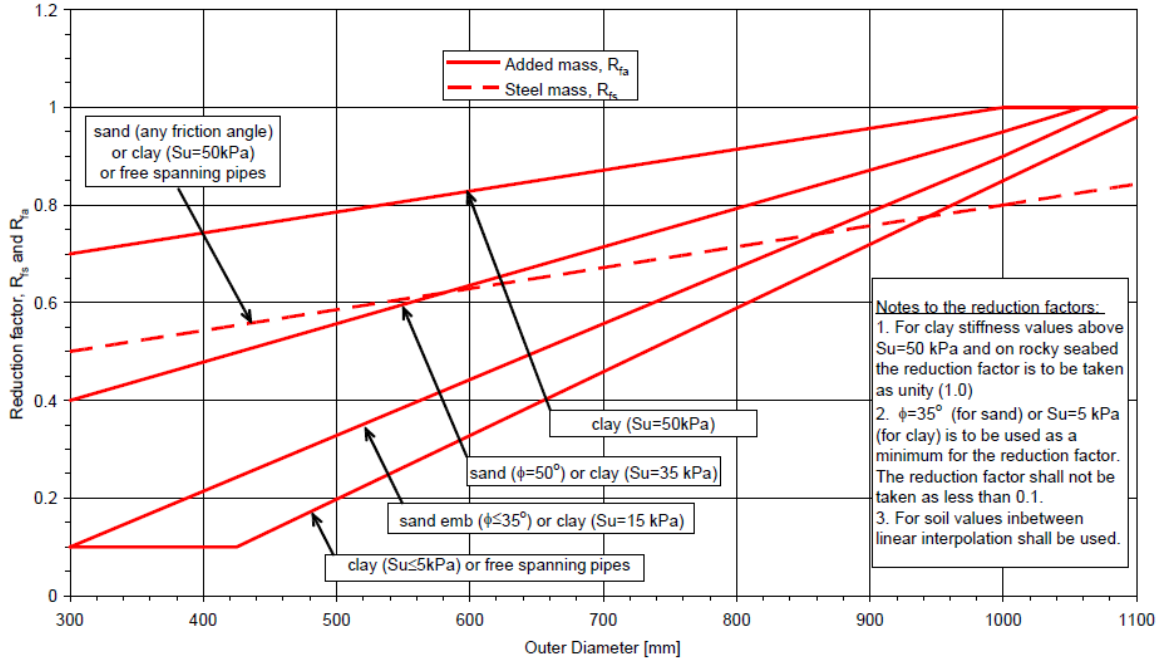


Figure 9: Reduction factor R_{fs} and R_{fa} , taking energy absorbed by global deformations and soil into account.

By observing Figure 9, it is clear that the impact energy absorbed by local deformations is reduced for all pipelines with a diameter less than 1000 mm. The magnitude of the reduction factor depends on both diameter and type of surrounding soil.

Trawl Boards

The impact energy from the steel mass of the trawl board E_s is given by:

$$E_s = R_{fs} \cdot \frac{1}{2} m_t (C_h \cdot V)^2 \quad (2.1)$$

where

R_{fs}	reduction factor for impact energy associated with steel mass, given by Figure 9
m_t	steel mass of trawl board
C_h	coefficient for effect of span height on impact velocity, given by Figure 8
V	tow velocity of trawler

The contribution of the hydrodynamic added mass is mainly acting perpendicular to the trawl board, and the associated force F_b is estimated by:

$$F_b = C_h \cdot V \cdot \sqrt{m_a \cdot k_b} \quad (2.2)$$

where

m_a hydrodynamic added mass
 k_b bending board stiffness. If not specified by geometry it is conservatively given by Table 1

The associated impact energy from the hydrodynamic added mass E_a is given by:

$$E_a = R_{fa} \cdot \frac{2 \cdot F_b^3}{75 \cdot f_y^2 \cdot t^3} \leq \frac{1}{2} m_a (C_h \cdot V)^2 \quad (2.3)$$

where

R_{fa} reduction factor for impact energy associated with hydrodynamic added mass, given by Figure 9
 t steel wall thickness
 f_y yield stress to be used in design, given by:

$$f_y = (SMYS - f_{y,temp}) \cdot \alpha_U \quad (2.4)$$

$SMYS$ Specified minimum yield strength
 $f_{y,temp}$ Temperature derating value according to DNV-OS-F101, ref. /4/, as illustrated in Figure 10
 α_U material strength factor. $\alpha_U = 0.96$, except for pipelines fulfilling supplementary requirement U in ref. /4/, where $\alpha_U = 1.0$

The temperature derating value $f_{y,temp}$ is given in Figure 10 according to DNV-OS-F101, ref. /4/. The temperature derating value accounts for a lower specified minimum yield strength SMYS or the specified minimum tensile strength SMTS due to higher temperatures.

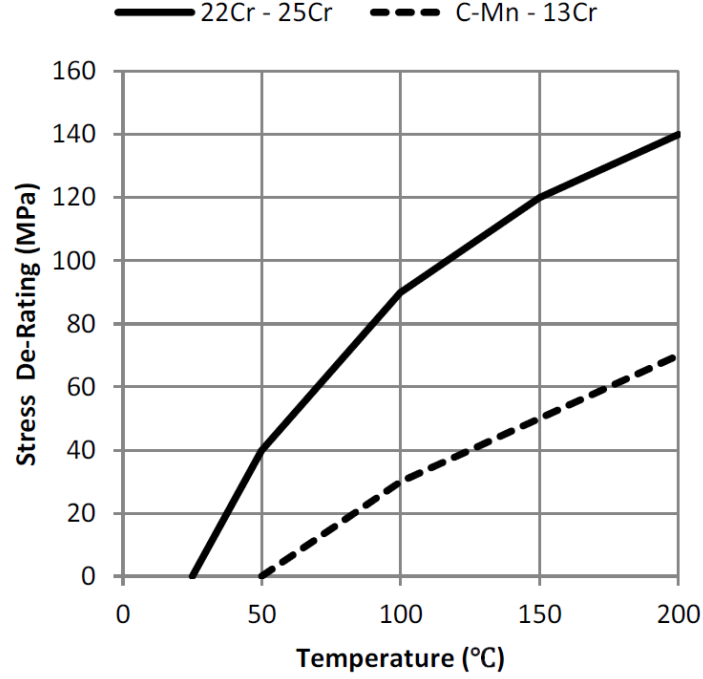


Figure 10: Temperature derating values according to DNV-OS-F101, ref. /4/.

Regarding the material strength factor α_U , the supplementary requirement U involves a higher quantity of material tests after fabrication of the pipe, ref. /4/. Thus, when assessing these simplified calculations in section 9, the yield strength is calculated from the assumption that this supplementary requirement U is not fulfilled, i.e. $\alpha_U = 0.96$.

A conservative relation between contact force F_{sh} and the expected dent H_t is given by:

$$F_{sh} = 5 \cdot f_y \cdot t^{\frac{3}{2}} \cdot \sqrt{H_t} \quad (2.5)$$

The dent depth H_t is both plastic and elastic. Finally, the impact energy absorbed by local deformations E_{loc} is conservatively taken as the maximum of eq. 2.1 and eq. 2.3:

$$E_{loc} = \max(E_s, E_a) \quad (2.6)$$

Beam Trawl

For beam trawls, the impact energy absorbed by local deformations E_{loc} is given by:

$$E_{loc} = R_{fs} \cdot \frac{1}{2} C_b (m_t + m_a) \cdot V^2 \quad (2.7)$$

where

- C_b coefficient of effective beam trawl mass during impact. Conservatively, C_b are set to 0.5 in lack of a more precise value.
- m_t steel mass of beam trawl inclusive shoes
- m_a hydrodynamic added mass from the beam trawl including the mass of water entrained by the hollow beam

Clump Weights

For clump weights the total energy absorbed by local deformations E_{loc} is given by:

$$E_{loc} = R_{fs} \cdot \frac{1}{2} (m_t + m_a) \cdot V^2 \quad (2.8)$$

- m_t steel mass of clump weight
- m_a hydrodynamic added mass from the clump weight including the mass of water entrained by the hollow section

Permanent Indentation of Pipe Shell

In lack of detailed relationship between the contact force and indentation of the pipe wall, the permanent plastic dent $H_{p,c}$ may be estimated from:

$$H_{p,c} = \left(\frac{F_{sh}}{5 \cdot f_y \cdot t^{\frac{3}{2}}} \right)^2 - \frac{F_{sh} \cdot \sqrt{0.005 \cdot D}}{5 \cdot f_y \cdot t^{\frac{3}{2}}} \quad (2.9)$$

where

$$F_{sh} = \left(\frac{75}{2} \cdot E_{loc} \cdot f_y^2 \cdot t^3 \right)^{\frac{1}{3}} \quad (2.10)$$

It is noted that the first term of eq. 2.9 is a conversion of eq. 2.5 which involves both plastic and elastic deformations, i.e. the first term of eq. 2.9 gives the total deformation of the pipe. As eq. 2.9 estimates the plastic deformation the second term must represent the elastic deformation. In other words eq. 2.9 expresses the following:

$$plastic\ def. = total\ def. - elastic\ def. \quad (2.11)$$

As this above described simple approach is based on the assumption that all energy is absorbed by local deformation, it will lead to rather conservative results for smaller and more flexible pipelines. Furthermore, this simple approach do not allow for other effects such as coating, pipe soil interaction and pipe inertia effects to be taken into account. Thus, DNV-RP-F111 has developed an advanced approach to give a more precise assessment of the trawl gear impact scenario by utilizing nonlinear static and dynamic FE-analyses. Though, the scope of this project is to analyse clad and lined pipes and comparing the results with the existing simplified approach as described above. Thus, the advanced approach will not be outlined here but a short description is given in Appendix 1.

2.3.3. Acceptance Criteria

The acceptance criteria for trawl gear impact, according to DNV-RP-F111, ref. /1/, is based on the permanent indentation of the pipeline $H_{p,c}$, given by eq. 2.9. The maximum accepted ratio between dent depth and diameter is given by:

$$\frac{H_{p,c}}{D} = 0.05 \cdot \eta \quad (2.12)$$

where η is the usage factor which is given by the frequency class. The frequency class is divided into three categories dependent on the number of trawl gear crossings of the pipeline in question. The frequency classification and associated usage factor is given in Table 2.

Table 2: Classification of crossing frequency and associated usage factor.

Frequency class	Impact frequency [/year/km]	Usage factor η
High	>100	0.0
Medium	1-100	0.3
Low	<1	0.7

The crossing frequency is classified by number of crossing per year per kilometre of pipeline. As this project deals with general assessment of clad and lined pipelines, no further studies are made regarding the acceptance criteria. Though, it is noted that the acceptance criteria is based on the permanent indentation of the pipe, i.e. eq. 2.9.

2.4. Conclusions

From the performed study it is concluded that various kinds of trawl gear is used in the North Sea and the Norwegian Sea. Thus, to determine the maximum possible impact energy from the design parameters given in Table 1, the maximum kinetic energy corresponding to each type of trawl gear is calculated by the solutions given in section 2.3. The results are summarized in Table 3.

Table 3: Maximum impact energy of the different types of trawl gear.

Type of trawl gear	Maximum impact energy [J]
Polyvalent/rectangular	37750
V-board	28224
Industrial	17334
Beam	20230
Clump weight	47589

Thereby it is concluded that the clump weight induces the largest amount of impact energy to the pipelines. Thus, the clump weight design parameters will be used during the FE pre-study in section 7.3, i.e. a total mass of 12140 kg with a velocity of 2.8 m/s.

Regarding the shape of the indenter to represent the trawl gear, parameter studies by ref. /2/ shows that the difference between a round shaped and a sharp edged indenter is negligible. Thus, it is decided to use a round shaped indenter with radius $r=25$ mm.

The above described simple approach is based on the assumption that all energy is absorbed by local deformations and the project scope involves assessments of clad and lined pipes by comparing with these analytical solutions. Thus, it is decided to use a rigid surface as boundary condition of the pipes while performing the FE impact analyses. This is further supported by ref. /2/, which recommends a rigid surface as boundary condition to ensure pure local deformations.

The yield strength used while assessing the simplified analytical solutions is calculated from:

$$f_y = (SMYS - f_{y,temp}) \cdot \alpha_U \quad (2.13)$$

The temperature derating value $f_{y,temp}$ is disregarded as no temperature data is available, and α_U is set to 0.96 as described in section 2.3.

As the acceptance criteria for trawl gear impact is based on the permanent indentation of the pipeline, the FE results will be compared with eq. 2.9. Furthermore, the contact force-displacement relation given by eq. 2.5 will be assessed as it is directly related to eq. 2.9; see section 9 for further studies.

3. Clad and Lined Steel Pipes

As this project deals with clad and lined steel pipes, this section studies the composition of these pipes to ensure an optimal approach when creating the FE-model. The study includes fabrication methods, commonly used materials and types of contact between outer pipe and internal layer of corrosion resistant alloy CRA.

3.1. General

The transport of corrosive content in offshore pipelines is generally increasing due to higher concentrations of hydrogen sulphide H_2S and carbon dioxide CO_2 . This results in increasing expenses for conventional carbon steel pipelines due to chemical injection of corrosion inhibitor and higher demands regarding inspection and maintenance.

An alternative solution is to use bimetallic pipelines such as clad and lined pipelines. The concept of clad and lined pipes is to utilize the structural capacity of carbon steel as backing material with an internal layer of corrosion resistant alloy CRA to prevent internal corrosion. Figure 11 gives an idea of the expenses for carbon steel pipelines vs. clad or lined pipelines during service lifetime, ref. /9/. The capital expenses CAPEX from production and material are higher for the clad and lined pipes, but due to lower operating expenses OPEX, clad and lined pipes are cost efficient over the service lifetime.

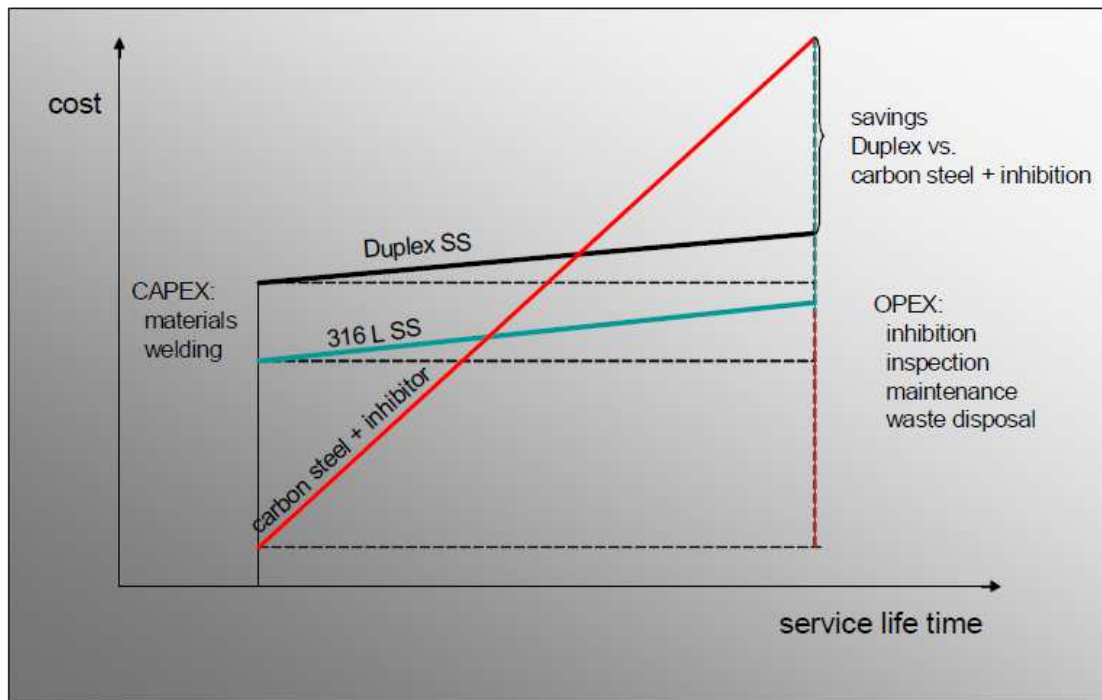


Figure 11: Expenses for carbon steel vs. clad or lined pipelines during service lifetime. Conventional pipelines (red line) are compared with bimetallic pipelines with either Duplex SS (black line) or 316 L SS (green line) as CRA, ref. /9/.

A DNV design and construction guideline for clad and lined pipelines is currently under development, but is not yet published. Alternatively, API 5LD ‘Specification for CRA Clad or Lined Steel Pipe’ is used as reference in this section, ref. /6/.

The minimum specified thickness of the CRA layer is 2.5 mm, ref. /6/, but a thickness of 3 mm is commonly used. The mechanical properties of the pipes are not specified directly in ref. /6/ as it may be specified in agreement between the supplier and the purchaser. Thus, a study is made below to determine these mechanical properties. The study includes manufacturing processes, residual stresses and most frequently used materials for both backing steel and CRA.

3.2. Clad Steel Pipes

The definition of clad steel pipes is an internal layer of CRA which is metallurgical bonded to the backing material. The fabrication methods are hot-rolling, co-extrusion, weld overlay, explosion bonding, powder metallurgy and other metallurgical bonding processes, ref. /6/. It is assumed that clad pipes are heat treated after fabrication to relief any residual stresses.

3.3. Lined Steel Pipes

The definition of lined steel pipes is a CRA which is mechanical bonded to the backing material. The liner, which could be a seamless pipe or a rolled sheet metal, is inserted into the backing pipe with subsequent expansion creating a mechanical bond. Alternatively, the CRA and backing material is sheet rolled into a cylinder resulting in a mechanical bond due to expansion of the liner and/or shrinkage of the backing material, ref. /6/.

Manufacturing the lined pipe by expansion induces limitations to the material selection as the elastic spring-back must be larger for the backing material, i.e. the yield strength of the backing material must be noticeable larger than for the CRA. Thus, the largest bond force between the two materials is created when the yield strength of the CRA is approximately 50 % of the yield strength of the backing material, ref. /9/.

However, to avoid the above mentioned material limitations, a thermo-hydraulic shrink-fit manufacturing process is developed by Kuroki T&P Co, ref. /10/. This method involves heating of the outer pipe during manufacturing which makes the bond force less dependent of the yield strength of the materials. Pipes manufactured by this method are also referred to as tight fit pipes TFP. The manufacturing process is illustrated in Figure 12 and described below.

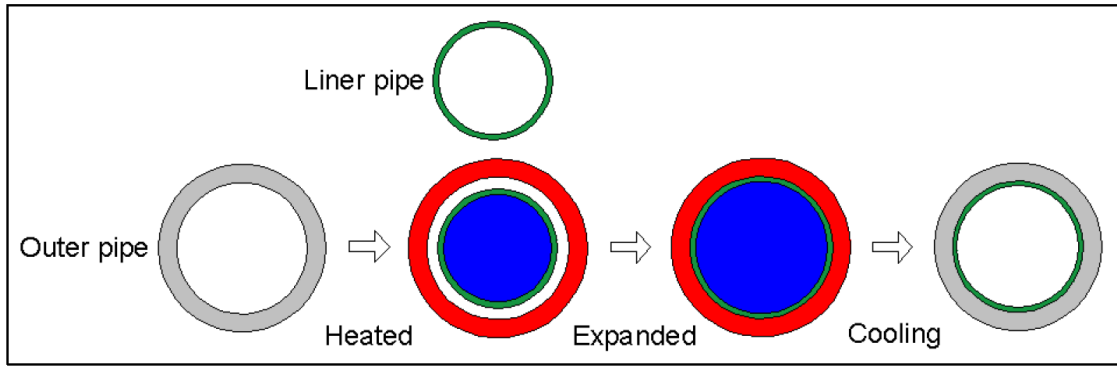


Figure 12: Manufacturing process for tight fit pipes TFP, ref. /10/

Manufacturing process:

1. The outer pipe is heated to 300-400°C
2. The liner is inserted into the outer pipe and hydraulically expanded to fit the outer pipe, i.e. the material of the outer pipe is still in the elastic range
3. The composed pipe is cooled both with water from the inside and air from the outside

The thermal and elastic shrinkage of the outer pipe ensures a tight uniform fit between the pipes, i.e. the outer pipe is in tension and the liner in compression. The theoretical development of hoop stress as a function of diameter is illustrated in Figure 13. The liner is represented by a green line and the outer pipe by a red line. The liner is exposed to strain hardening while the outer pipe is in the elastic range.

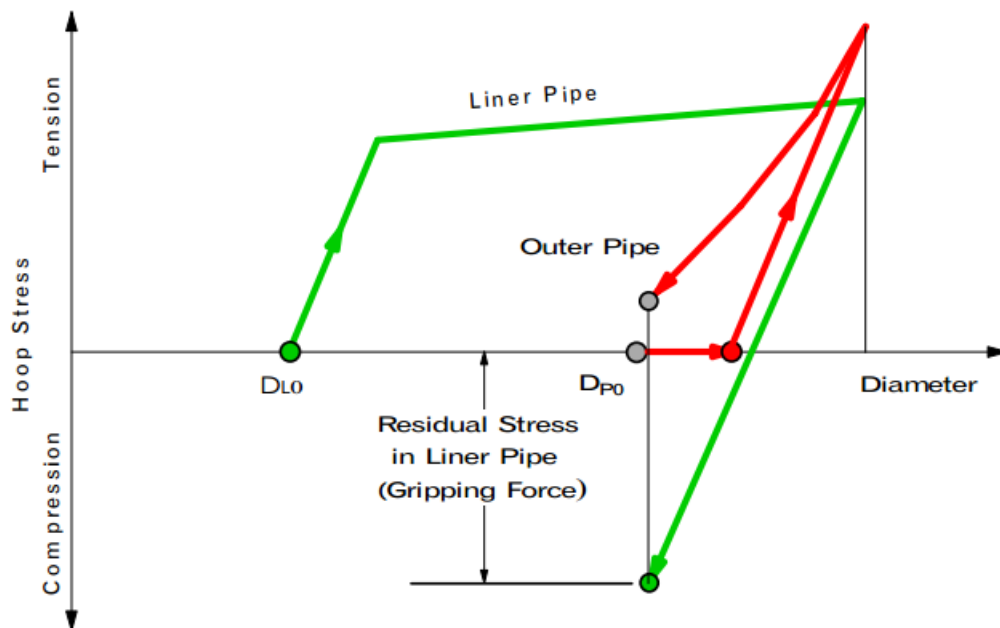


Figure 13: the theoretical development of hoop stress as a function of diameter, ref. /10/.

Even though, the described TFP manufacturing process is limited to pipe dimensions up to 12” in diameter, it is deemed to be developed in the future to span larger pipe diameters.

Furthermore, the only available information regarding the value of the residual stresses in a lined pipe is from TFP as described next.

The paper ‘Mechanical Behavior of Lined Pipe’ by A. Hilberink, ref. /11/, investigates the behavior of lined pipes during bending and reeling. The pipes used in the study are TFP manufactured by Kuroki T&P Co as described above. Tensile tests are carried out to determine the mechanical properties of 8 different 12” pipes. The liner residual hoop stresses lies in the range of -201 MPa to -86 MPa and the liner residual axial stresses in the range of -23 MPa to -3 MPa. Thus, it is decided to use constant residual liner stress values for all lined pipe analyses, i.e. -150 MPa and -20 MPa for residual hoop and axial stresses respectively. The corresponding residual stresses of the backing material depend on the wall thickness and are calculated separately in section 8.2.

To establish the friction coefficient between liner and backing material test results from ref. /12/ is used. Six push out tests are carried out with friction coefficients in the range of 0.32-0.63. Thus, an average value of 0.4 is used when defining contact between liner and backing in the FE-model.

3.4. Materials

A wide range of materials are used in clad and lined pipes, but to limit the scope of this project only one carbon steel material for backing and one CRA for clad/liner is selected.

The carbon steel material is selected as DNV SMYS 415 specified by DNV-OS-F101, ref. /4/. This is a commonly used material for pipelines and lies in the medium range of yield strengths. The CRA material is selected as Alloy 316L specified by ASTM, ref. /8/, since this is the material used in all tests performed in ref. /11/ and is commonly used as CRA material for clad and lined pipelines. All relevant material properties used in the FE-analyses are given in Table 4.

Table 4: Relevant material properties of the selected materials.

Application	Type/name	Yield strength [MPa]	Tensile strength [MPa]	Elongation in 50 mm [%]	Young’s modulus [MPa]	Density [kg/m ³]
Backing	SMYS 415	415	520	17.5	210000	7850
Clad/liner	Alloy 316L	170	485	40	193000	7900

The elongation in 50 mm for SMYS 415 is calculated from, ref. /4/:

$$A_f = C \cdot \frac{A_{XC}^{0.2}}{U^{0.9}} \quad (3.1)$$

where

A_f	elongation in 50 mm
C	factor equal to 1940 when using SI units
A_{XC}	cross section area of the test specimen
U	Tensile strength

3.5. Conclusions

For clad pipes the metallurgical bond between CRA and backing material must be defined in the FE-model as fully bonded. No residual stresses are present in clad pipes.

For lined pipes the mechanical bond between CRA and backing material must be defined by contact with a friction coefficient of 0.4. Furthermore, liner residual stresses of -150 MPa and -20 MPa must be defined in the hoop and axial directions respectively. Corresponding stresses of the backing material are calculated to create force equilibrium between the two pipes. As illustrated in Figure 13, the liner is exposed to some strain hardening but as no quantification is available, this strain hardening is neglected in the material models in this project.

The materials are selected as DNV SMYS 415 and Alloy 316L for backing and clad/liner respectively with mechanical properties given in Table 4. The thickness of the clad and liner is set to be 3 mm as commonly used.

4. The Abaqus Software

The Abaqus version 6.12 finite element software is used for all analyses in this project. Generally, the Abaqus system includes five programs:

- Abaqus/Standard, a finite element program for general purpose
- Abaqus/Explicit, a finite element program for explicit dynamic simulations
- Abaqus/CFD, a computational fluid dynamics program
- Abaqus/CAE, an interactive environment used for modelling, job execution and results evaluation
- Abaqus/Viewer, a subset of CAE containing the results evaluation part

As the trawl gear impact simulations in this project are highly dynamic and undergo relatively large deformations, Abaqus/Explicit is used for all impact simulations; see section 4.1 for further explanations. Abaqus/Standard is used for all verification examples and calibration of material models as outlined in section 6, and all modelling is carried out in Abaqus/CAE.

The following sections studies the Abaqus applications relevant to this project, including the explicit solver, material modelling and constraints necessary to model these clad and lined pipes. Thus, the information in these sections is based on the Abaqus Documentation version 6.12, ref. /13/, when not specified otherwise.

4.1. Abaqus/Explicit

As mentioned above, the explicit dynamic solver is efficient for large models undergoing large deformations over a relatively short time period. Thus, Abaqus/Explicit is used for all impact analyses in this project. Without going into details, the explicit solver utilizes the central difference method where the dynamic equilibrium equation is satisfied at the start of each increment where time is t . The accelerations at time t are the used to calculate the velocities at time $t+\Delta t/2$ and the displacements at time $t+\Delta t$. The explicit solver is efficient because the mass matrix is a diagonal matrix, i.e. lumped masses are used. The explicit solver is conditionally stable with a critical time increment of, ref. /14/:

$$\Delta t_{cr} = \frac{2}{\omega_{max}} \quad (4.1)$$

where ω_{max} is the highest frequency of the structure. Abaqus/Explicit approximates a conservative stable time increment from the size of the smallest elements in the model and the dilatational wave speed of the material. A further explanation of the stable time increment in Abaqus/Explicit is given in section 7.3.

The solid continuum elements available in Abaqus/Explicit are limited to mainly first order elements with the exception of one special purpose tetrahedron element which is of second order. Though, the 8-node first order brick element is provided with the option of enhancing with incompatible modes to improve the bending behaviour of the element. The 8-node linear brick element is found to be too stiff when undergoing bending due to spurious shear strain, i.e. shear locking, ref. /15/. One disadvantage by using the incompatible element is that 13 internal DOF is added and thereby increases the calculation time. Furthermore, according to the Abaqus documentation the incompatible element should be used with caution in applications involving large strains, especially compressive strains. Thus, the regular 8-node and the incompatible element are tested by simple verification examples in section 6.2.

4.2. Material Modelling in Abaqus

Since this project deals with material plasticity and dynamic simulations, a study is performed to explore the possibilities regarding the metal plasticity models available in Abaqus, including rate dependence, damage, failure and initial conditions.

4.2.1. General

Abaqus utilize incremental plasticity in which the mechanical strain rate is divided into an elastic part and a plastic part. These plasticity models are usually formulated by a yield surface, a flow rule and hardening behaviour.

When working with plasticity models for ductile materials such as metals, stress and strain measures are defined by:

- True stress (Cauchy stress), σ_{true}
- Logarithmic plastic strain, ε_{ln}^{pl}

The conversions of nominal test data are given by eq. 4.2 and eq. 4.3:

$$\sigma_{true} = \sigma_{nom}(1 + \varepsilon_{nom}) \quad (4.2)$$

$$\varepsilon_{ln}^{pl} = \ln(1 + \varepsilon_{nom}) - \frac{\sigma_{true}}{E} \quad (4.3)$$

where σ_{nom} and ε_{nom} are the nominal stress and strain, respectively, and E is the Young's modulus.

4.2.2. Metal Plasticity

Metal plasticity in Abaqus uses either Mises or Hill yield surfaces, which both assumes, that yielding is independent of the hydrostatic pressure. The Mises yield surface is used to define isotropic yielding by the values of the uniaxial yield stress and corresponding equivalent plastic strain. The Hill yield surface is used to model anisotropic yielding. Figure 14 illustrates the Mises criterion in principal stress space.

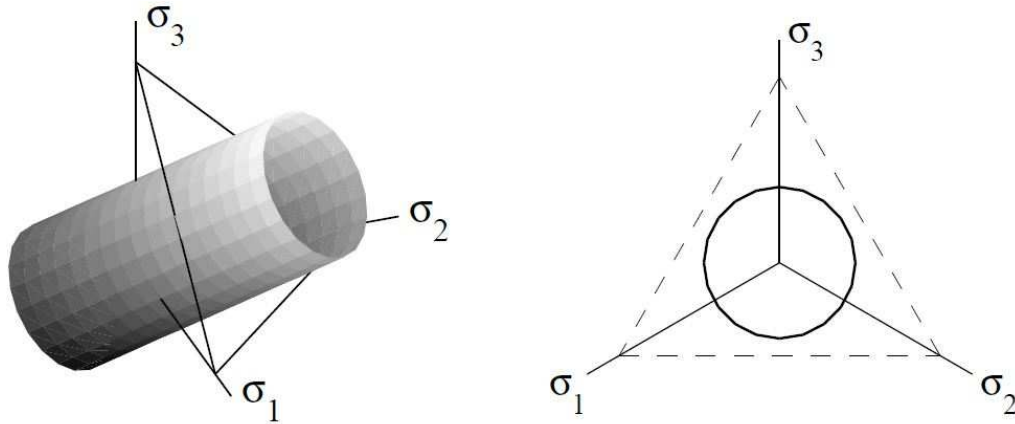


Figure 14: Mises yield criterion in principal stress space, ref. /16/.

Abaqus uses the associated flow rule, meaning that the direction of the plastic deformation rate is normal to the yield surface.

Hardening

The following hardening models are available in Abaqus:

- Isotropic hardening
- Kinematic hardening
- Johnson-Cook isotropic hardening
- Hardening defined through user subroutine
- Combined hardening

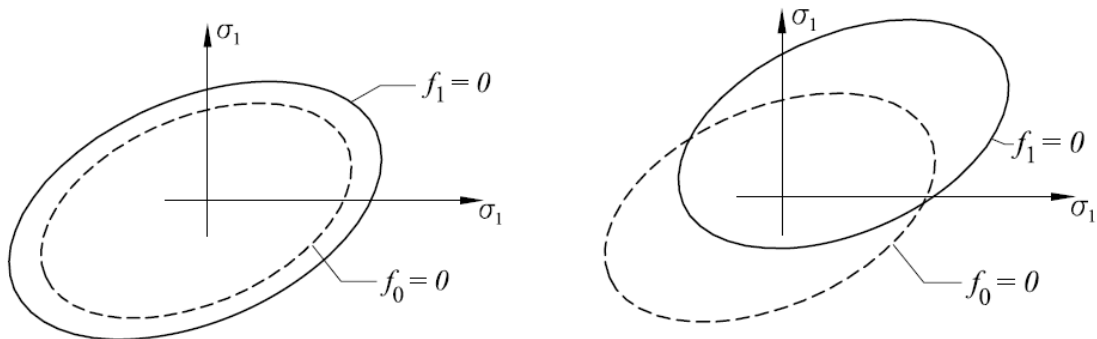


Figure 15: Isotropic hardening (left) and kinematic hardening (right) illustrated in plane stress. f_0 is the yield surface prior to hardening and f_1 is the hardened yield surface, ref /17, plast/.

Isotropic hardening assumes that the yield surface expands in all directions when yielding occurs as illustrated in Figure 15. Isotropic hardening is defined by giving the stresses as a tabular function of equivalent plastic strains. The stresses at a given state of deformation are then interpolated from the given tabular data, with no stresses exceeding the last value given in the table.

Kinematic hardening assumes a translation or movement of the yield surface in stress space, and is suitable for cyclic loading of metals.

Johnson-Cook isotropic hardening expresses the stress σ_0 at a given state as an analytical function of equivalent plastic strain, strain rate and temperature, eq. 4.4.

$$\sigma_0 = (A + B(\varepsilon^{pl})^n) \left(1 + C \cdot \ln \left(\frac{\dot{\varepsilon}^{pl}}{\dot{\varepsilon}_0} \right) \right) (1 - \hat{T}^m) \quad (4.4)$$

where

A, B, C, n and m	Material parameters to be estimated from testing
ε^{pl}	Equivalent plastic strain
$\dot{\varepsilon}^{pl}$	Equivalent plastic strain rate
$\dot{\varepsilon}_0$	Reference strain rate
\hat{T}	Dimensionless temperature given by eq. 4.5:

$$\hat{T} = \begin{cases} 0 & \text{for } T < T_r \\ \frac{T - T_r}{T_m - T_r} & \text{for } T_r \leq T \leq T_m \\ 1 & \text{for } T > T_m \end{cases} \quad (4.5)$$

T	Current temperature
T_r	Reference temperature
T_m	Melting temperature

The Johnson-Cook isotropic hardening model is well suited for high rate deformation analyses, including impact analyses, as rate dependency is directly incorporated.

Hardening defined through user subroutine allows the user to specify the material hardening through a user subroutine, meaning that the stress state is calculated from a separate script at every step.

Combined hardening combines isotropic and kinematic hardening and is well suited for cyclic loading of metals.

Rate Dependence

During impact analysis or other analysis with high strain rates, the corresponding yield stress increases. Figure 16 illustrates the difference in yield stress for tensile tests performed with various strain rates.

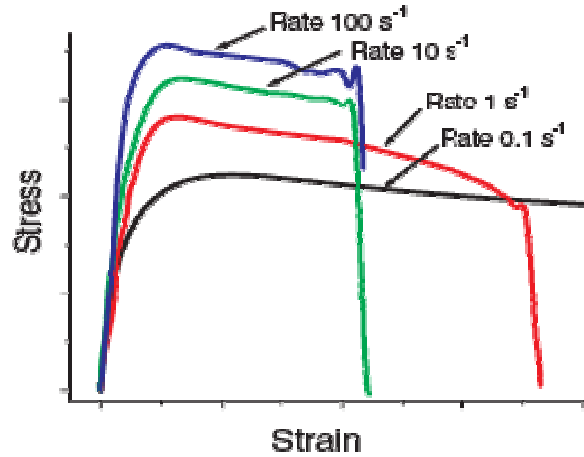


Figure 16: Stress-strain relations for different strain rates, ref. /18/.

Rate dependence is directly included in the Johnson-Cook isotropic hardening, but can also be defined in multiple other ways:

- Tabular data
- Scaling function
- User subroutine

Test data can be specified by **tabular data** with stresses as a function of equivalent plastic strain at different equivalent plastic strain rates – one table per strain rate.

By using a **scaling function**, the specified static hardening curve is scaled:

$$\bar{\sigma}(\bar{\epsilon}^{pl}, \dot{\epsilon}^{pl}) = \sigma^0(\bar{\epsilon}^{pl}) \cdot R(\dot{\epsilon}^{pl}) \quad (4.6)$$

where

$\bar{\sigma}$	Scaled yield stress
σ^0	Static yield stress
R	Scaling factor defined as $R=1.0$ at $\dot{\epsilon}^{pl}=0$
$\bar{\epsilon}^{pl}$	Equivalent plastic strain
$\dot{\epsilon}^{pl}$	Equivalent plastic strain rate

Alternatively, strain rate can be defined through a **user subroutine**.

4.2.3. Damage and Failure

To implement an upper limit to the load bearing capacity of a material, several damage and failure models are available in Abaqus. Generally, damage and failure in Abaqus is divided into two types:

- Progressive damage and failure
- Shear and tensile dynamic failure

Progressive damage and failure, which is well suited for ductile materials in quasi-static and dynamic simulations, can be specified in Abaqus using the following required specifications:

- Undamaged elastic-plastic response of the material
- Damage initiation criterion
- Damage evolution response

Several different damage initiation criteria are available in Abaqus:

- Ductile
- Shear
- Forming limit diagram, FLD
- Forming limit stress diagram, FLSD
- Müshenborn-Sonne forming limit diagram, MSFLD
- Marciniak-Kuczynski criteria, M-K

The ductile and shear criteria are used to define fracture of metals, while FLD, FLSD, MSFLD and M-K are intended to define necking stability of sheet metal.

Common for these damage initiation criteria is that the material stiffness is degraded progressively after damage initiation also referred to as damage evolution. Several damage evolution laws are available in Abaqus but since this project deals with ductile metals only the ductile damage evolution law is considered and discussed later in this section.

The **shear and tensile dynamic failure** models are only recommended for high strain rate dynamic simulations in which inertia effects are important. These failure models are used to limit subsequent loadbearing capacity of an element e.g. by removing it once the stress limit is reached. The shear failure model uses the equivalent plastic strain as a failure measure, while the tensile failure model uses the hydrostatic pressure stress as a failure measure. Though, it is recommended to use the progressive damage and failure models since these are suited for both static and dynamic simulations.

Figure 17 illustrates the difference between the damage evolution laws and the instant failure corresponding to the shear and tensile dynamic failure models.

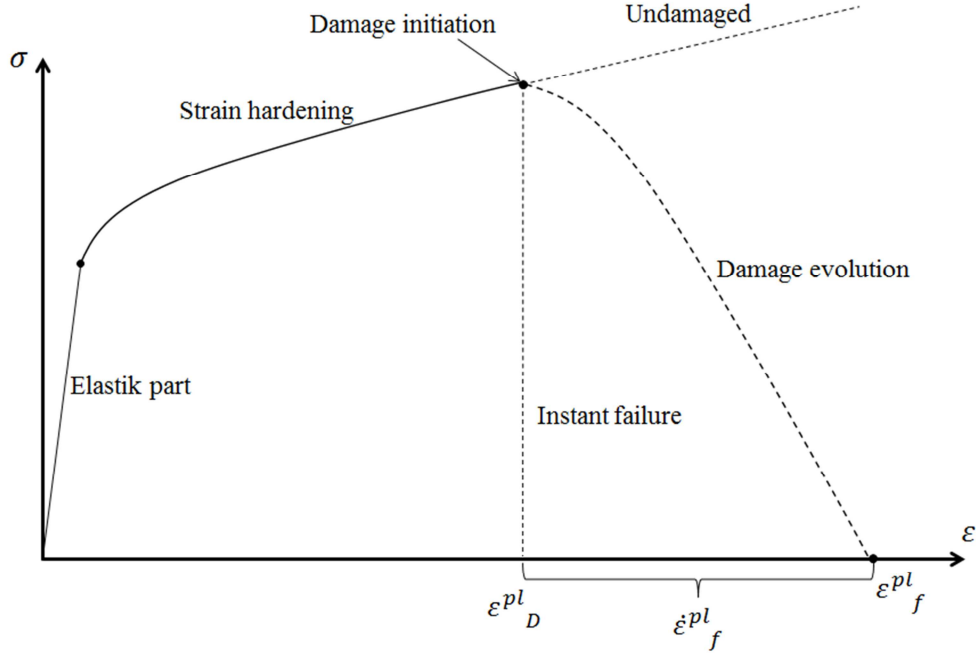


Figure 17: Illustrates the difference between the damage evolution laws and instant failure.

Ductile Damage and Failure

The ductile damage initiation is specified by the equivalent plastic strain at the onset of damage ε_D^{pl} . The ductile damage evolution law is governed by specifying the equivalent plastic strain increment at failure ε_f^{pl} as illustrated in Figure 17, but to avoid mesh dependence due to strain localization the equivalent plastic displacement after damage initiation \dot{u}_f^{pl} and characteristic length L are introduced, with \dot{u}_f^{pl} being the input variable in Abaqus, defined by:

$$\dot{u}_f^{pl} = L \cdot \varepsilon_f^{pl} \quad (4.7)$$

The definition of the characteristic length L depends on the element geometry and formulation. For continuum elements the characteristic length is given by the distance across the element for a first-order element or half the distance across the element for a second-order element. The implementation and verification of the ductile damage and failure is carried out in section 6.1.

4.2.4. Initial Conditions

As described in section 3.3, lined pipes are subjected to residual hoop and axial stresses in order to create the mechanical bond between liner and backing steel. Thus, the possibility for defining residual stresses as an initial condition is shortly introduced here.

Abaqus allows for residual stresses to be defined as a predefined field variable by defining the six stress components:

$$\begin{pmatrix} \sigma_{11} \\ \sigma_{22} \\ \sigma_{33} \\ \sigma_{12} \\ \sigma_{13} \\ \sigma_{23} \end{pmatrix}$$

To define residual hoop stresses the selected stress component must be related to the curvature of the pipe. This is done by specifying local material directions by relating them directly to the surface of the pipe.

4.3. Constraints Options Available in Abaqus

As the scope of this project involves a relatively large number of analyses, the computational costs should be minimized when possible. Thus, the possibility of creating models with a combination of solid and shell elements using coupling constraints is studied here. Furthermore, the metallurgical bond between cladding and backing material involves constraint to create full bonding between the two materials.

4.3.1. Shell-to-Solid Coupling Constraints

Abaqus offers the special purpose shell-to-solid coupling constraints, which is a surface based coupling designed to use in mesh refinement purposes as relevant to this project. The shell-to-solid coupling constraint couples the displacements and rotations of the shell nodes on the edge of the shell part, to the average displacement and rotation of the adjacent solid surface; see Figure 18.

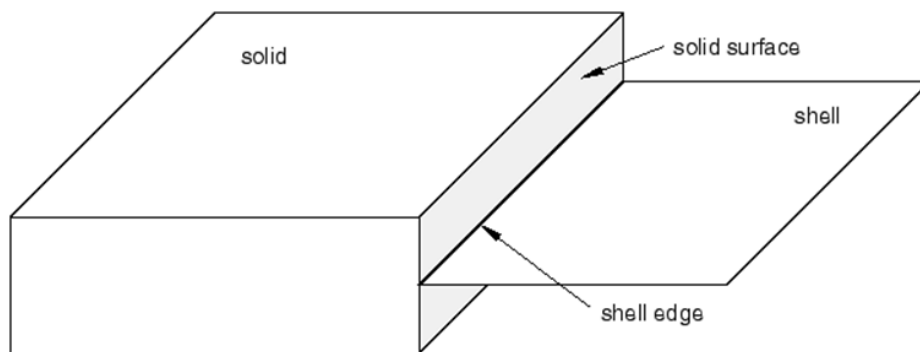


Figure 18: The shell-to-solid coupling constraint couples the displacements and rotations at the shell edge, to the average displacement and rotation of the adjacent solid surface, ref. /13/.

The usage of the shell-to-solid coupling constraints is verified by a simple verification example in section 6.3.

4.3.2. Mesh Tie Constraints

The mesh tie constraint option available in Abaqus is a surface based constraint, which ties two surfaces together during an analysis. The two surface tied together is referred to as master surface and slave surface, where each node of the slave surface is constrained to have the same motion as the nearest node of the master surface.

The mesh tie constraint is applicable for surfaces based on various element types. The two types relevant to this project are the Solid-to-solid and shell-to-shell mesh tie constraints as illustrated in Figure 19. The distance between the two shell surfaces h is automatically calculated from the specified element thicknesses of the two tied shell surfaces.

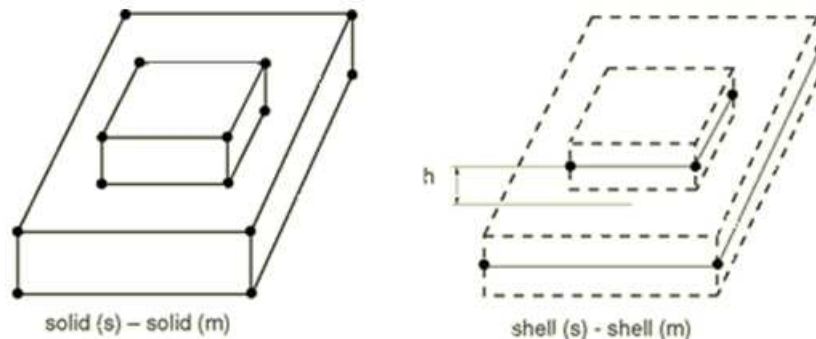


Figure 19: Illustration of the Solid-to-solid and shell-to-shell mesh tie constraints, ref. /13/.

4.4. Conclusions

Generally, there are no limitations to the use of hardening models, while the hardening curve can be specified through tabular data allowing the hardening curve to be calculated externally. Though, it should be noted that strain rate dependency in combination with tabular stress-strain data must be defined by the means of a scaling function, eq. 4.6. Even though, the Johnson-Cook isotropic hardening law is well suited for high rate deformation analyses, the lack of test data for calibration of the relevant parameters excludes this option. Thus, it is decided to use the Ramberg-Osgood hardening law as outlined in section 5, as it is fitted using the specified minimum requirements of the materials.

Strain rate dependency is implemented by using the scaling function, and the implementation is verified in section 6.1. The actual strain rate dependence of the trawl gear impact simulations is put to the test in section 7.3 using the Cowper-Symonds relation.

It is preferred to use the progressive damage and failure model for ductile metals as it is suited for both static and dynamic simulations.

Residual hoop and axial stresses are defined by stress components related to local material directions related to the pipe geometry.

The shell-to-solid coupling constraint and the mesh tie constraint are used to create a model with a combination of shell, and solid elements and to define the metallurgical bond between cladding and backing material, respectively.

5. The Ramberg-Osgood Material Model

As material modelling in this project is based on minimum specified material requirements from the standards instead of performed material tests, the Ramberg-Osgood material model is selected to represent the stress-strain relation in Abaqus. The advantage by using the Ramberg-Osgood model is that the specified material requirements SMYS and SMTS can be used as fitting parameters in conjunction with the corresponding strains ε_y and ε_u as outlined in this section.

The Ramberg-Osgood material model was first introduced in 1941 by W. Ramberg and W.R. Osgood, ref. /19/, but has been presented in numerous different versions since then, depending on the type of material and application. DNV-RP-F110, ref. /5/, has proposed the following version, eq. 5.1, which is commonly used by DNV as material model in Abaqus.

$$\varepsilon = \frac{\sigma}{E} \left(1 + \frac{3}{7} \left(\frac{\sigma}{\sigma_0} \right)^{n-1} \right) \quad (5.1)$$

where

ε	equivalent strain
σ	equivalent stress
E	young's modulus
σ_0, n	Ramberg-Osgood parameters

The parameters σ_0 and n are derived by inserting two points from the stress-strain curve into eq. 5.1, and solving the two equations with two unknowns, namely σ_0 and n , ref. /20/. In this case the two points are chosen as the minimum specified material requirements, but as described in section 4.2, the stress and strain measures in Abaqus must be given as true stresses and logarithmic strains. Thus, the stresses and strains are converted by:

$$\sigma_{true,1} = SMYS(1 + \varepsilon_y), \quad \sigma_{true,2} = SMTS(1 + \varepsilon_u) \quad (5.2)$$

$$\varepsilon_{ln,1} = \ln(1 + \varepsilon_y), \quad \varepsilon_{ln,2} = \ln(1 + \varepsilon_u) \quad (5.3)$$

Giving the two points on the curve $(\varepsilon_{ln,1}, \sigma_{true,1})$ and $(\varepsilon_{ln,2}, \sigma_{true,2})$ by which the parameters σ_0 and n are derived:

$$\sigma_0 = \frac{\sigma_{true,1}}{\frac{7}{3} \left(\frac{E \cdot \varepsilon_{ln,1}}{\sigma_{true,1}} - 1 \right)^{\frac{1}{n-1}}} \quad (5.4)$$

$$n = \frac{\ln \left(\varepsilon_{ln,2} - \frac{\sigma_{true,2}}{E} \right) - \ln \left(\varepsilon_{ln,1} - \frac{\sigma_{true,1}}{E} \right)}{\ln \left(\frac{\sigma_{true,2}}{\sigma_{true,1}} \right)} \quad (5.5)$$

As an example the true stress-logarithmic strain curve for DNV SMYS 415 steel are calculated by using the parameters in Table 5 and plotted in Figure 20.

Table 5: Material specifications for DNV SMYS 415 steel.

Parameter	Value
Yield strength SMYS	415 MPa
Tensile strength SMTS	520 MPa
Yield strain ε_y	0.005
Ultimate tensile strain ε_u	0.1
Young's modulus E	210,000 MPa
$\sigma_{true,1}$	417.07 MPa
$\sigma_{true,2}$	572.00 MPa
$\varepsilon_{ln,1}$	0.00499
$\varepsilon_{ln,2}$	0.09531

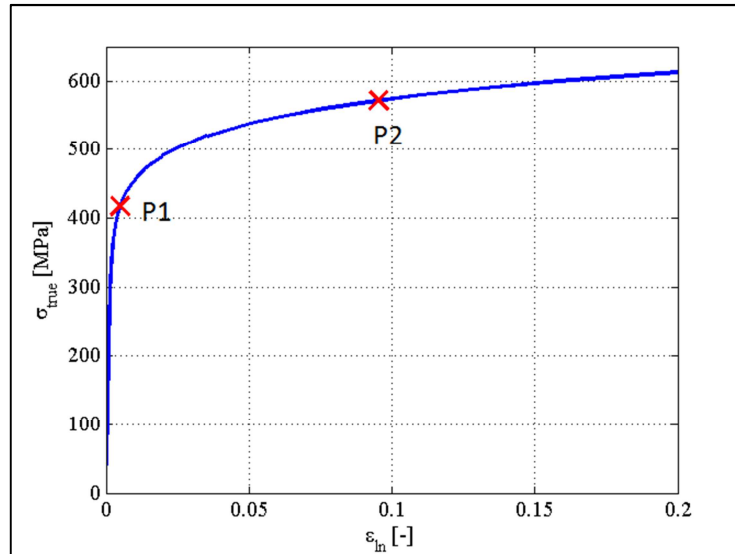


Figure 20: True stress-logarithmic strain curve for DNV SMLS 415 steel, plotted with the two fitting points P1 and P2.

It should be noted that only the plastic part is used as input in Abaqus. The above described formulation of the Ramberg-Osgood material model is implemented and verified in section 6.1.

6. Simple Verification Examples

A number of simple verification examples are performed in this section. The objective is to verify the use of Abaqus with material and element definitions relevant to this project.

Three tensile tests are performed to verify the implementation of the Ramberg-Osgood plasticity model with strain rate dependence and damage and failure. The results from the tensile tests are used to calibrate the material models for later use in the trawl gear impact analyses.

Furthermore, two bend tests are carried out to study the performance of first order elements subjected to bending. The stress distribution through the cross section and the transverse deformation are compared with existing analytical solutions.

Finally, the usage of shell-to-solid coupling constraints is verified by comparing the stress distribution of two identical geometries, one modelled with solid elements and one with a combination of shell and solid elements.

6.1. Material Model Verification and Calibration

A simple uniform tensile test specimen with quadratic cross section is modelled with the dimensions 10x10x100 mm. The test specimen is divided into five sections in the axial direction to define different mesh sizes and material properties; see Figure 21.

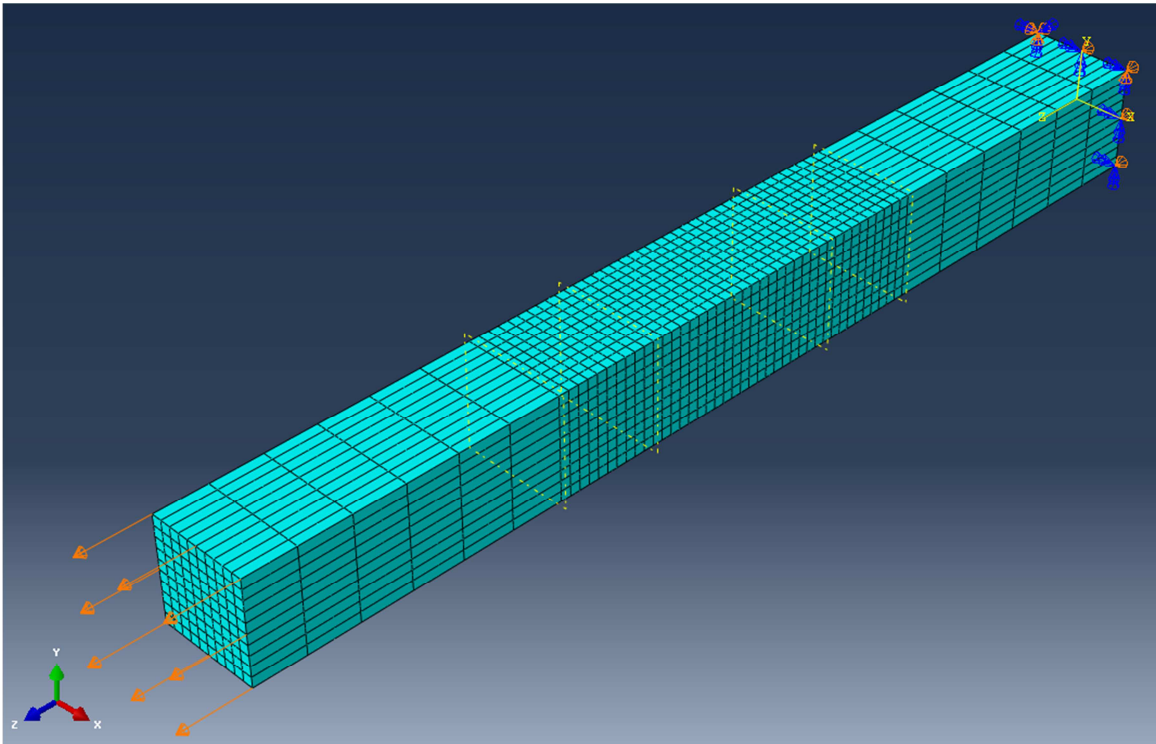


Figure 21: The test specimen is divided into five sections to define different mesh sizes and material properties.

The geometry is meshed with the C3D20R element, a 20-node quadratic brick element with reduced integration, and the mesh is refined in the middle three sections.

Mises yield surface with isotropic hardening is defined with the Ramberg-Osgood plasticity model. The steel is taken as DNV SMYS 415 with material properties as listed in Table 6, and the Ramberg-Osgood stress-strain relation is generated externally, as described in section 5, and typed in as table data.

Table 6: Material parameters used in the analyses.

Parameter	Value
Yield strength SMYS	415 MPa
Tensile strength SMTS	520 MPa
Yield strain ϵ_y	0.5 %
Ultimate tensile strain ϵ_u	10 %
Young's modulus E	210000 MPa
Poisson's ratio ν	0.3

The test specimen is fixed in one end and given a displacement in the other end of up to 50 mm over a time period of 10 seconds. All tensile analyses are carried out with geometric nonlinearities and automatic step control with a full Newton solver scheme.

6.1.1. Verification of Material Model

Tensile test no. 1 is carried out to verify the implementation of the Ramberg-Osgood plasticity model by comparing the output stress-strain relation from the Abaqus analysis with the analytical solution for the Ramberg-Osgood model.

The solution is plotted in Figure 22 as Mises equivalent stresses with both the initial and deformed geometry. The stress-strain relation from a random node is compared with the analytical solution in Figure 23.

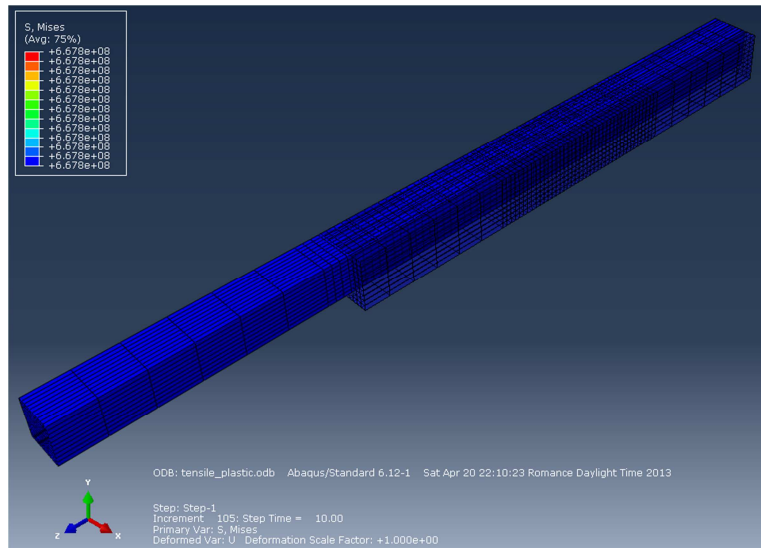


Figure 22: Initial geometry and deformed shape plotted with Mises equivalent stresses.

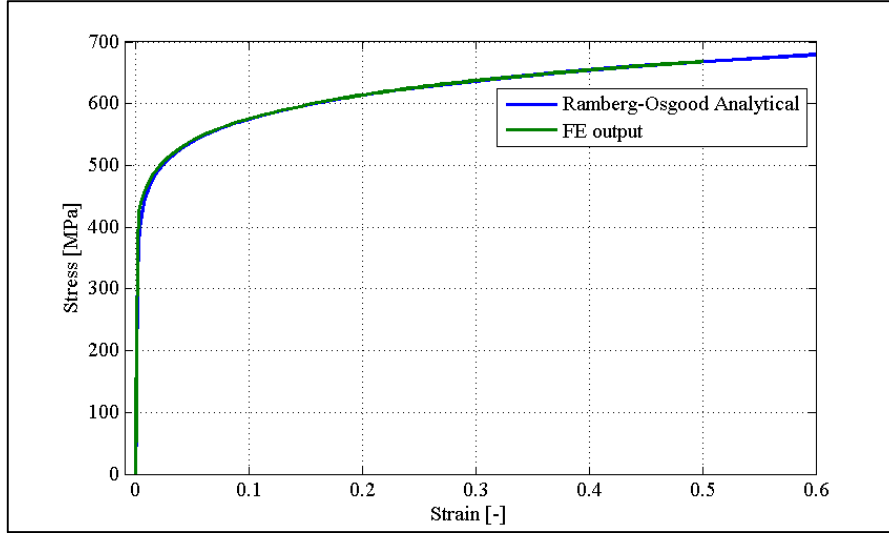


Figure 23: Stress-strain relation from the FE-analysis compared with the analytical solution.

The stress-strain relation from the FE-analysis shows good compliance with the Ramberg-Osgood analytical solution.

6.1.2. Implementation of Strain Rate Dependency

Tensile test no. 2 is carried out to verify the implementation of strain rate dependence by using the scaling function as outlined in section 4.2:

$$\bar{\sigma}(\bar{\varepsilon}^{pl}, \dot{\bar{\varepsilon}}^{pl}) = \sigma^0(\bar{\varepsilon}^{pl}) \cdot R(\dot{\bar{\varepsilon}}^{pl}) \quad (6.1)$$

To give a somewhat realistic value of the yield stress ratio R , test results from ref. /2/ are studied. The tests shows a large variations of the yield stresses, but the largest strain rate from the performed tests is 1079 s^{-1} with a corresponding yield stress ratio of $R=1.33$. Thus, as an approximation and for simplicity, R is given as a linear function of strain rate, with $R=1.0$ at zero strain rate; see Figure 24.

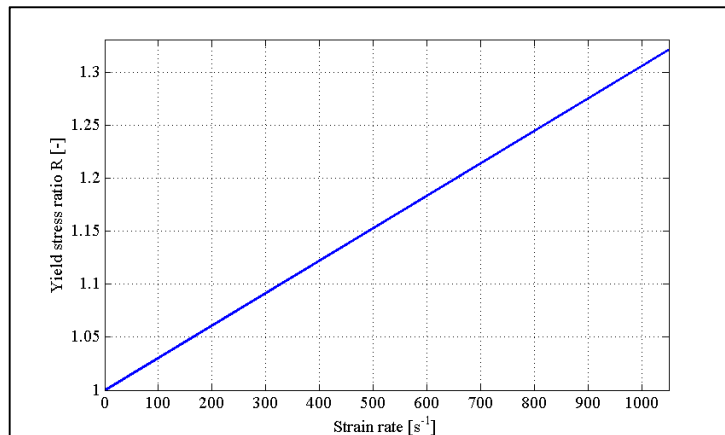


Figure 24: Yield stress ratio R as a function of strain rate.

Two simulations are carried out with strain rates of 100 s^{-1} and 500 s^{-1} , and the output stress-strain relations are compared in Figure 25. As expected the strain rate dependence results in increasing stresses for higher strain rates.

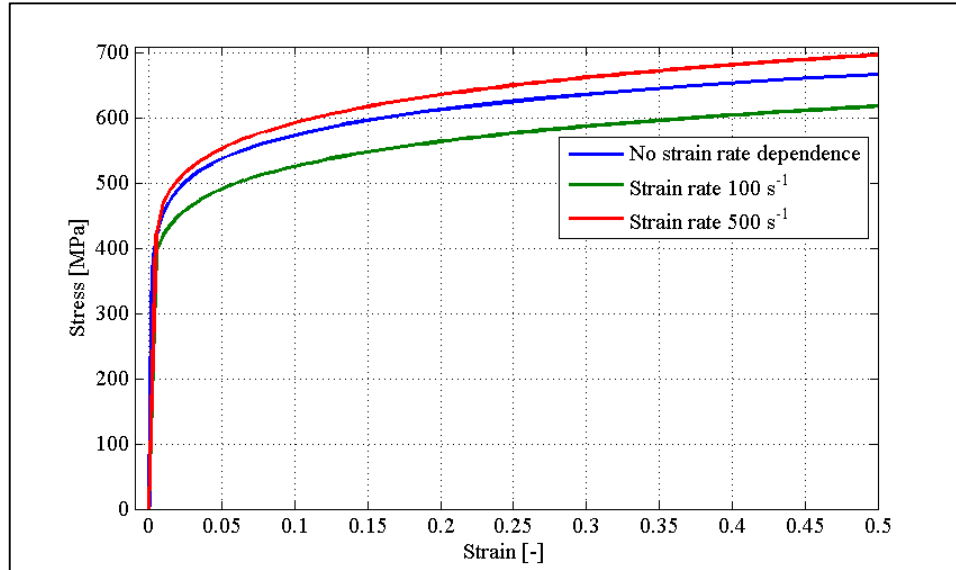


Figure 25: Output from simulations with strain rates of 100 s^{-1} and 500 s^{-1} compared with no strain rate dependence output.

6.1.3. Implementation and verification of the Ductile Damage and Failure Model

Tensile test no. 3 is carried out to implement an upper limit to the load bearing capacity of the material by means of ductile damage and failure as described in section 4.2. Two parameters govern the characteristics of the ductile damage and failure, namely the equivalent plastic strain at damage initiation ε_D^{pl} and the equivalent plastic displacement after damage initiation \dot{u}_f^{pl} given by:

$$\dot{u}_f^{pl} = L \cdot \varepsilon_f^{pl} \quad (6.2)$$

The characteristic length L is defined as half the distance across an element for second order elements giving a constant value of $L=0.0005 \text{ m}$ for these analyses with an element size of 1 mm . The equivalent plastic strain at damage initiation ε_D^{pl} and the equivalent plastic strain increment after damage initiation $\dot{\varepsilon}_f^{pl}$ are illustrated in Figure 26.

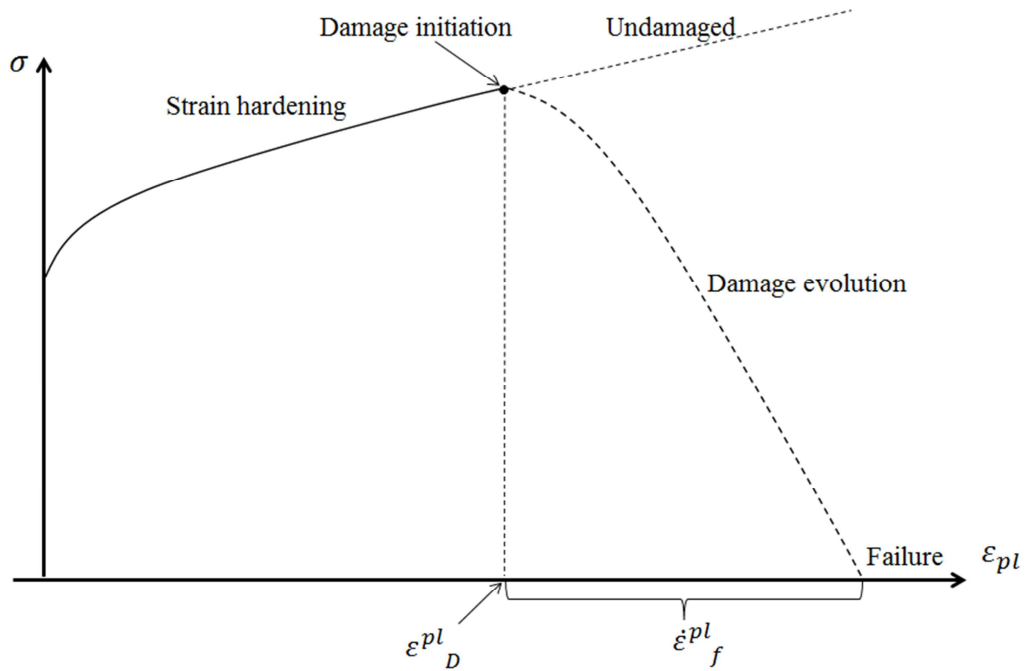


Figure 26: Definition of the two governing damage and failure parameters.

To evaluate the influence of the two governing parameters, two simulations are carried out with values as given in Table 7.

Table 7: Values used in the two simulations.

Test ID	L [m]	$\dot{\epsilon}_f^{pl}$ [-]	\dot{u}_f^{pl} [m]	ϵ_D^{pl} [-]
TT3-1	0.0005	0.1	0.00005	0.1
TT3-2	0.0005	0.2	0.0001	0.2

To ensure damage and failure in the middle section of the geometry, the end sections are given higher yield stresses and only the middle 20 mm are specified with damage and failure as illustrated in Figure 27.

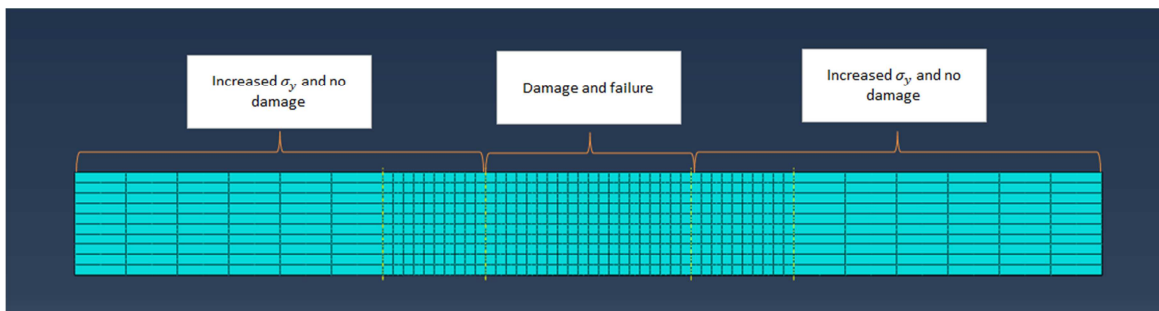


Figure 27: To ensure damage and failure in the middle section the yield stress is increased for the end sections and damage and failure are only specified for the middle 20 mm of the geometry.

The deformed geometry and Mises stresses from the last frame before complete failure of the two analyses are plotted in Figure 28 with a section cut through the middle of the geometry.

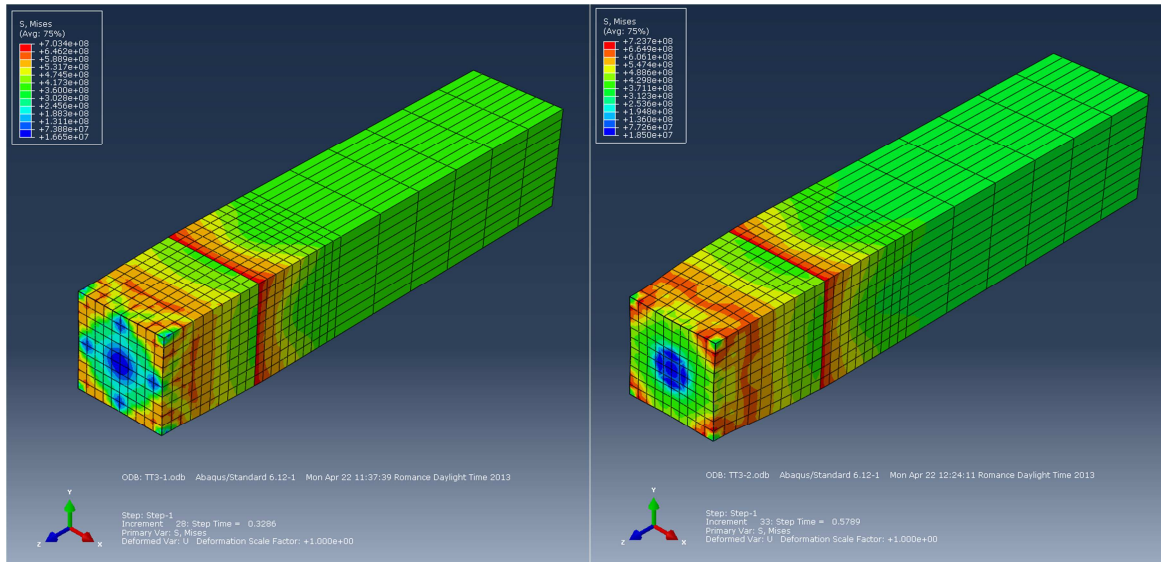


Figure 28: Deformed geometry plotted with Mises stresses from the last frame before complete failure of the cross section. TT3-1 to the left and TT3-2 to the right.

The damaged sections show the expected necking shape and it is noted that damage is severe in the middle of the cross section with a large degradation of the Mises stresses. To evaluate the material behaviour during damage and failure, the true stresses and logarithmic strains from the central node in the cross section are plotted in Figure 29, i.e. stresses and strains from the blue area of the geometries in Figure 28.

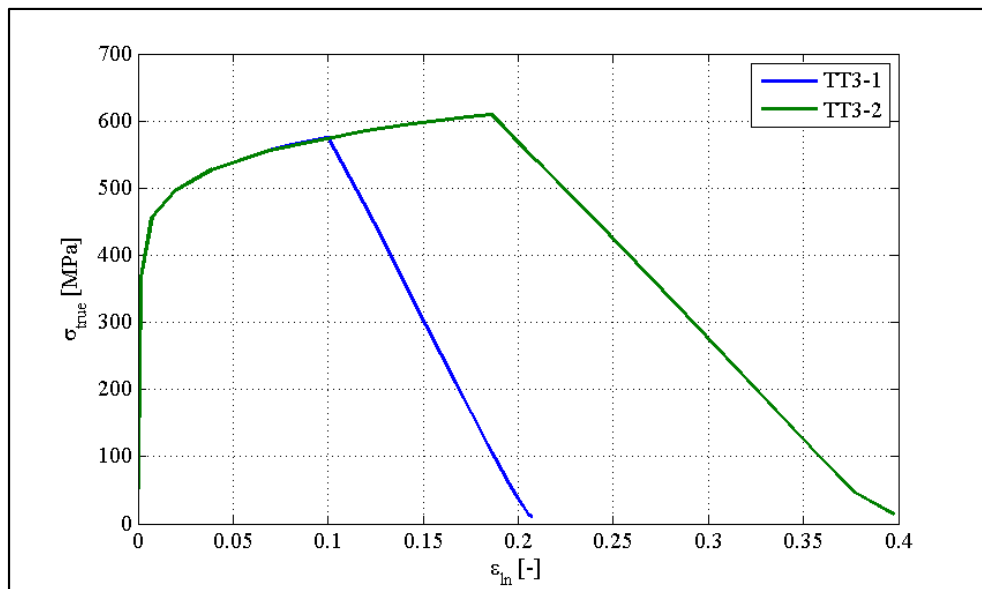


Figure 29: True stress-logarithmic strain plots from the central node of the cross sections.

With reference to the governing parameters specified in Table 7 it is noted that they are directly related to the true stresses and logarithmic strains with a linear degradation of the

material strength from ε_D^{pl} to ε_f^{pl} . Though, it is desired to relate the damage and failure to the engineering stresses and strains corresponding to known material parameters as outlined in section 3.4. The engineering stresses and strains are given by:

$$\sigma_{eng} = \frac{F}{A_0} \quad (6.3)$$

$$\varepsilon_{eng} = \frac{L - L_0}{L_0} = \frac{\Delta L}{L_0} \quad (6.4)$$

It is concluded from the engineering stresses and strains plotted in Figure 30 that the ductile damage and failure gives somewhat realistic results compared with theoretical stress-strain relations, ref. /21/. In addition, the specified strength parameters, ref. Table 6, SMYS=415 MPa and SMTS=520 MPa are in compliance with the test results. Thus, the results are used to calibrate the material models in the following section.

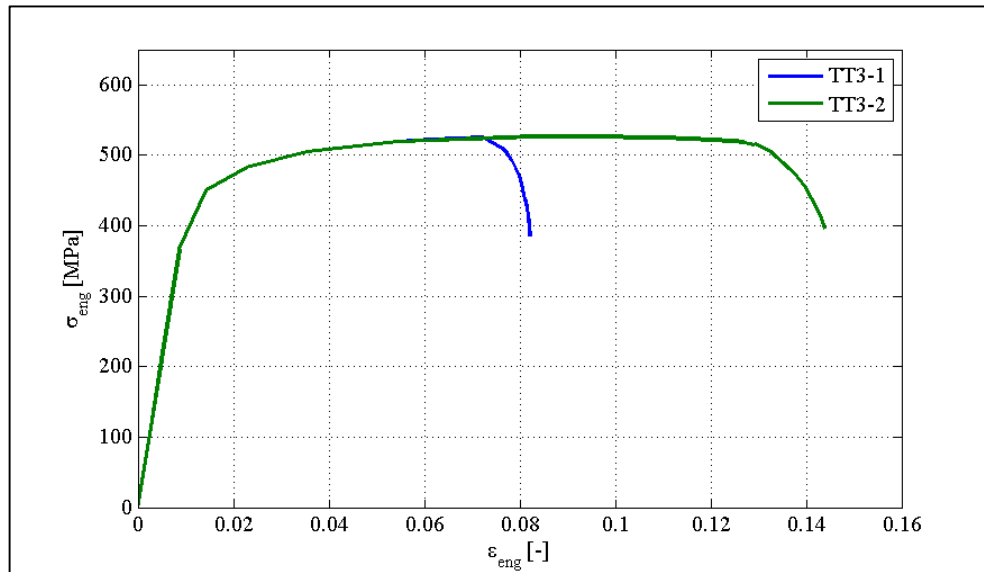


Figure 30: Engineering stresses and strains from the two analyses.

6.1.4. Calibration of Material Models

The materials selected for all clad and lined pipes in the trawl gear impact analyses are DNV SMYS 415 and Alloy 316L; see section 3.4. The Ramberg-Osgood material model is calibrated to fit the given material parameters as outlined in section 5, but to implement damage and failure in compliance with the specified minimum elongation of the material A_f , further calibration is needed. The relevant material properties are given in Table 8.

Table 8: Material properties relevant to the material model calibration.

Application	Type/name	Yield strength [MPa]	Tensile strength [MPa]	Elongation in 50 mm A_f [%]
Backing	SMYS 415	415	520	17.5
Clad/liner	Alloy 316L	170	485	40

The approach is to calibrate the two Abaqus input parameters ε_D^{pl} and \dot{u}_f^{pl} by “trial and error” to fit the specified minimum elongation A_f , i.e. on the basis of FE tensile tests as described in section 6.1.3. The calibrated engineering stress-strain curves from the tensile tests are plotted in Figure 31 and the corresponding input parameters are given in Table 9.

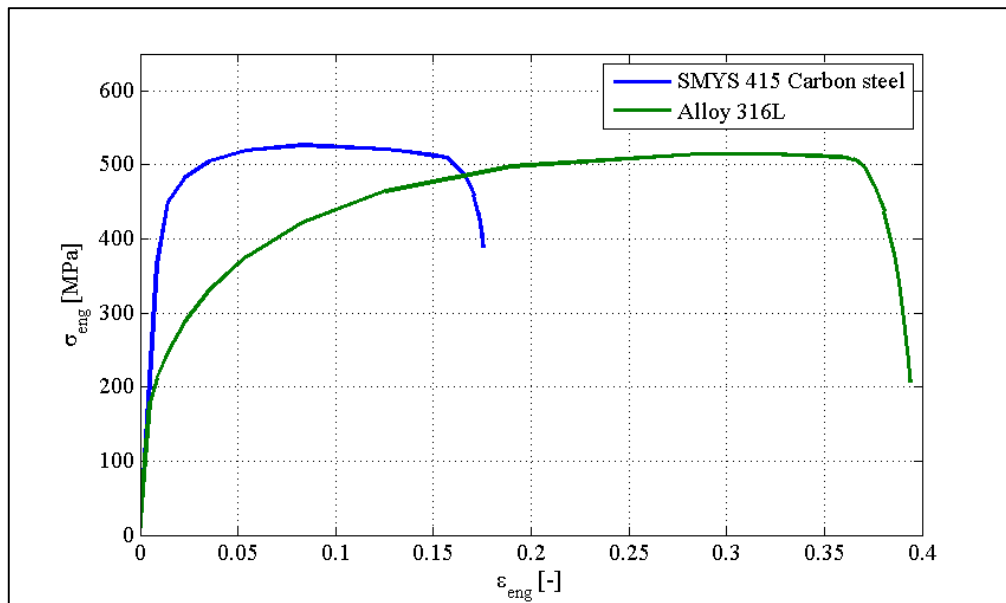


Figure 31: The calibrated engineering stress-strain curves.

Table 9: Abaqus input parameters calibrated to fit the specified minimum elongation of the material.

Material	ε_D^{pl} [-]	\dot{u}_f^{pl} [m]
SMYS 415	0.3	0.00008
Alloy 316L	0.5	0.00015

The results show good compliance with the material parameters given in Table 8. Though, it should be noted that the ultimate tensile strength of Alloy 316L in Figure 31 is higher than the one specified in Table 8. This is due to the large difference between yield strength and tensile strength of the material, i.e. 170 MPa and 485 MPa respectively, which would

cause a discontinuous stress-strain curve if the tensile strength should be obtained. This relatively small error is assessed as negligible and disregarded.

6.1.5. Preliminary Conclusions

The tensile tests show good compliance with the analytical Ramberg-Osgood stress-strain relation verifying the implementation of the plasticity model. Strain rate dependence is taken into account by the scaling function, which for this simple example the yield stress ratio R was approximated as a linear function of strain rate. If strain rate dependence is to be used for the trawl gear impact analyses, a more specific R -strain rate relation must be obtained. Finally, a maximum load bearing capacity is defined by the ductile damage and failure criterion. The results are evaluated as realistic compared with theoretical solution and the engineering stress-strain plots are in compliance with the specified minimum requirements, i.e. the SMYS and SMTS. Thus, the results are used to calibrate the material models for DNV SMYS 415 and Alloy 316L to be used in the trawl gear impact analyses.

6.2. Element Performance during Bending

As outlined in section 4.1, the use of Abaqus/Explicit induces some element limitations as only first order brick elements are available with the possibility to enhance with incompatible modes to improve bending behaviour. Thus, bend tests are carried out to study the stress distribution and deformations of these elements while undergoing bending, i.e. tests are carried out with 8-node brick elements with and without incompatible modes. The results are compared with known analytical solutions.

By using symmetry, only half the test specimen is modelled with the dimensions 10x10x50 mm corresponding to the full geometry of 10x10x100 mm; see Figure 32.

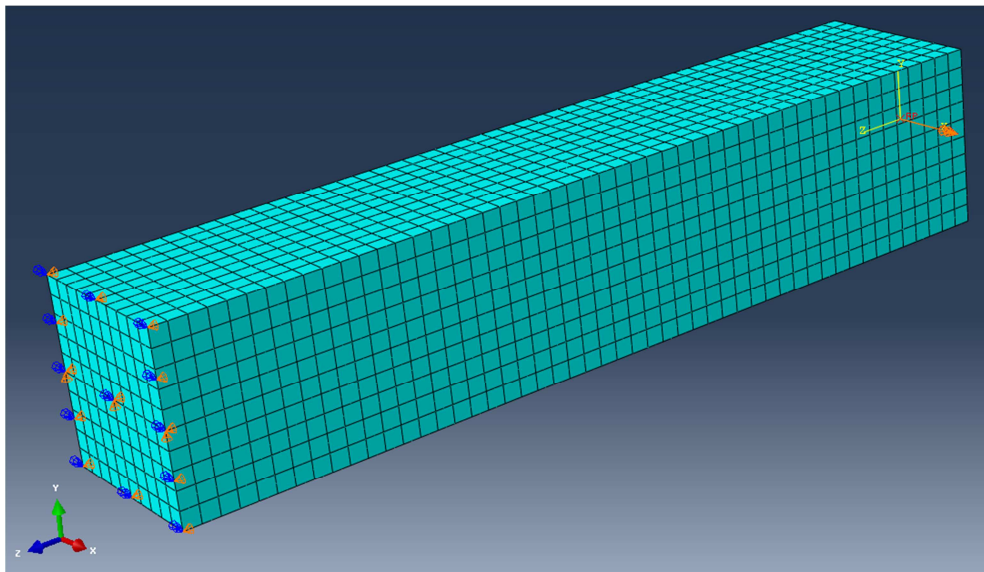


Figure 32: Half of the geometry modelled with boundary conditions corresponding to a symmetry plane on the left end surface.

The boundary conditions $u_z=0$ and $r_x=0$ are applied to the surface on the left in Figure 32 corresponding to a symmetry plane, and $u_y=0$ is applied to the centre line on the same surface. The test specimen is loaded in the opposite end with a moment m_x acting on the entire surface.

The geometry of the first test specimen BT1 is meshed with first order 8-node brick element C3D8R with reduced integration and hourglass control. The second test specimen BT2 is meshed with first order 8-node brick element C3D8I enhanced with incompatible modes. The initial element size is 1x1x1 mm.

The material is specified as linear-elastic/ideal-plastic with a yield stress of 400 MPa, Young's modulus of 210 GPa and Poisson's ratio of 0.3. The analyses are carried out with automatic step control and a full Newton solver scheme.

6.2.1. Pure Elastic Bending

The first bend tests are carried out to verify the elastic bending capacity, to show a correct stress distribution in the cross section and finally to verify the maximum transverse displacement.

The elastic bending capacity M_e of a rectangular cross section is given by, ref. /22/:

$$\begin{aligned} M_e &= \frac{1}{6} \cdot \sigma_y \cdot b \cdot h^2 = \frac{1}{6} \cdot 400 \text{ MPa} \cdot 10\text{mm} \cdot (10\text{mm})^2 \\ &= 66,666.67 \text{ Nmm} \end{aligned} \quad (6.5)$$

which is applied to the end of the test specimens and the results are plotted in Figure 33, with the deformed geometries and normal stresses. The test specimen meshed with regular first order elements, BT1, shows normal stresses of 363.6 MPa in the outer fibres, while the specimen meshed with incompatible elements BT2 shows normal stresses of 400 MPa in the outer fibres.

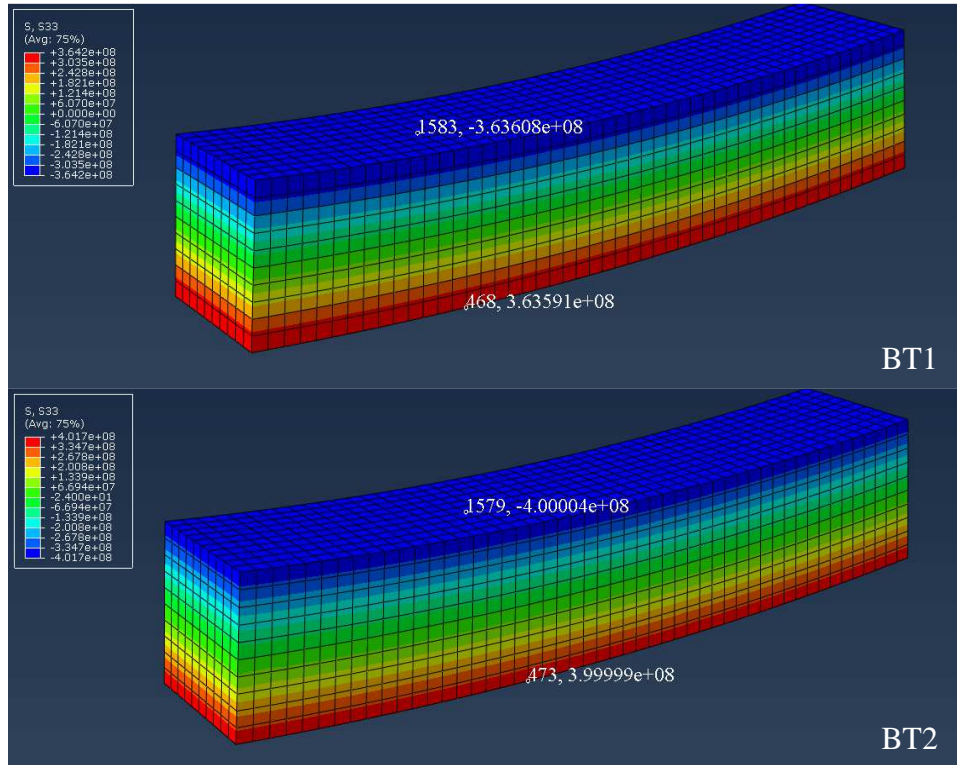


Figure 33: Normal stress distribution in the two test specimens. BT1 meshed with regular first order elements and BT2 with incompatible elements.

The results are clear as the incompatible elements shows good compliance with the yield strength of the material, i.e. the elastic bending capacity is reached. The result from the analysis with regular first order elements BT1 confirms the predicted problems when undergoing bending as outlined in section 4.1.

Furthermore, the maximum transverse displacements are studied by comparing the FE-analyses with beam theory analytical solution, ref /23/. The maximum displacement for a simply supported beam with applied moments is given by:

$$\begin{aligned}
 u_{max} &= \frac{1}{8} \cdot \frac{M \cdot l^2}{E \cdot I_x} = \frac{1}{8} \cdot \frac{66,666.67 \text{ Nmm} \cdot (100\text{mm})^2}{2.1e5 \text{ MPa} \cdot \frac{1}{12} \cdot 10\text{mm} \cdot (10\text{mm})^3} \\
 &= 0.476 \text{ mm}
 \end{aligned} \tag{6.6}$$

The FE results gives maximum deformations of 0.480 mm and 0.476 mm for BT1 and BT2 respectively. Again the incompatible elements shows good compliance while the regular first order elements show larger deformations than calculated by eq. 6.6. This is somewhat surprising as the shear locking are predicted to add stiffness to the elements while undergoing bending, and thereby should result in a smaller transverse deformation, ref. /15/.

Though, as later studies confirms, there are limitations to the incompatible element while undergoing large deformations; see Appendix 2. Thus, further studies are made with bending of the regular first order elements, i.e. with refined mesh to test the convergence of the solution with respect to the normal stress distribution and the maximum transverse deformation. The element length is reduced to half the size giving 2^3 times more elements in the mesh. The results are a normal stress in the outer fibres of 382 MPa and a maximum transverse deformation of 0.476 mm. This shows that the mesh refinement produces a fully converged solution with respect to the transverse deformation, while the stress distribution is closer to the analytical solution, but not fully converged.

6.2.2. Bending with Partly Plastic Cross Section

As the trawl gear impact simulations involve material plasticity, further bend tests are carried out to verify the plastic material response when subject to bending. This is done by comparing the FE results with an applied plastic moment calculated by eq. 6.8, ref. /22/. The aim is to show yielding of the material in the outer fibres of the cross section while maintaining an elastic part in the middle 2 mm corresponding to x in Figure 34.

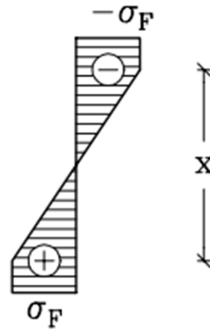


Figure 34: Stress distribution in partly plastic cross section, ref. /22/.

$$M_p = \frac{1}{4} \cdot \sigma_y \cdot b \cdot h^2 \left(1 - \frac{1}{3} \left(\frac{x}{h} \right)^2 \right) \quad (6.7)$$

$$\begin{aligned} M_{p,2mm} &= \frac{1}{4} \cdot 400 \text{ MPa} \cdot 10 \text{ mm} \cdot (10 \text{ mm})^2 \left(1 - \frac{1}{3} \left(\frac{2 \text{ mm}}{10 \text{ mm}} \right)^2 \right) \\ &= 98,666.67 \text{ Nmm} \end{aligned} \quad (6.8)$$

which is applied to the end of the test specimen and the normal stresses are plotted with the deformed geometry in Figure 35 and the stress distribution through the cross section is plotted in Figure 36. The stress distribution is not exactly as the theoretical solution illustrated in Figure 34, but this is due to the three-dimensional stress state, as Mises stresses shows fully plastic regions besides the middle 2 mm.

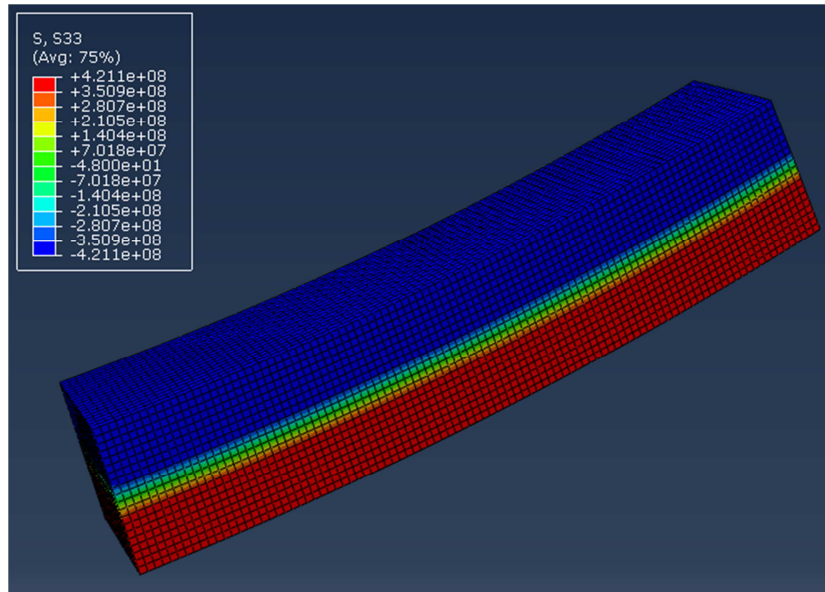


Figure 35: Normal stresses plotted with the deformed geometry.

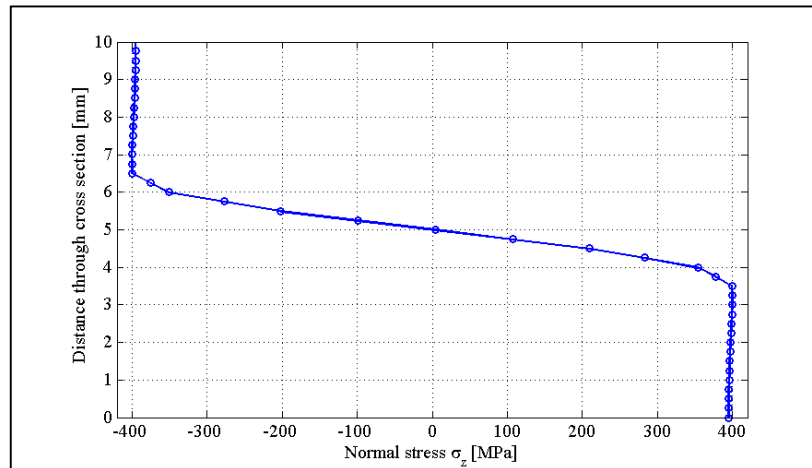


Figure 36: Stress distribution through the partly plastic cross section.

6.2.3. Preliminary Conclusions

The trawl gear impact simulations in this project are carried out mainly to study deformation of the pipes. Thus, the regular first order element as tested above is evaluated to be sufficient as the transverse deformation is fully converged with the analytical solution. Though, uncertainties are still present regarding the stresses calculated by the regular first order element as relatively fine meshing is necessary to obtain reliable results, wherefore a convergence study is performed during the model calibration in section 7.3.

6.3. Verification of the Shell-to-Solid Coupling Constraint

As described in section 4.3, Abaqus offers the option of a shell-to-solid coupling constraint which enables the possibility of creating a model with a combination of shell and solid elements. Thus, the usage of this feature is verified by a simple bend test with two identical

geometries, i.e. two cantilever beams with quadratic cross sections. The difference between the two beams is that one is modelled with solid elements while the other is modelled with a combination of shells and solids. All elements, both shells and solids, are first order elements.

Both beams are fixed in one end and given a displacement of 1 mm in the other end, and the results are plotted in Figure 37 as Mises stresses. The two beams show close to identical stress distributions and the shell-to-solid coupling constraint is considered verified.

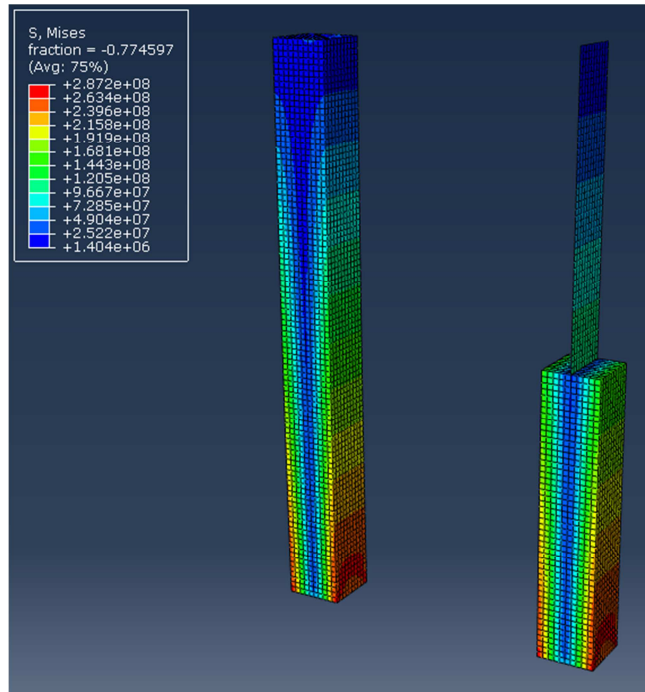


Figure 37: Two identical geometries modelled with solids and a combination of shells and solids. The stress distribution is identical in the two beams.

6.4. Conclusions

The Ramberg-Osgood material model is verified from FE-analyses, including the implementation of strain rate dependence and ductile damage and failure. Furthermore, the material models representing DNV SMYS 415 and Alloy 316L are calibrated to comply with the governing material parameters, including the maximum elongation of the materials.

The first order element available in Abaqus/Explicit is tested in pure bending to evaluate the influence of shear locking. The results show a converged solution with respect to the transverse deformations, but the stresses deviates from the analytical solution, even with a relatively fine mesh. A solution to the shear locking of first order elements is to use the incompatible element available in Abaqus, but as later studies reveals other limitations excludes the use of this element in the trawl gear impact simulations. Thus, with the

options limited to the first order element, focus should be on verifying the model when performing the impact analyses in section 7.2.

Finally, the usage of shell-to-solid coupling constraint is verified which enables the possibility of modelling the pipes with a combination of shell and solid elements.

7. Model Calibration, Verification and Optimization

As the general usage of Abaqus is verified through simple verification examples, the concept of the dynamic trawl gear impact analyses is outlined in this section. The concept is verified by comparing with test results from ref. /2/.

Furthermore, a pre-study is carried out with a 16" bare carbon steel pipe to optimize the model regarding mesh size and computational costs. During the pre-study, strain rate dependency is implemented by the Cowper-Symonds relation to study the influence. Additionally, general observations are made during the pre-study to ensure reliable results during the subsequent parameter study; see section 9.

7.1. General Modelling Considerations

The general setup of the FE-model is outlined in this section including boundary conditions, element types and contact definition. As outlined in section 2.4, it is recommended to use a rigid surface to support the pipe as this ensures that most energy is absorbed locally, i.e. the most conservative with respect to indentation of the pipe.

As the model is symmetric across two planes, only $\frac{1}{4}$ of the full geometry is modelled. A bare steel pipe model is assembled from four parts as illustrated in Figure 38 and further described below.

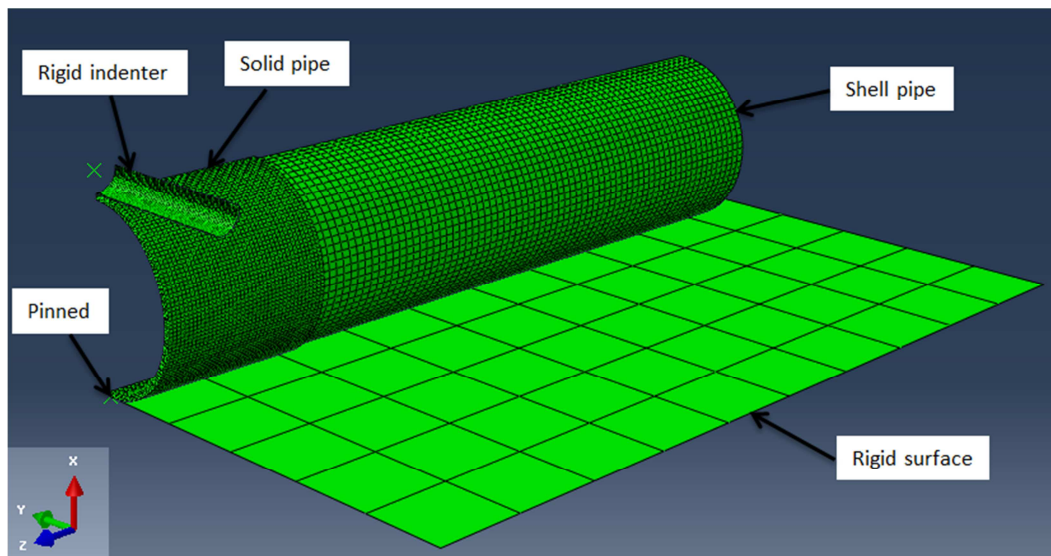


Figure 38: Concept of the FE-model. The model is assembled from four parts as described below.

The model is supported by a rigid surface to ensure that most energy is absorbed by local deformations as discussed in section 2.3. The mesh is coarse as the surface acts as foundation and no output is required for this part.

The trawl gear is represented by a round shaped rigid indenter with a radius of 25 mm as outlined in section 2.4. The indenter is modelled as a shell with relatively fine mesh as the contact force is integrated over the surface as output. The indenter is given a mass and initial velocity in the negative x-direction.

The pipe is modelled with both shell and solid elements. The impact zone and the surrounding geometry are modelled with solid elements with a relatively fine mesh and several elements in the pipe wall thickness direction. The rest of the pipe is modelled with shell elements with a coarser mesh to reduce computational costs. The two parts are connected with shell-to-solid coupling constraints as discussed in section 4.3.

As outlined in section 6.2, the incompatible first order element C3D8I performs better while undergoing pure bending, but due to limitations in large straining applications the element is found as not suitable for these impact simulations; see Appendix 2 for further discussion and testing of this element. Thus, the solid section is modelled with element type C3D8R, an 8-node first order brick element with reduced integration and hourglass control; see section 6.2 for verification of this element. The shell section is modelled with element type S4R, a 4-node first order shell element with reduced integration and hourglass control.

The pipe and indenter are given boundary conditions corresponding to the two symmetry planes. Furthermore, the pipe is pinned to the rigid surface at the intersection between the two symmetry planes to prevent the pipe from “jumping” on the surface; see Figure 38.

The indenter-pipe and pipe-surface contacts are defined as frictionless in the tangential direction and “hard” in the normal direction. The definition of “hard” contact is that contact pressure only is present at contact with no transmission phase as illustrated in Figure 39, ref. /13/.

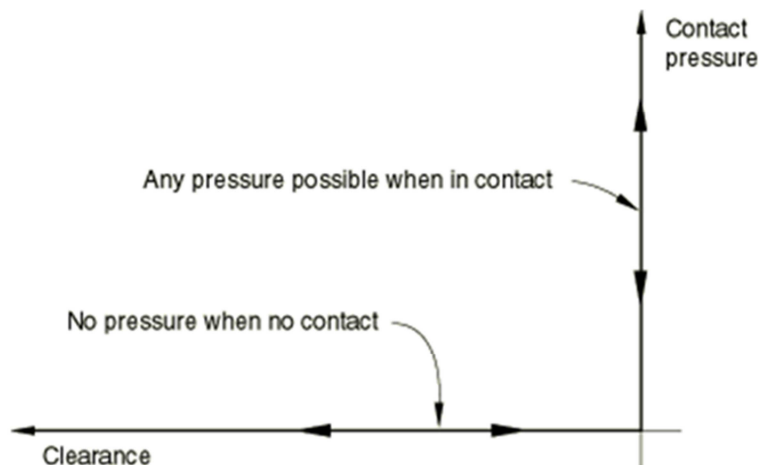


Figure 39: Definition of “hard” contact, ref. /13/.

7.2. Model Verification

To verify the concept of the FE-model, test results from ref. /2/ are used as a benchmark by comparing the contact force-displacement relationships. The tests in ref. /2/ are carried out with a so-called kicking machine, where a sledge is “kicked” towards the test specimen. On the sledge is mounted a round shaped indenter with a radius of 25 mm representing the trawl gear. The test specimen is held against a stiff plate with large mass compared to the mass of the sledge and pipe. Furthermore, static and dynamic tensile tests are performed in ref. /2/ to calibrate a Johnson-Cook material model which includes strain rate dependency. To ensure comparable results, this material model is implemented in the following verification of the FE-model. One test with a 12” structural steel pipe is picked out for the verification. Pipe dimensions and test parameters are given in Table 10.

Table 10: Pipe dimensions and test parameters for the 12” dynamic test, ref. /2/.

Parameter	Value
Outer diameter	219.1 mm
Wall thickness	6.27 mm
Length	1800 mm
Material	s355
Sledge velocity	2.144 m/s
Mass of the sledge	1000 kg

The contact force-displacement curves from the test and the FE-model are plotted in Figure 40. In general, the results are similar with respect to the shape of the curves. The test result shows a larger maximum deformation while the FE-model shows a larger maximum contact force. This could be the result of various factors such as lack of homogeneity in the material and geometry of the test specimen. The Johnson-Cook material model used in the FE-model is calibrated from test results which could lead to some deviation in the stress-strain relationship as a result of the fitting goodness of the curve. Furthermore, the material model does not take damage and failure into account which is shown later to be a factor for these impact analyses. And last but not least, the smaller deformation of the FE-model is likely to be a result of shear locking of the elements undergoing bending as described in section 4.1. Thus, the concept of the FE-model is considered as verified with respect to geometry, boundary conditions and contact definition.

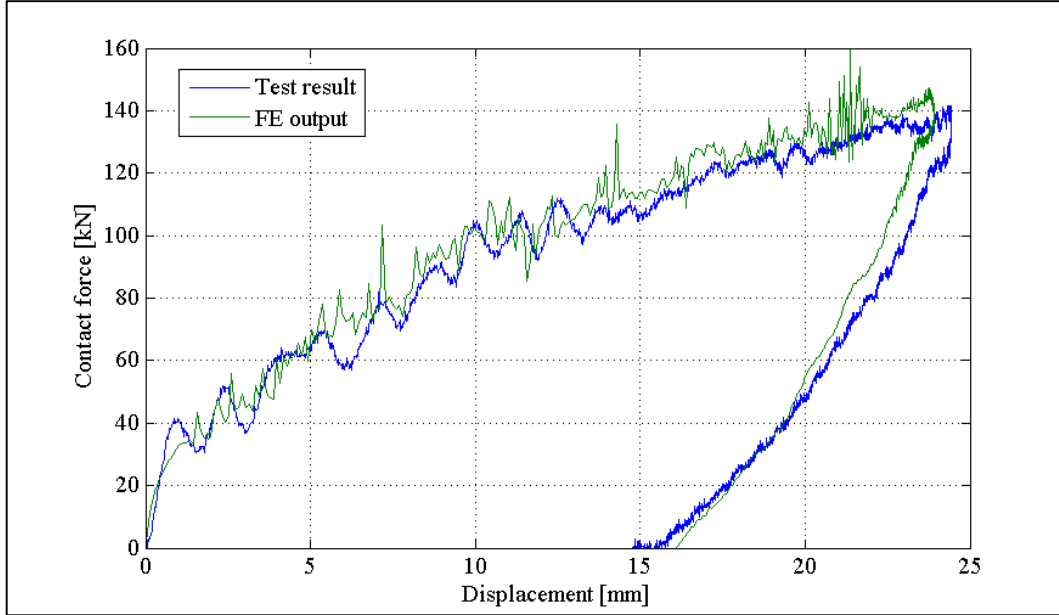


Figure 40: Result from the FE-model is compared with test result.

From this preliminary verification analysis it is observed that the contact force-displacement curve shows varying excitations as the contact force increases. These excitations will be studied further in the following pre-study, section 7.3.

The deformed shape of the pipe with Mises stresses is plotted in Figure 41. For further verification of the boundary conditions at the symmetry planes, the geometry is mirrored in both planes creating the full geometry of the pipe. On the basis of the deformations the boundary conditions are evaluated as satisfactory. Additionally, it is observed that the time period of contact between pipe and indenter is 0.0318 seconds, and the computational time is approximately 60 minutes.

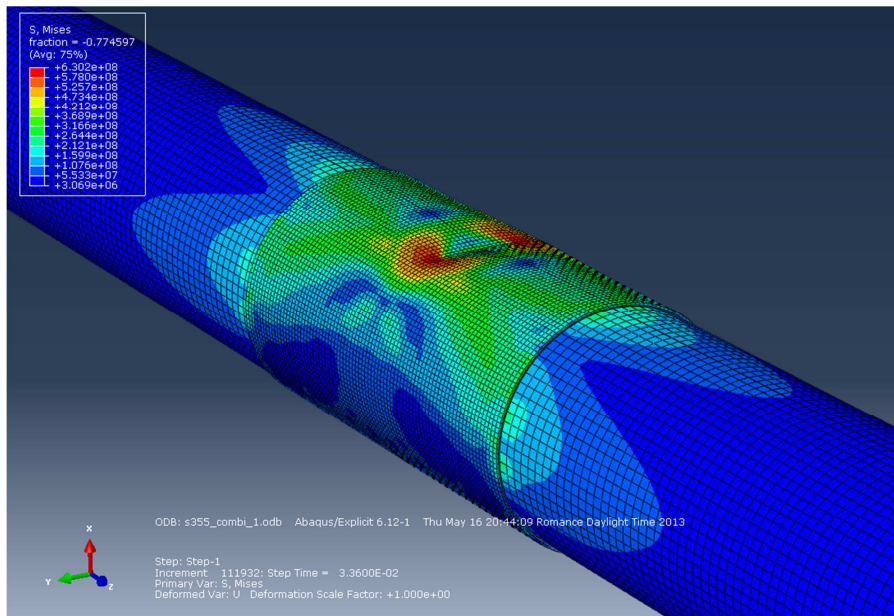


Figure 41: Deformed geometry of the pipe mirrored in both symmetry planes to create the full geometry.

7.3. Pre-study of Bare Carbon Steel Pipe

A pre-study is carried out in this section with a bare carbon steel pipe. The objective is to optimize the model with respect to mesh density and computational costs. Additionally, other subjects of interest are studied, such as strain rate dependency and the source of excitations in the contact force as observed in section 7.2.

Part of the scope of this project is to analyse pipes with diameters in the interval 12''-28'' with D/t relations in the range of 15-40. Thus, the pipe selected for this pre-study is a 16'' pipe with a wall thickness of 15.88 mm corresponding to $D/t=25$, as this is a medium size and thereby better represent the wide range of pipe dimensions to be analysed. The material used is the calibrated DNV SMYS 415 carbon steel; see section 6.1. The mass and velocity of the indenter are set to the maximum possible values recommended by DNV-RP-F111, i.e. 12140 kg and 2.8 m/s respectively; see section 2.4, ref. /1/.

7.3.1. Convergence Study

To ensure an optimized mesh size without using too many elements, a convergence study is carried out by comparing the contact force-deformation curves from analyses with different mesh sizes. The approach is to refine the mesh in the impact region of the pipe until the solution shows similar results, which indicates a converged solution.

The contact force-displacement relations from five analyses with different mesh sizes are plotted in Figure 42. A mesh size of 10 mm x 10 mm x 6 pc. refers to an element size of 10x10 mm with a density of six elements in the pipe wall thickness direction, which for this pipe is 15.88 mm. The mesh size refers to the smallest elements in the mesh, which are located just around the impact area and gets coarser further away from the impact area as illustrated in Figure 43.

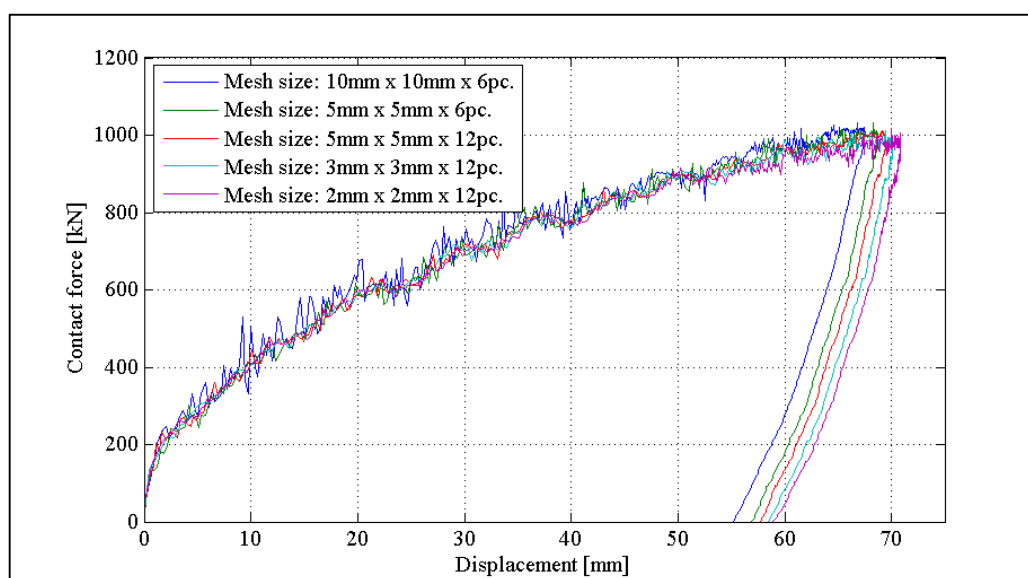


Figure 42: Contact force-displacement curves for different mesh sizes.

The study shows a not yet converged solution by changing the mesh from 3 mm to 2 mm, but with a calculation time of approximately 8 hours, the solution is assumed converged at the mesh size of 2 mm x 2 mm x 12 pc. The reason for the non-converged solution is considered to be due to the first order elements used in the analyses as they require a relatively fine mesh compared with second order elements.

By studying the solutions from the different analyses, a difference is noticed regarding damaged elements. The two analyses with coarsest mesh sizes have no damaged elements, but the three analyses with finer meshes all have damaged elements. Figure 43 illustrates the deformed geometry from the analysis with mesh size 2x2 mm. It is evident that the pipe is severely damaged, both inside and outside. In reality, the damaged material would still be present without load bearing capacity, but to better illustrate the actual damage, the elements are removed in Figure 43.

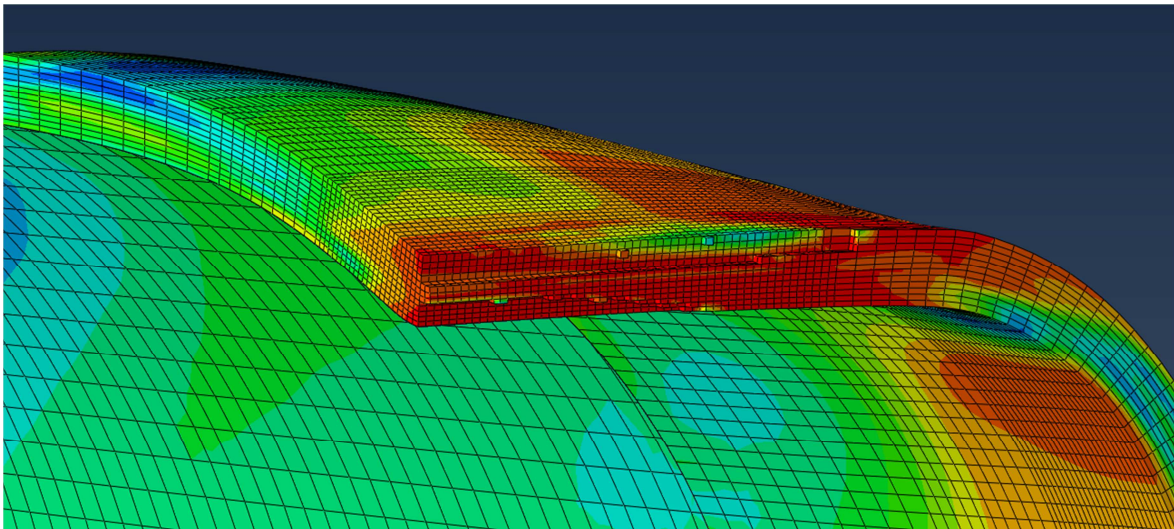


Figure 43: The solution for mesh size 2 mm x 2 mm x 12 pc. shows severe damage around the impact area.

Preliminary Conclusions

Due to limitations in computer capacity the solution is assumed as converged at a mesh size of 2 mm x 2 mm x 12 pc. However, a calculation time of 8 hours is not acceptable considering the desired parameter study which involves a large number of analyses. Thus, several optimization options are discussed in section 7.3.4.

The damaged elements in the analyses indicate that the damage and failure model is implemented and perform as intended.

7.3.2. Strain Rate Dependency

To determine whether the analyses are strain rate dependent, the material model is updated to be rate dependent by using the Cowper-Symonds relation, ref. /24/:

$$\frac{\sigma_1}{\sigma_0} = 1 + \left(\frac{\dot{\epsilon}}{D}\right)^{\frac{1}{q}} \quad (7.1)$$

where

σ_0	static yield stress
σ_1	dynamic rate dependent yield stress
$\dot{\epsilon}$	strain rate
D, q	material constants

As no test data is available the values $D=40 \text{ s}^{-1}$ and $q=5$ is used as commonly applied for mild steel, ref. /25/. The rate dependency is implemented in the material model by the scaling function as described in section 4.2, and two simulations are carried out in Abaqus, both with and without strain rate dependence. The two analyses are made with relatively coarse mesh as the focus is on the difference in using strain rate dependency. The contact force-displacement curves for the two analyses are plotted in Figure 44.

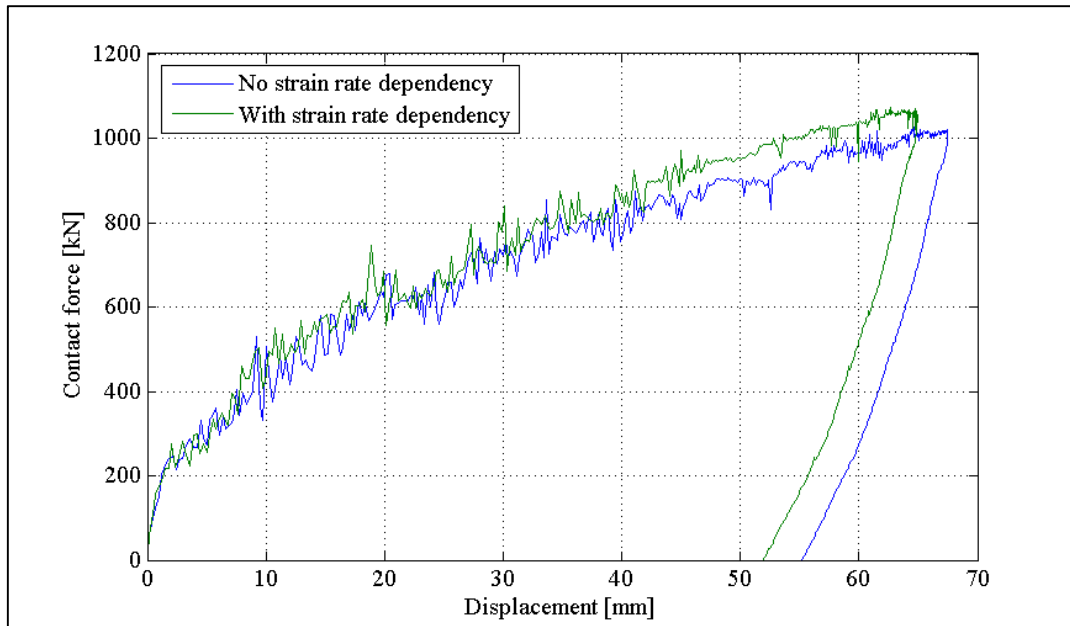


Figure 44: Contact force-displacement curves for analyses with and without strain rate dependency.

The effect of the strain rate dependency is distinct, as the deformation is smaller and the contact force larger for the analysis with rate dependency. This is due to an increase in the material strength for the rate dependent analysis which clearly indicates that strain rates are non-negligible. Thus, strain rate dependency is implemented in the material models for

both carbon steel and CRA for further analyses. Though, it should be noted that the rest of the analyses in this pre-study are carried out without strain rate dependent material if not noticed otherwise. The Cowper-Symonds material parameters for the CRA are taken as $D=100 \text{ s}^{-1}$ and $q=10$, ref. /25/, and both curves are plotted in Figure 45.

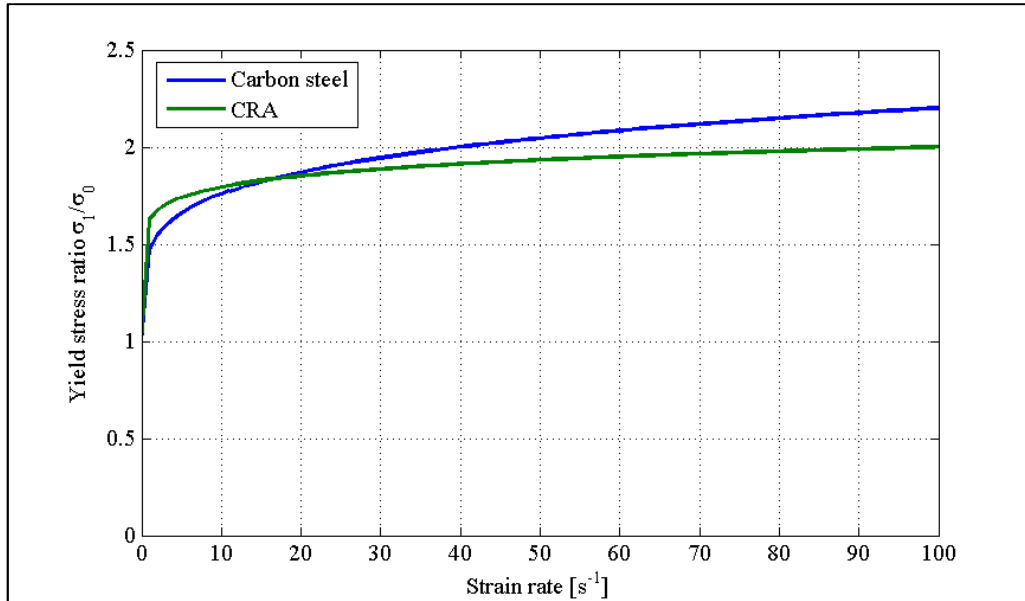


Figure 45: The Cowper-Symonds relation for carbon steel and CRA.

7.3.3. Studying the Source of Contact Force Excitations

As observed during the model verification, section 7.2, the contact force is exposed to excitations as it increases. However, studying the contact force-displacement curves from the convergence study; see Figure 42, it is evident that the excitations decrease as the mesh density increases. This indicates that the excitations are due to variations of the contact area as a result of mesh interaction between pipe and indenter. Thus, an analysis is carried out with a finer meshed indenter. The output frequency is also increased for this analysis to ensure that all “noise” will be evident, and the result is plotted in Figure 46. Most of the observed larger excitations are removed which confirms that they are mesh related. Though, some excitations still remains, but they are judged to be elastic excitations in the pipe as the same excitations are present in the test pipe from section 7.2, Figure 40.

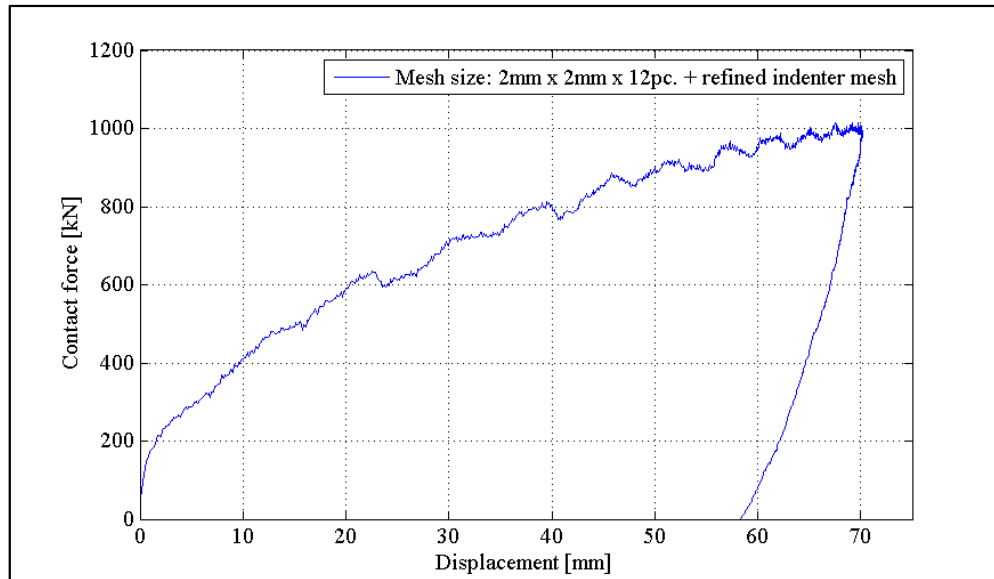


Figure 46: Contact force-displacement curve from the analysis with refined indenter mesh.

7.3.4. Model Optimization

With a calculation time of approximately 8 hours a study is made to optimize the model with respect to computational costs without noticeable deviation in the contact force-displacement relation. Three optimization options are discussed and put to the test in this section.

Mass Scaling

The total calculation time of an analysis in Abaqus/Explicit depends on the stable time increment, ref. /13/. The stable time increment Δt is approximated from the smallest element dimension in the model L_{min} and the dilatational wave speed C_d :

$$\Delta t \approx \frac{L_{min}}{C_d} \quad (7.2)$$

The dilatational wave speed is given by:

$$C_d = \sqrt{\frac{\lambda + 2\mu}{\rho}} \quad (7.3)$$

Where λ and μ are Lamé's constants which are defined in terms of Young's modulus E and Poisson's ratio ν :

$$\lambda = \frac{E \cdot \nu}{(1 + \nu)(1 - 2\nu)} \quad (7.4)$$

$$\mu = \frac{E}{2(1 + \nu)} \quad (7.5)$$

The dilatational wave speed is the speed at which stresses propagate through the material equal to the speed of sound through the material, ref. /26/.

Studying eq. 7.2 and 7.3 it is clear that the stable time increment is directly related to the density ρ . By increasing the density the dilatational wave speed is lowered resulting in a larger stable time increment, which is the methodology used in mass scaling. As the stable time increment relates to the smallest element dimension; see eq. 7.2, it is proposed to only scale the mass of the smallest elements in the model, corresponding to the refined mesh in the contact region, ref. /13/. However, tests shows the necessity of scaling the full solid element section of the model marked with red colour in Figure 47. The reason for this is that the other elements in the solid section becomes controlling for the stable time increment as the smallest elements are mass scaled.

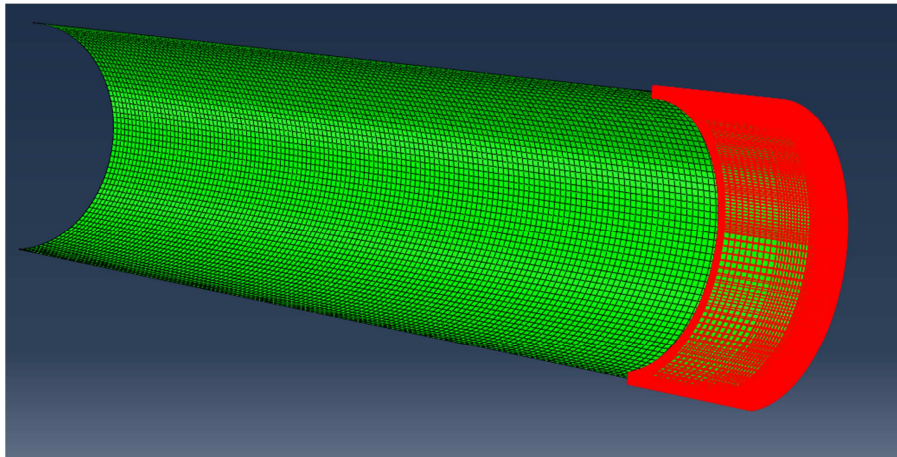


Figure 47: Mass scaling is defined for the full solid section of the model marked with red colour.

Mass scaling is defined by a scaling factor f , which directly scales the density of the selected elements. Scaling factors of 3 and 10 is used and the results of the analyses are plotted in Figure 48. It is evident that the mass scaling introduces different dynamic responses, which is not surprising taking the increased mass of the scaled part into account. As the stable time increment increases with a factor of approximately the square root of f , giving an increase of 1.73 times the stable time increment for $f=3$, this solution is judged as not applicable for this type of geometry. If mass scaling is to be used with efficiency, the model must have a small region with small elements surrounded by much larger elements, or the analysis must be nearly quasi-static to prevent the scaled mass having any or little effect.

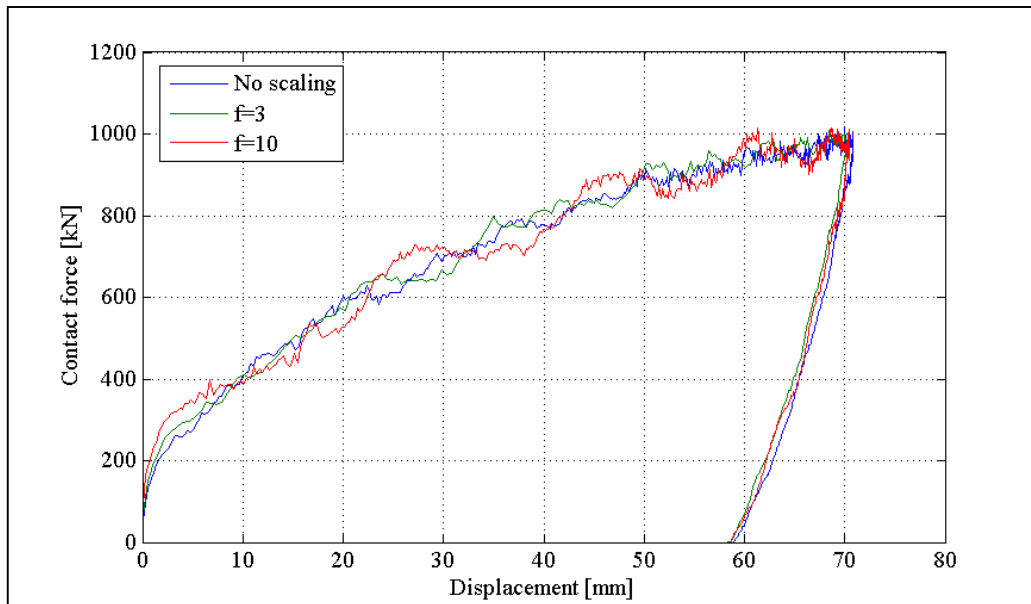


Figure 48: Results from analyses with mass scaling factors of 3 and 10, compared with an analysis without mass scaling.

Multiple Processors

Another option is to use multiple processors, but this option induces certain limitations when analysing in Abaqus/Explicit. Features such as Kinematic constraints and contact pairs cannot be split across domains, ref. /13/. Furthermore, splitting the analysis could affect the consistency of the result. Thus, two analyses was carried out, one with a lined pipe and one with a clad pipe. The results were that the calculation time was reduced with approximately 10-20%, and small deviations were observed in the solution compared with an analyses solved using one processor. Though, the deviations in the solutions were below 1%, it is decided not to use multiple processors taking the relatively small reductions of calculation time into account. The fact that these analyses show some deviations in the solutions also supports this decision, as these deviations could be larger at different pipe geometries.

Model Variable Reduction

The last option studied is to reduce calculation time by reducing the number of variables in the model. Thus, the solid part is reduced to represent only half the circumference of the pipe as illustrated in Figure 49. Furthermore, the length of the pipe is shortened to represent a 2 m pipe instead of the initial 3 m, and the mesh size of the shell elements are increased from 10 mm to 20 mm.

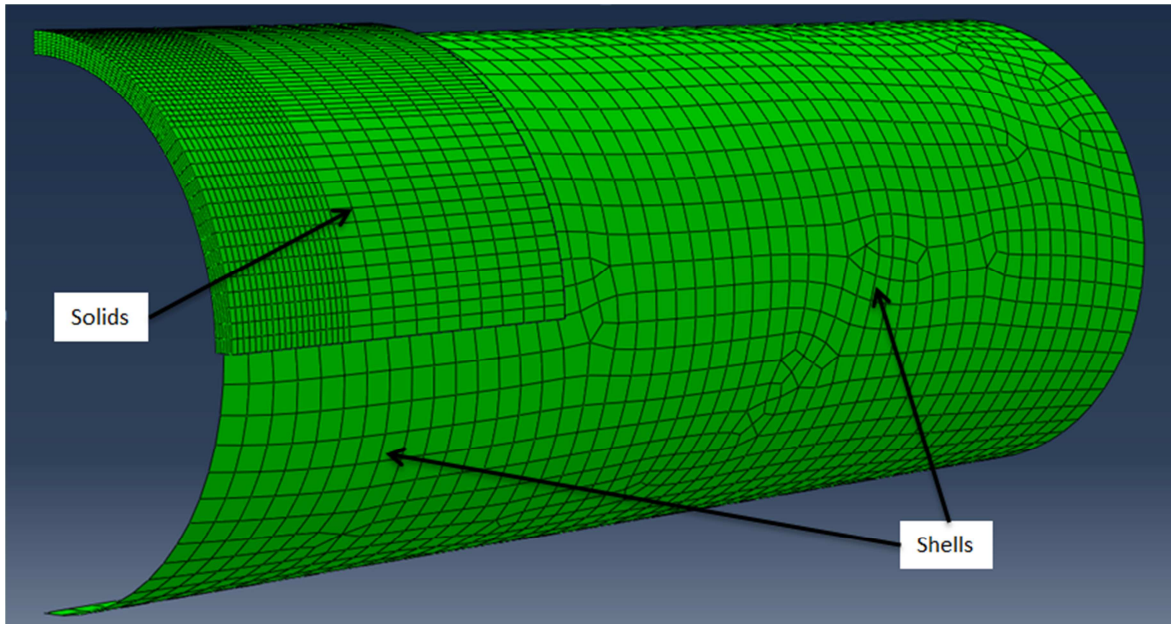


Figure 49: The solid part is reduced to represent half only half the circumference and the length of the pipe is reduced from 3 m to 2 m with a coarser mesh for the shell elements.

The contact force-displacement curve from the analysis is compared with the result from the initial geometry in Figure 50. It should be noted that strain rate dependency is implemented in the material model for these analyses. By comparing the two curves, the reduced model shows a larger maximum contact force while the indentation of the pipe is smaller, which could indicate that the reduction has slightly stiffened the model. However, the calculation costs are reduced by approximately 80% giving a total calculation time of 90 minutes.

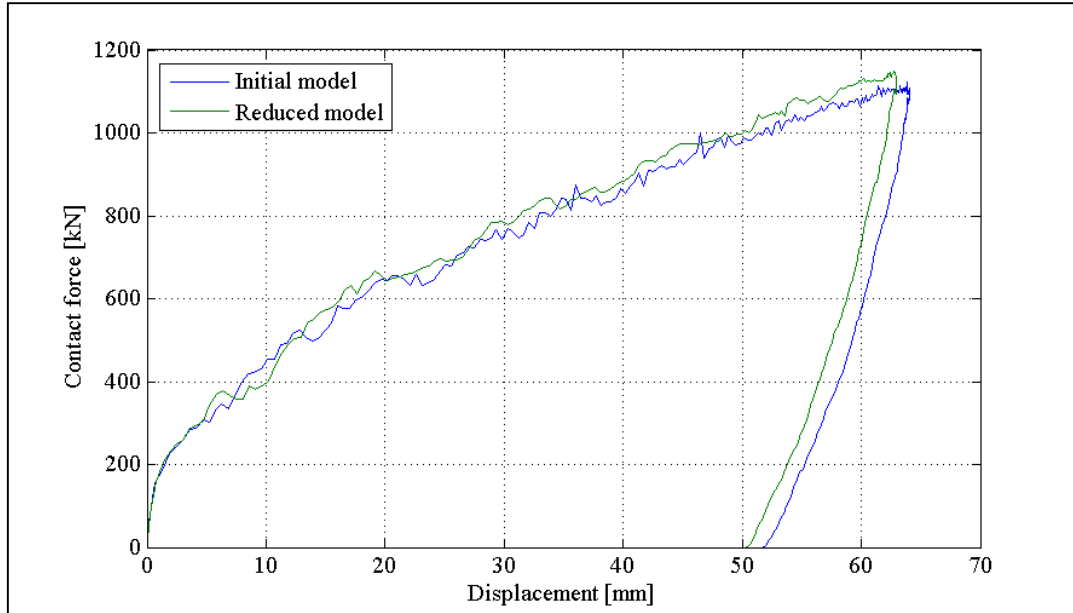


Figure 50: Output from the reduced model is compared with results from the initial model.

Preliminary Conclusions

None of the above described optimization options are found to be ideal with respect to either the consistency of the results or the reduction of the computational costs. Though, the scope of the project is to study the difference between conventional pipes and clad or lined pipes with different diameters and D/t relations, which results in a relatively high number of analyses. Thus, it is decided to proceed with the reduced model as illustrated in Figure 49, as the reduction of calculation time is largest for this option. The fact that the reduced model induces some inaccuracies and non-conservative results with respect to the indentation of the pipe will be taken into account when interpreting the results in section 9. Additionally, analyses with bare steel pipes will be carried out with the same reduced model to ensure comparable results.

7.4. Conclusions

The initial model with symmetry and a combination of shell and solid first order elements is verified by comparing the contact force-displacement curve with test results. Thus, this concept is used in all subsequent analyses in this project.

During the convergence study it becomes evident that this type of impact analysis requires a fine mesh as the solution fails to converge between mesh sizes 3 mm and 2 mm. The calculation time of the analysis with 2 mm mesh is approximately 8 hours leading to an optimization study, where different optimization options are discussed and put to the test. The solution selected is a reduced model with the solid section representing half the circumference of the pipe. The result is a calculation time of approximately 90 minutes, but the reduced model induces some inaccurate results which should be accounted for when interpreting the results in section 9.

The strain rate dependency of the model is put to the test with a distinct difference in contact force-displacement curves. Thus, strain rate dependency is implemented in the material models by the Cowper-Symonds relation; see Figure 45.

During the pre-study severe damage is observed around the impact area verifying the implementation of the damage and failure model. Though, it should be noted that subsequent implementation of the strain rate dependency could prevent or reduce damage of the pipe.

The mass and velocity of the indenter, i.e. the maximum specified by DNV-RP-F111, ref. /1/, of 12140 kg and 2.8 m/s respectively, is found to be suitable for further studies, as no excessive deformations are noted during the pre-study.

Generally, the model is considered as verified and optimized to give the best possible results taking the relatively large number of analyses into account.

8. Implementation of Clad and Liner in the FE-model

With a verified and optimized bare steel pipe model, clad and liner are implemented in this section. As outlined in section 3, the thickness of clad and liner is set to 3 mm for all analyses. Furthermore, it is decided to model clad and liner with a combination of shell and solid elements, i.e. the part of the internal pipe near the impact zone is modelled with solid elements as the case for the outer pipe.

The following sections describe the modelling considerations while implementing the cladding and liner, including difficulties occurred during the implementation.

8.1. Clad Pipe Modelling Considerations

As described in section 3.2, the internal layer of CRA in clad pipes is metallurgical bonded to the backing material. This means that full contact must be defined between cladding and backing material during the analyses. The mesh tie constraint available in Abaqus is appropriate for this application, as it ties the mesh from the two materials together; see section 4.3 for further explanation of the mesh tie constraint. However, the use of the mesh tie constraint between clad and backing produces some modelling difficulties as described below.

As the pipe geometry is modelled with a combination of shell and solid elements constrained with shell-to-solid coupling constrains, the implementation of the mesh tie constraint over-constrains the nodes involved in both constrains. Over-constraining appears when multiple constraints are applied to the same degree of freedom, ref. /13/. The result is that the shell-to-solid coupling constrains are partly suppressed during the solution process creating a slip, as illustrated in Figure 51 where the thickness of the shell elements is included.

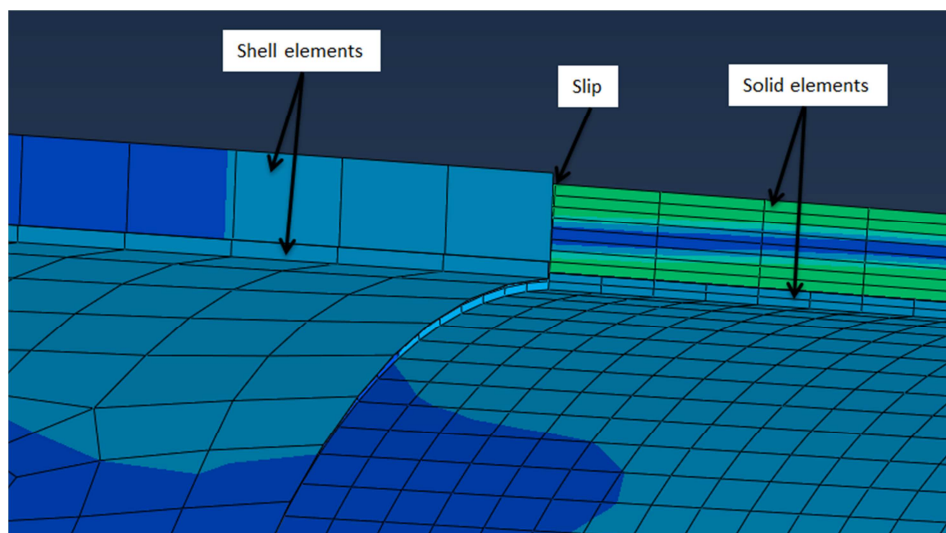


Figure 51: The over-constrained model shows a slip in the shell-to-solid coupling constraints. The thickness of shell elements is included.

The solution to the over-constrained model is to remove the mesh tie constraints at the nodes where shell-to-solid coupling constraints are present. Figure 52 illustrates the pipe solid part with the surrounding shells to the left with the same geometry illustrated as a wireframe in the right picture. Here the mesh tie constraints are represented by the purple lines, and it is evident that the nodes containing the shell-to-solid coupling is not included in the mesh tie constraints which solves the problem with over-constrained nodes.

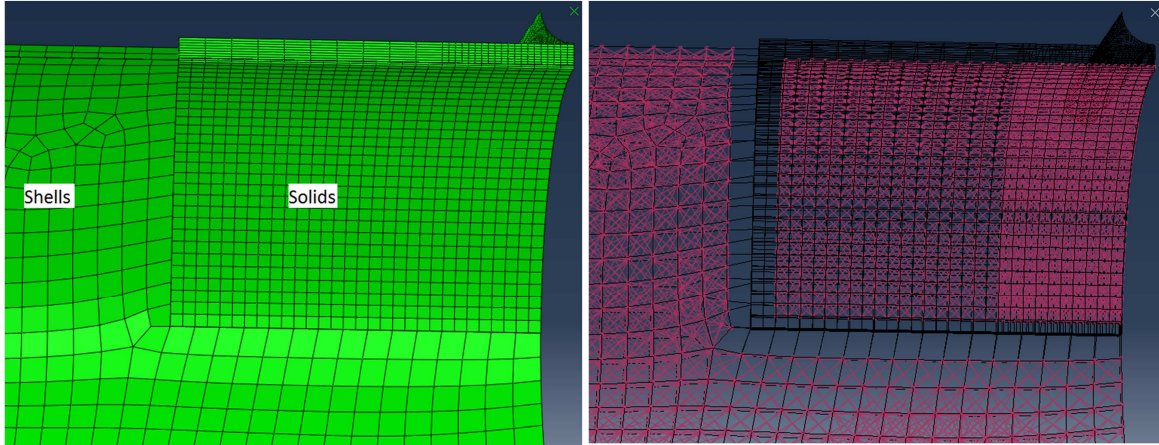


Figure 52: Left picture shows the solid part of the pipe surrounded by shells. Right picture shows the same geometry as a wireframe with the mesh tie constraints represented by purple lines.

As the problem with over-constrained nodes is solved another error is created. The full contact between clad and backing material is not present at the intersection between shell and solid elements. However, this error is considered negligible as it only exists in a small area and is located at a considerable distance from the impact zone. To further support this choice, all later performed analyses with clad pipes is examined for possible delamination between clad and backing without any noticeable defects.

8.2. Lined Pipe Modelling Considerations

The lined pipes are manufactured with a mechanical bond between liner and backing material as described in section 3.3. The contact between liner and backing is defined with a tangential friction coefficient of 0.4. Furthermore, residual stresses of -150 MPa and -20 MPa are defined as the liner hoop $\sigma_{liner,hoop}$ and axial $\sigma_{liner,axial}$ stresses respectively. The corresponding residual stresses of the outer pipe, $\sigma_{outer,hoop}$ and $\sigma_{outer,axial}$ are calculated to create equilibrium between liner and outer pipe as illustrated in Figure 53 and Figure 54. The residual stresses of the outer pipe are calculated from eq. 8.1 and 8.2.

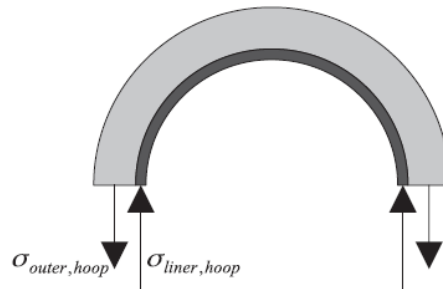


Figure 53: Hoop stress equilibrium between liner and outer pipe, ref. /11/.

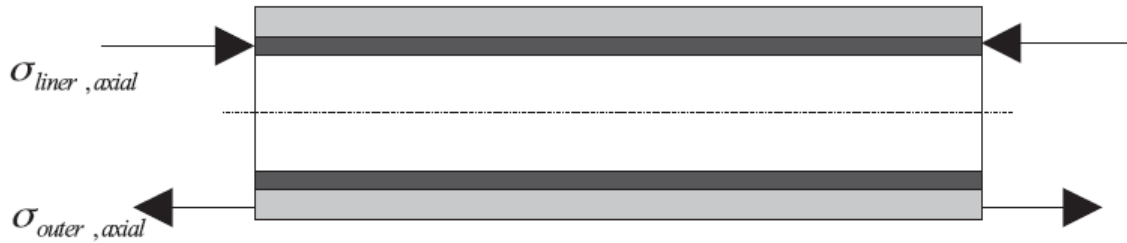


Figure 54: Axial stress equilibrium between liner and outer pipe, ref. /11/.

$$\sigma_{outer, hoop} = -\sigma_{liner, hoop} \cdot \frac{t_l}{t_b} \quad (8.1)$$

$$\sigma_{outer, axial} = -\sigma_{liner, axial} \cdot \frac{A_l}{A_b} \quad (8.2)$$

The hoop stress is calculated from the ratio between the wall thicknesses of liner and backing pipe, t_l and t_b , and the axial stress is calculated from the ratio between the cross sectional areas of the two pipes, A_l and A_b .

To implement the hoop and axial stresses in Abaqus, local material directions must be defined as illustrated for the pipe solid section in Figure 55, i.e. the local material directions are defined to follow the curvature of the pipe.

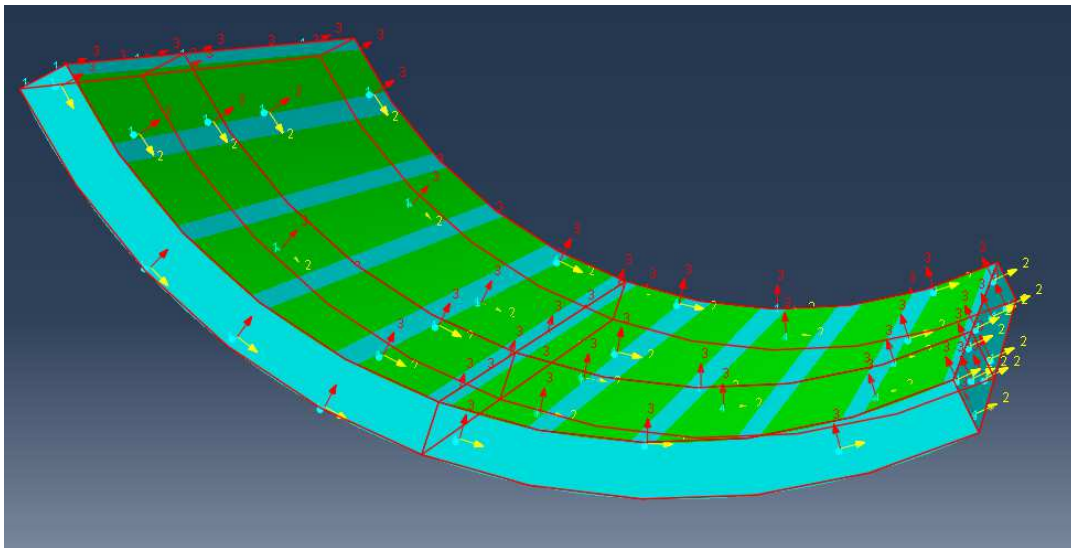


Figure 55: Local material directions defined to follow the curvature of the pipe.

To verify the implementation of the residual stresses, i.e. that the two pipes are in equilibrium, the stresses and deformations of the composed pipe is examined at the last increment before impact. The stresses are held against the entered values as described above, and the deformation of the pipe should be close to none if equilibrium is fulfilled. As an example, the deformations of the 16" $D/t=25$ lined pipe are plotted in Figure 56. The

result is a maximum deformation of approximately 0.2 mm which verifies that the pipe is in equilibrium from the start of the analysis. The relatively small deformation of 0.2 mm is judged to be due to the contact between liner and outer pipe, as the contact surfaces adjust to avoid any over-closure during the analysis.

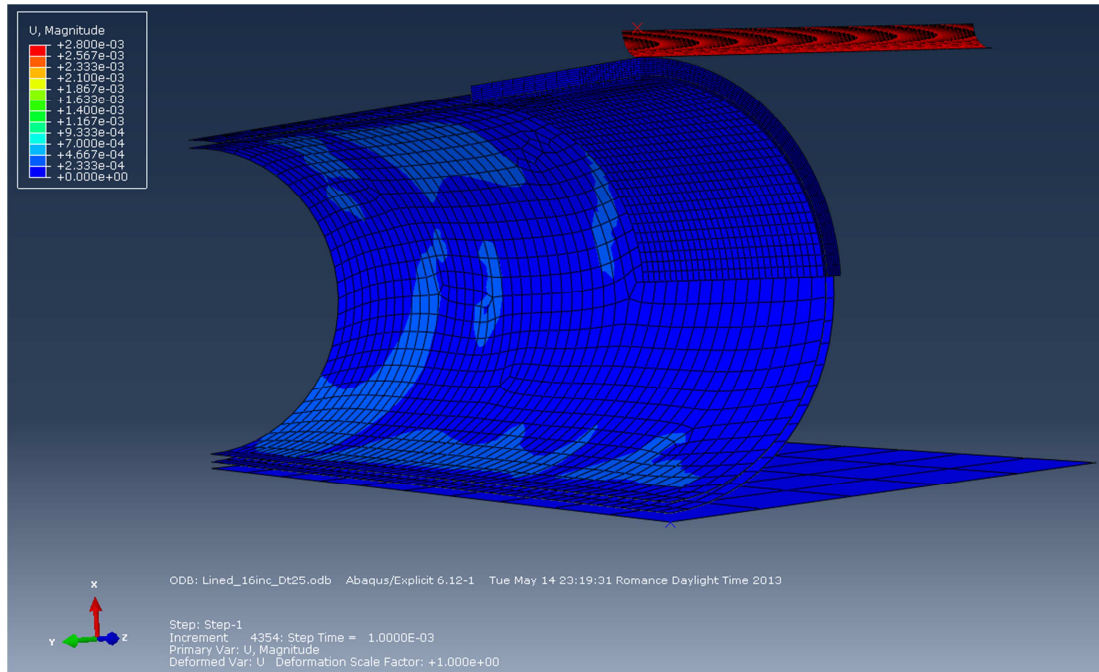


Figure 56: Deformations are plotted from the last frame before impact to verify the implementation of residual stresses.

8.3. Conclusions

The implementation of cladding using the mesh tie constraint induces over-constrained degrees of freedom DOF where the shell-to-solid coupling is present. The problem is solved by removing the mesh tie constraint at the DOF where the shell-to-solid coupling is active. Though, this solution creates another error as the metallurgic bond is removed, right at and around the intersection between shells and solids; see Figure 52. Thus, all performed clad pipe analyses must be examined for any delamination in this area.

The lined pipe residual stresses are implemented by defining local material directions following the curvature of the pipe. The residual stresses of the outer pipe are calculated to obtain equilibrium between liner and outer pipe. To verify that equilibrium is fulfilled, all lined pipe analyses must be examined at the last frame before impact, i.e. no excessive deformations or stress deviations must be present.

9. Trawl Gear Impact Simulations: Parameter Study, Evaluations of Analytical Solutions From DNV-RP-F111 and General Observations

With the FE-model calibrated and optimized as outlined in section 7, this section deals with the results of the FE-analyses. First, a parameter study is carried out to evaluate the influence of clad and liner on the plastic deformation of the pipe. Next, the analytical solutions stated by DNV-RP-F111, ref. /1/, are evaluated regarding the applicability for all types of pipes, including bare steel pipes. Furthermore, the contact force-displacement curves are studied and compared with the estimate given by DNV-RP-F111. Finally, general observations made during the parameter study are outlined, including problems with contact over-closure, time of impact and maximum strain rates observed during the analyses.

9.1. Parameter Study: The Influence of Clad and Liner on the Permanent Indentation of Different Pipe Dimensions

As described in section 2.3 and according to DNV-RP-F111, ref. /1/, the acceptance criteria for trawl gear impact is based on the permanent indentation of the pipe. Thus, a study is carried out to look at the differences in permanent indentation for clad and lined pipes compared with bare steel pipes at different pipe dimensions. Furthermore, the results are compared with the analytical solution given by DNV-RP-F111.

9.1.1. Pipe Specifications

Part of the scope for this project is to study pipes in the range of 12"-24" with D/t relations ranging from 15 to 40 with D being the outer pipe diameter and t the wall thickness; see section 1.1 for further clarification of the project scope. To limit the number of analyses, it is decided to study three different pipe dimensions and five D/t relations, namely 12", 16" and 24" pipes with D/t of 15, 20, 25, 30 and 40. The wall thicknesses calculated by the specified D/t are rounded to the nearest available dimension according to ASME, ref. /7/. The outer pipe dimensions used in the analyses are given in Table 11.

Table 11: Pipe dimensions used in the analyses with the wall thicknesses rounded to the nearest available dimension according to ASME, ref. /7/.

D		D/t				
		15	20	25	30	40
[inch]	[mm]	t [mm]	t [mm]	t [mm]	t [mm]	t [mm]
12"	323.8	21.44	15.88	12.7	11.13	7.92
16"	406.4	26.97	20.62	15.88	14.27	10.31
24"	610	39.67	30.18	24.61	20.62	15.88

The materials used in all analyses are DNV SMYS 415 and Alloy 316L for backing and clad/liner respectively; see section 3.4 for material properties. The thickness of the clad/liner are set to 3 mm for all analyses. The mass and velocity of the indenter are 12140 kg and 2.8 m/s respectively.

9.1.2. Parameter Study

Some uncertainties are present in the model due limitations in the mesh convergence and inaccuracies in reduction of the model as outlined in section 7.3. Thus, the analyses are carried out not only with clad and liner but also with bare steel pipes, as the scope is to look into the differences between clad/lined pipes and bare steel pipes. This means that three types of pipes are analysed with 15 different dimensions, giving a total of 45 analyses. The contact force-displacement curves for all analyses are found in Appendix 3.

The results of the analyses are plotted as plastic deformation of the pipe as a function of wall thickness, and Figure 57, Figure 58 and Figure 59 represents 12", 16" and 24" pipes respectively. Furthermore, the results are compared with DNV-RP-F111, eq. 3.9, i.e. eq. 9.1 in this report, which estimates the plastic deformation of the pipe H_{pc} as a function of maximum contact force $F_{sh,max}$, yield strength f_y , wall thickness t and diameter D :

$$H_{pc} = \left(\frac{F_{sh,max}}{5 \cdot f_y \cdot t^2} \right)^2 - \left(\frac{F_{sh,max} \sqrt{0.005 D}}{5 \cdot f_y \cdot t^2} \right) \quad (9.1)$$

where

$$F_{sh,max} = \left(\frac{75}{2} \cdot E_{loc} \cdot f_y^2 \cdot t^3 \right)^{\frac{1}{3}} \quad (9.2)$$

E_{loc} is the impact energy, i.e. the kinetic energy of the trawl gear given by:

$$E_{loc} = E_{kin} = \frac{1}{2} \cdot m \cdot v^2 = \frac{1}{2} \cdot 12140 \text{ kg} \cdot \left(2.8 \frac{\text{m}}{\text{s}} \right)^2 = 47588,8 \text{ J} \quad (9.3)$$

The yield strength used in eq. 9.1 and eq. 9.2 are calculated as $0.96 \cdot SMYS$ as it is assumed that the material do not fullfill suplimentary requirement U in DNV-OS-F101, ref. /4/; see section 2.3.

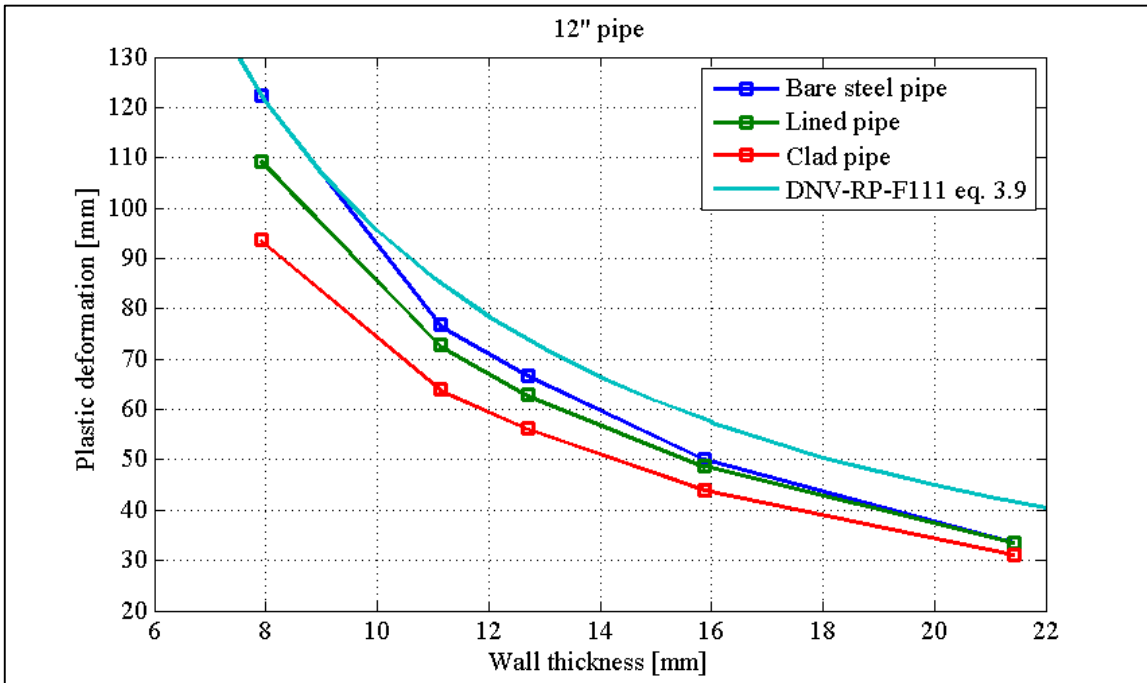


Figure 57: Plastic deformations of the 12'' pipes with the different wall thicknesses analysed. The FE results are compared with DNV-RP-F111, eq. 3.9.

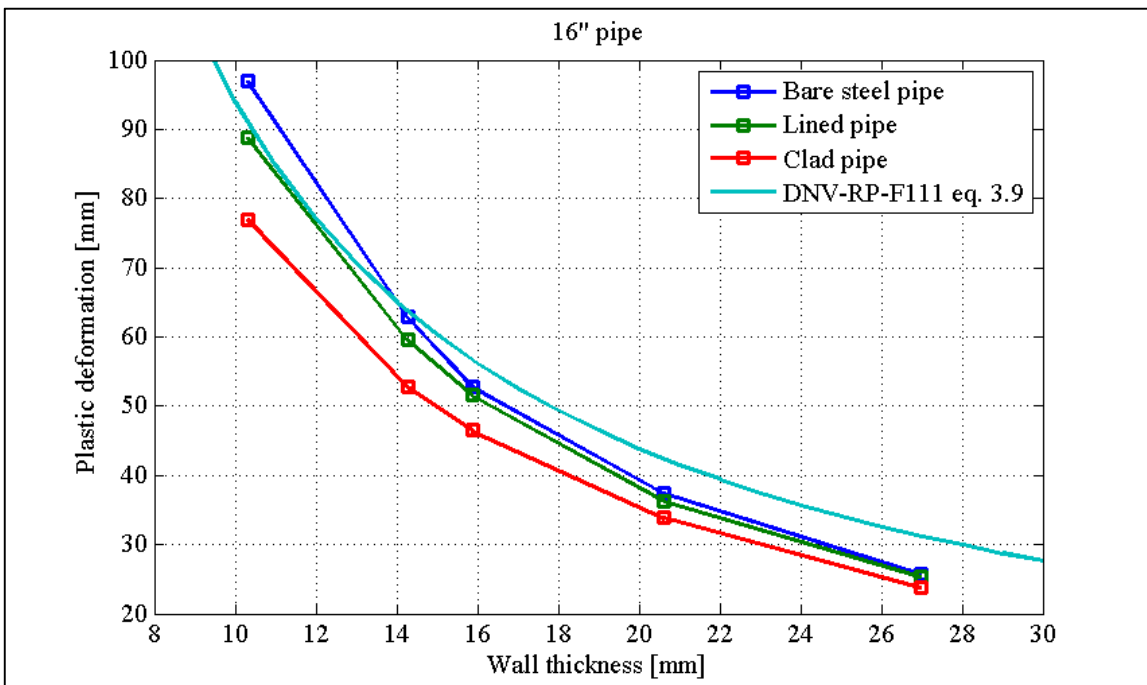


Figure 58: Plastic deformations of the 16'' pipes with the different wall thicknesses analysed. The FE results are compared with DNV-RP-F111, eq. 3.9.

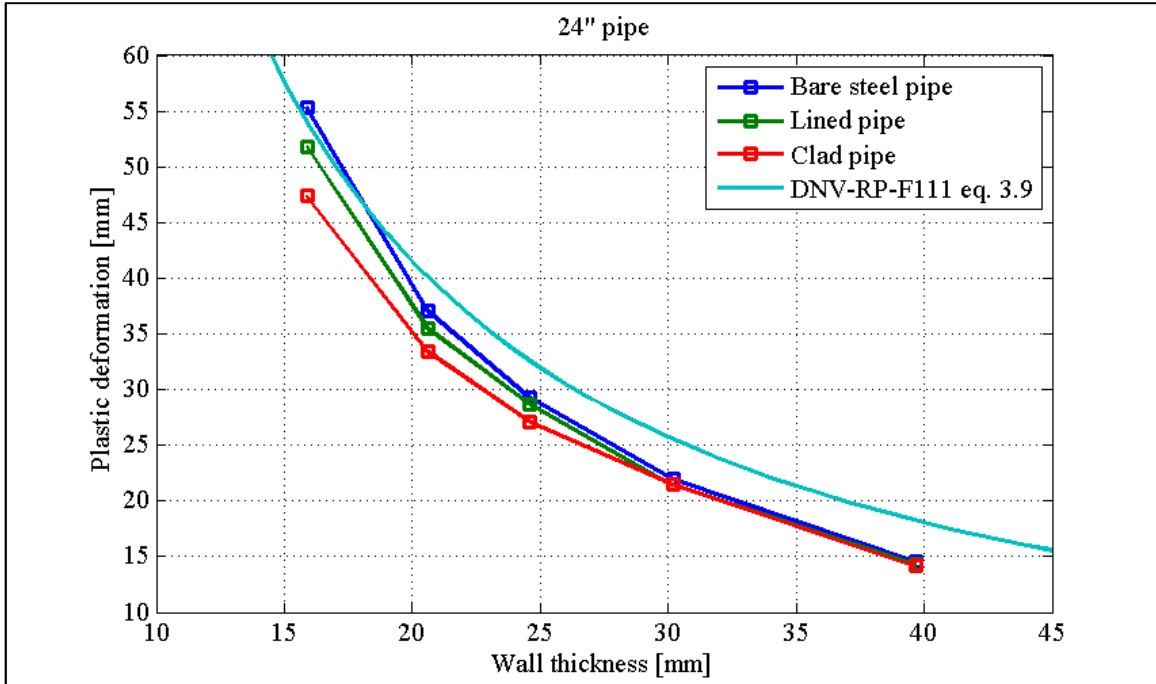


Figure 59: Plastic deformations of the 24" pipes with the different wall thicknesses analysed. The FE results are compared with DNV-RP-F111, eq. 3.9.

By comparing the results it is clear that both clad and liner contributes to the structural integrity of the pipes with respect to trawl gear impact, as the plastic deformations is smaller for these pipes compared with bare steel pipes. Though, it is noted that the plastic deformation is smallest for clad pipes at all analysed pipe dimensions. Furthermore, the magnitude of the plastic deformation, for the three different types of pipes, is converging as the wall thickness increases, especially for the 24" pipes.

While comparing the FE results with DNV-RP-F111, eq. 3.9, it is observed that the bare pipes with $D/t=40$ all shows larger deformations than estimated by eq. 9.1. Thus, the following section evaluates the proposed analytical solutions in DNV-RP-F111.

9.2. Evaluation of DNV-RP-F111 Analytical Solution

The following sections evaluate the analytical solution stated by DNV-RP-F111. Initially, the estimate of plastic deformation and maximum contact force, are evaluated with respect to bare steel pipes. Subsequently, the analytical solutions are held against FE results from clad pipes with suggestions of changes in the analytical solution to estimate the plastic deformation of clad pipes.

9.2.1. Bare Steel Pipes

As outlined in section 9.1, DNV-RP-F111, eq. 3.9, i.e. eq. 9.4 in this report, shows non-conservative results regarding bare pipes with $D/t=40$. Eq. 9.4 estimates the plastic deformation of the pipe on the basis of the maximum contact force, eq. 9.5. For further explanation see section 2.3 and 9.1.

$$H_{pc} = \left(\frac{F_{sh,max}}{5 \cdot f_y \cdot t^{\frac{3}{2}}} \right)^2 - \left(\frac{F_{sh,max} \sqrt{0.005 D}}{5 \cdot f_y \cdot t^{\frac{3}{2}}} \right) \quad (9.4)$$

$$F_{sh,max} = \left(\frac{75}{2} \cdot E_{loc} \cdot f_y^2 \cdot t^3 \right)^{\frac{1}{3}} \quad (9.5)$$

To evaluate eq. 9.5, the maximum contact forces from the performed analyses are plotted in Figure 60, Figure 61 and Figure 62, representing 12", 16" and 24" pipes respectively. The FE results are compared with DNV-RP-F111, eq. 3.10, i.e. eq. 9.5 in this report.

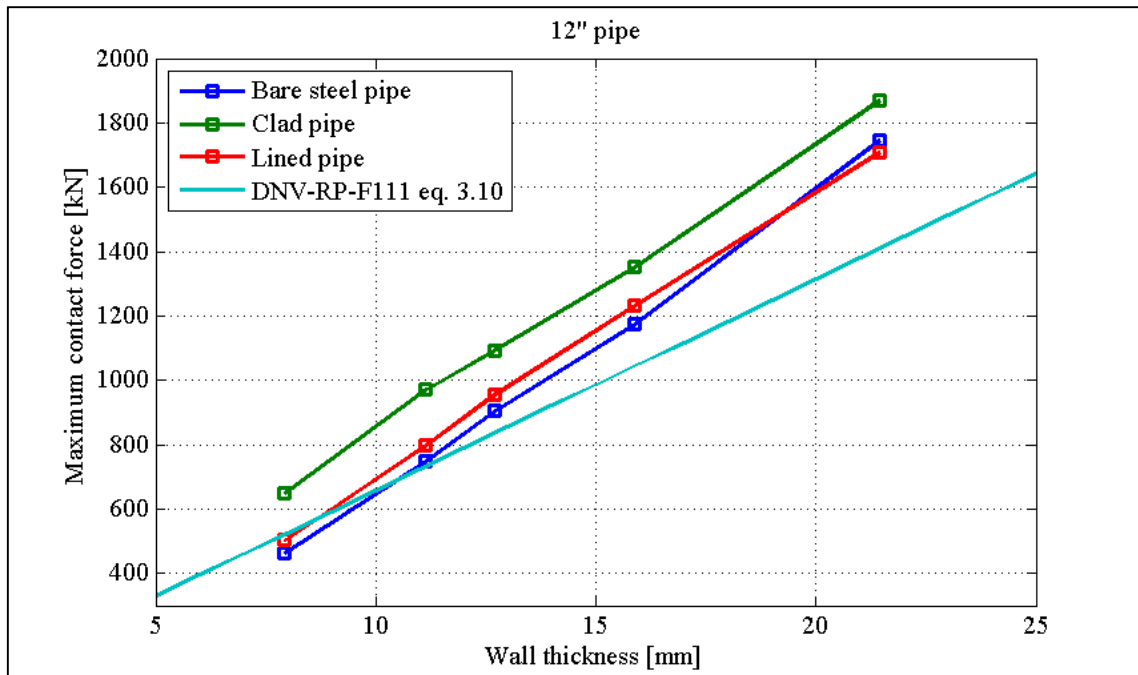


Figure 60: Maximum contact force for the 12" pipes with the different wall thicknesses analysed. The FE results are compared with DNV-RP-F111, eq. 3.10.

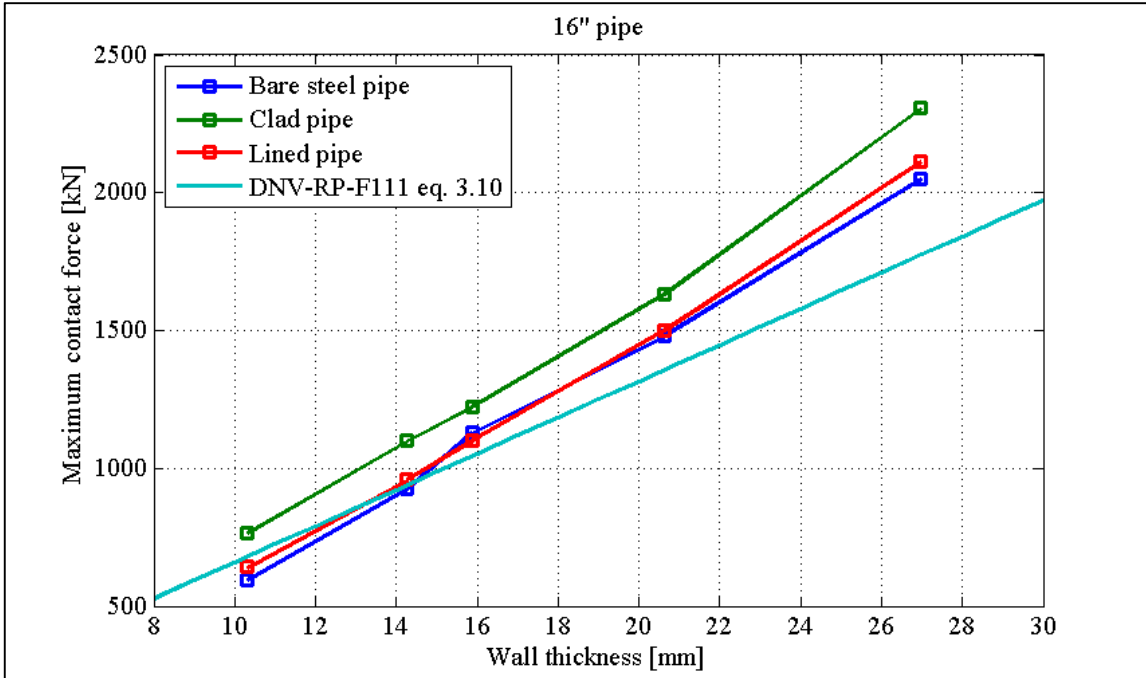


Figure 61: Maximum contact force for the 16" pipes with the different wall thicknesses analysed. The FE results are compared with DNV-RP-F111, eq. 3.10.

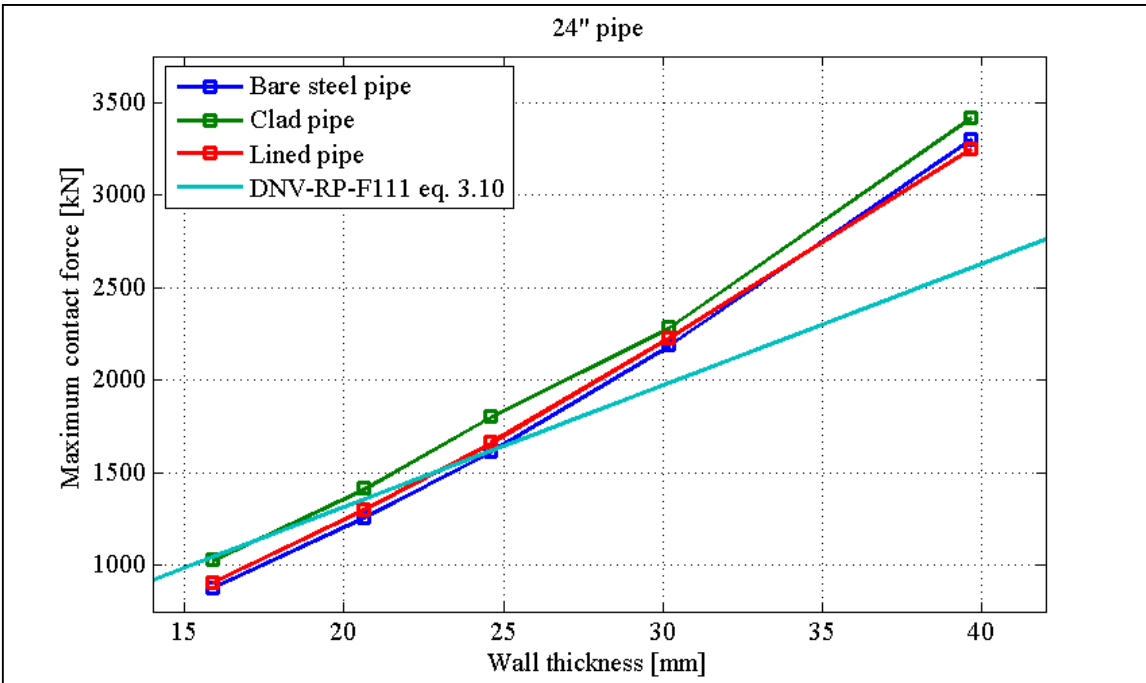


Figure 62: Maximum contact force for the 24" pipes with the different wall thicknesses analysed. The FE results are compared with DNV-RP-F111, eq. 3.10.

By evaluating Figure 60 - Figure 62 it is evident that eq. 9.5 under-predicts the maximum contact force for the larger wall thicknesses. This is somewhat surprising as eq. 9.4 over predicts the plastic deformation for these same wall thicknesses as concluded in section 9.1. Furthermore, it is noted from Figure 60 - Figure 62 that the maximum contact force depends on the pipe diameter. This becomes clear as the wall thickness of 15.88 mm is

analysed for all three pipe diameters, and the results shows a considerable difference in maximum contact force as illustrated in Figure 63. However, this is not surprising as the pipes with smaller diameters are more compact compared with larger diameters.

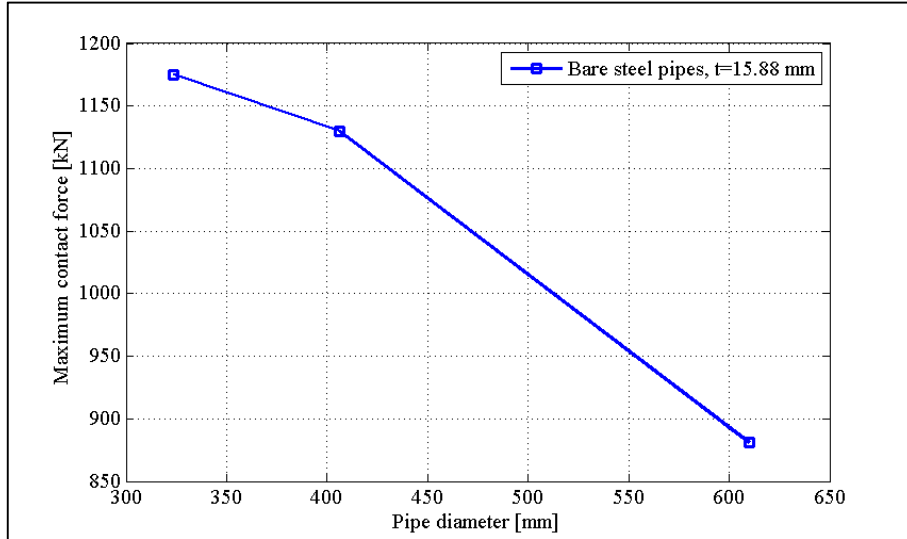


Figure 63: Maximum contact force for different diameters but with the same wall thickness, $t=15.88$ mm.

Following the above evaluation it is recommended to revise eq. 9.5 to include the pipe diameter as the maximum contact force is dependent of the diameter as illustrated in Figure 63. Furthermore, the general composition of eq. 9.5 is considered as non-conservative for larger wall thicknesses, i.e. D/t relations smaller than 20-25 depending on the pipe diameter.

As the above recommended revisions of eq. 9.5 would cause larger estimations of the maximum contact force for some wall thicknesses, the influence of the maximum contact force in eq. 9.4 is studied further. This is done by plotting the plastic deformation calculated by eq. 9.4 as a function of the maximum contact force; see Figure 64.

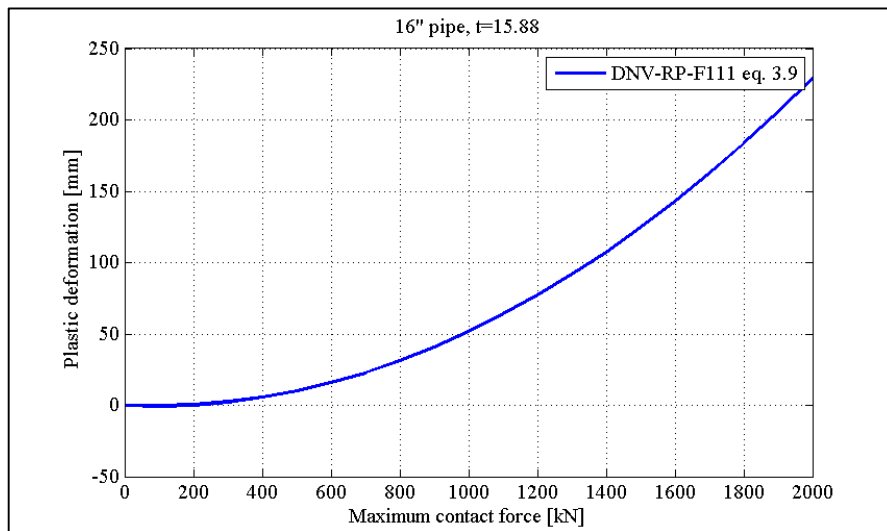


Figure 64: Plastic deformation calculated by eq. 9.4 as a function of Maximum contact force.

It is clear that for a 16" pipe with $t=15.88$ mm, that plastic deformation increases as the maximum contact force increases, which is assumed to be the case for all relevant pipe dimension. Knowing this while looking at the proposed revision of eq. 9.5, which causes larger estimates of the maximum contact force for large values of t , it is evident that this would increase the plastic deformations estimated by eq. 9.4 for the same values of t . Though, eq. 9.4 already shows conservative results for these large values of t , which indicates that eq. 9.4 would become over-conservative. On the other hand, it is concluded in section 9.1 that eq. 9.4 shows non-conservative results for low values of t ; see Figure 57 - Figure 59. Thus, it is generally recommended to revise both eq. 9.5 and 9.4 in that order.

The above recommended revisions of eq. 9.4 and 9.5 are evaluated on the basis of FE results for bare steel pipes. Regarding lined pipes it is recommended to treat them as bare steel pipes when estimating that plastic deformation.

9.2.2. Clad Pipes

On the contrary, when calculating the plastic deformation for clad pipes, it could be a solution to increase the wall thickness in eq. 9.4 to include the clad material as the two materials are metallurgical bonded. Furthermore, the lower yield strength of the cladding material should be taken into account. This could be done by calculating a weighted average yield strength $f_{y,mean}$ given by:

$$f_{y,mean} = \frac{f_{y,backing} \cdot t_{backing} + f_{y,clad} \cdot t_{clad}}{t_{tot}} \quad (9.6)$$

where

$f_{y,backing}$	yield strength of backing material
$f_{y,clad}$	yield strength of clad material
$t_{backing}$	wall thickness of backing material
t_{clad}	wall thickness of backing material
t_{tot}	total wall thickness of the composed pipe

Thereby, eq. 9.4 is changed to the following for clad pipes:

$$H_{pc,clad} = \left(\frac{F_{sh,max}}{5 \cdot f_{y,mean} \cdot t_{tot}^{\frac{3}{2}}} \right)^2 - \left(\frac{F_{sh,max} \sqrt{0.005 D}}{5 \cdot f_{y,mean} \cdot t_{tot}^{\frac{3}{2}}} \right) \quad (9.7)$$

To evaluate the above calibrated expression it is plotted in Figure 65 and compared with both FE results for clad pipes and the existing solution. It should be noted that the clad pipe FE results (blue) are plotted as a function of the total wall thickness t_{tot} .

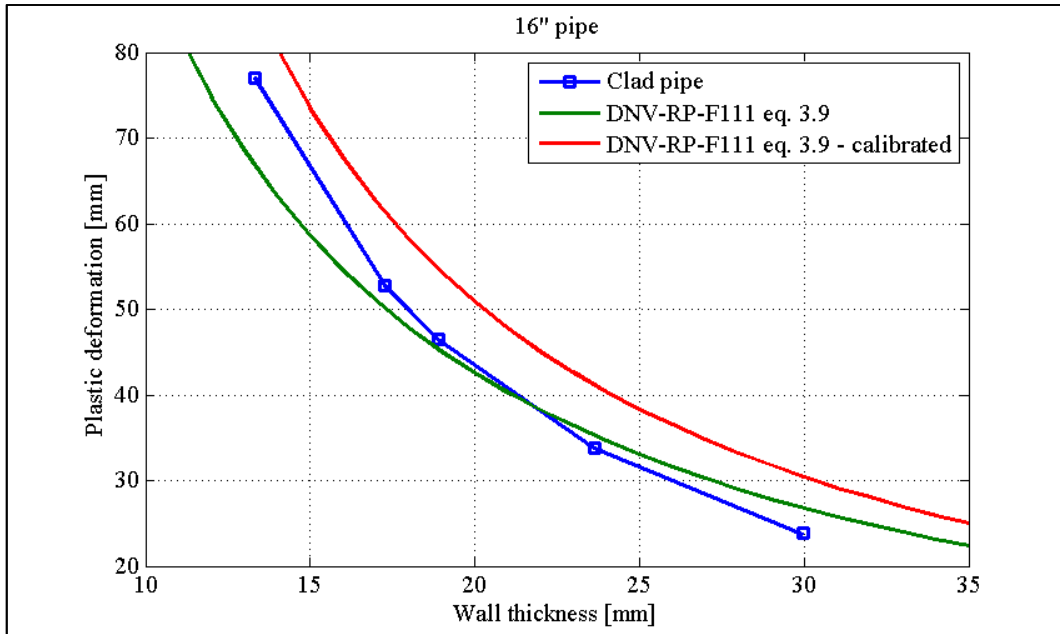


Figure 65: The existing expression (green) and the calibrated expression (red) are compared with FE results for 16" clad pipes (blue).

The calibrated expression shows conservative results as the plastic deformation is over estimated compared with FE results. Though, it should be noted that the proposed revision of the maximum contact force, eq. 9.5, is not accounted for in the above calibrated expression. It should only be seen as a proposal to possible solutions on how to treat clad pipes in the future.

9.3. Studying Contact Force-Displacement Curves

The contact force-displacement curves are not directly related to the acceptance criteria as the permanent indentation of the pipe is. Though, they bring a good understanding of the differences in the three different types of pipes analysed. DNV-RP-F111, eq. 3.5, i.e. eq. 9.8 in this report also gives a so-called conservative estimate of the contact force-displacement relationship, ref. /1/:

$$F_{sh} = 5 \cdot f_y \cdot t^{\frac{3}{2}} \cdot H_t^{\frac{1}{2}} \quad (9.8)$$

where F_{sh} is the contact force and H_t is the deformation of the pipe. It should be noted that by isolating H_t in eq. 9.8 one get the first term of eq. 9.4.

Eq. 9.8 is described in DNV-RP-F111 as a conservative estimate of the relation between contact force and deformation of the pipe, but it is not clearly stated in what sense the expression is conservative. However, two pipe dimensions are picked to compare the different types of pipes analysed, namely 12" pipes with $D/t=20$ and 24" pipes with $D/t=40$. The reason for picking these two dimensions is that the wall thickness is the same for both

pipes, i.e. 15.88 mm. The contact force-displacement curves are plotted in Figure 66 and Figure 67 with the analytical solution stated by DNV-RP-F111, i.e. eq. 9.8. All contact force-displacement curves are plotted in Appendix 3.

By comparing the bare steel pipes with eq. 9.8 the difference is evident between the two pipe dimensions. Regarding the 12” pipe, eq. 9.8 under-predicts the contact force, while the opposite is the case for the 24” pipe. Again, this indicates that impact calculations are highly dependent on the pipe diameter which further supports the observations made in section 9.2.

Whether eq. 9.8 is conservative for either the 12” or the 24” pipe is highly dependent of the application. An under-prediction of the contact force-displacement curve as the case for the 12” pipes could induce a larger deformation of the pipe if the energy absorbed during impact is assumed to be constant, i.e. the estimate is conservative with respect to the acceptance criteria. The assumption of constant energy absorption is supported by comparing the contact force-displacement curves in Figure 66 or Figure 67, where the energy absorbed by deformation is equal to the area under the curves.

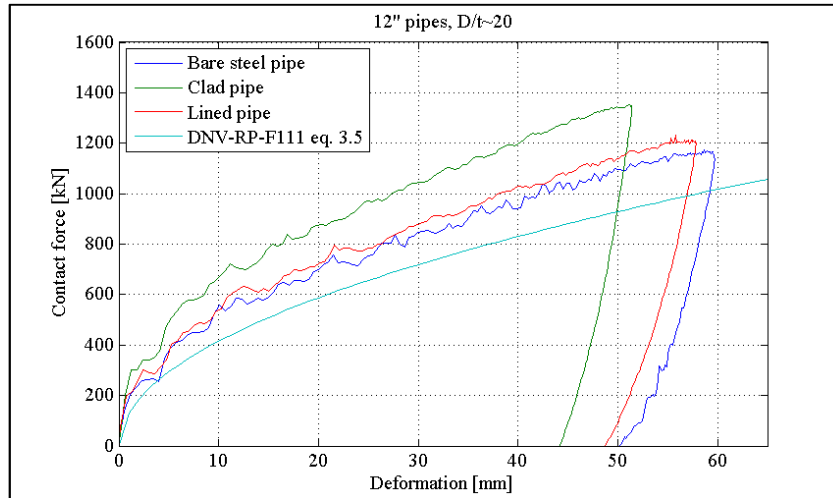


Figure 66: Contact force-displacement curves for 12”, $D/t=20$, FE-analyses compared with DNV-RP-F111 eq. 3.5.

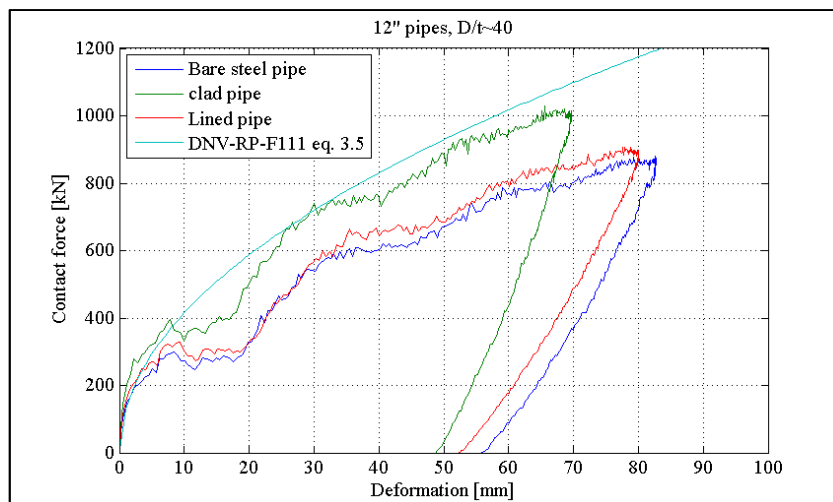


Figure 67: Contact force-displacement curves for 24”, $D/t=40$, FE-analyses compared with DNV-RP-F111 eq. 3.5.

Another observation made is the excitations of the contact force for the 24” pipes. This is judged to be due to elastic vibrations in the pipe induced by the impact. Furthermore, the study of the contact force-displacements curves from the FE-analyses generally supports the observations made in section 9.1, regarding the influence of clad and liner on the indentation of the pipes during impact.

9.4. General Observations

General observations made during the parameter study are outlined in this section, including problems with contact over-closure, time of impact and maximum strain rates during the analyses.

9.4.1. Decoupling of $D/t=40$ Pipes

During the performed analyses an error was discovered as the shell-to-solid coupling of the outer pipe is decoupled during the simulation of all $D/t=40$ lined pipes as illustrated in Figure 68.

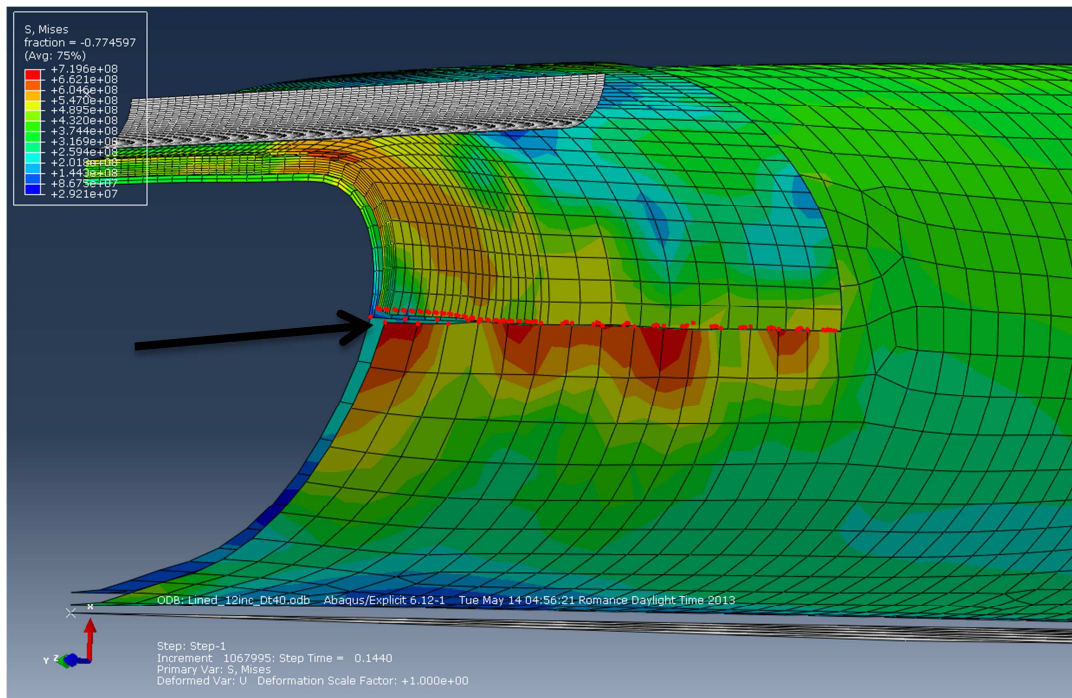


Figure 68: Decoupling of the shell-to-solid coupling constraint, here illustrated with the 12” $D/t=40$ lined pipe plotted with Mises stresses. The red dots represent all nodes involved in the failure as described below.

By studying the output status file it is clear that the decoupling failure is due to initial over-closure of contact surfaces. The warning message involves all nodes represented by red dots in Figure 68. The definition of initial over-closure is that two contact surfaces intersect each other at the beginning of the analysis. As the failure could not be solved by changing the contact definitions, the problem is solved by modelling the full circumference with solid elements. The fact that this resolves the problem could indicate that the over-closure was due to contact difficulties between the shell surfaces representing liner and

outer pipe respectively. Anyway, the geometries representing all $D/t=40$ pipes are modelled with a full solid cross section around the impact area as illustrated in Figure 69.

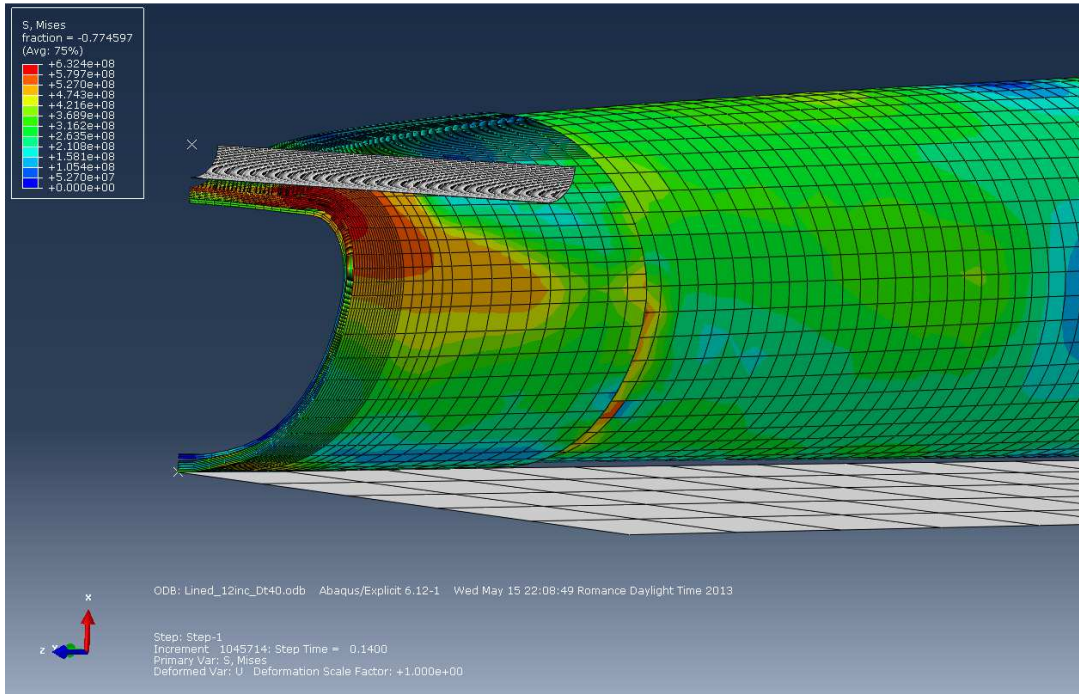


Figure 69: All $D/t=40$ lined pipes are modelled with a full solid cross section around the impact area.

9.4.2. Time of impact

To give an idea of the time periods involved in these trawl gear impact simulations all impact time periods for lined pipes are given in Table 12, i.e. the time from initial contact to separation between pipe and indenter t_i .

Table 12: Time of impact t_i for lined pipes.

D [inch]	D/t				
	15	20	25	30	40
	t_i [s]				
12"	0.0377	0.0538	0.0694	0.0826	0.1384
16"	0.0312	0.0444	0.0608	0.0699	0.1056
24"	0.0241	0.0347	0.0458	0.059	0.0831

It is clear that the longest and shortest times of impact are from the 12" $D/t=40$ and 24" $D/t=15$ analyses respectively. This supports the assumption made by DNV-RP-F111, ref. /1/, that smaller pipe dimensions absorb more energy through global deformation due to longer impact times and flexibility.

9.4.3. Strain Rates

As concluded during the pre-study, section 7.3, the impact simulations are strain rate dependent. Thus, observations are made to quantify the maximum strain rate experienced by the pipe during impact. Abaqus lacks the option of integrating the maximum value of all nodes at all time steps, wherefore the maximum strain rate is detected manually. As illustrated with the 12" $D/t=40$ bare steel pipe in Figure 70 local strain rates of 3817 s^{-1} is detected at the impact zone of the pipe. Though, strain rates of this magnitude are rare and localized in a small area represented by one element. A more general evaluation of the strain rates during the analysis is $100\text{-}200 \text{ s}^{-1}$, which are present during most of the analysis and for larger areas than one element.

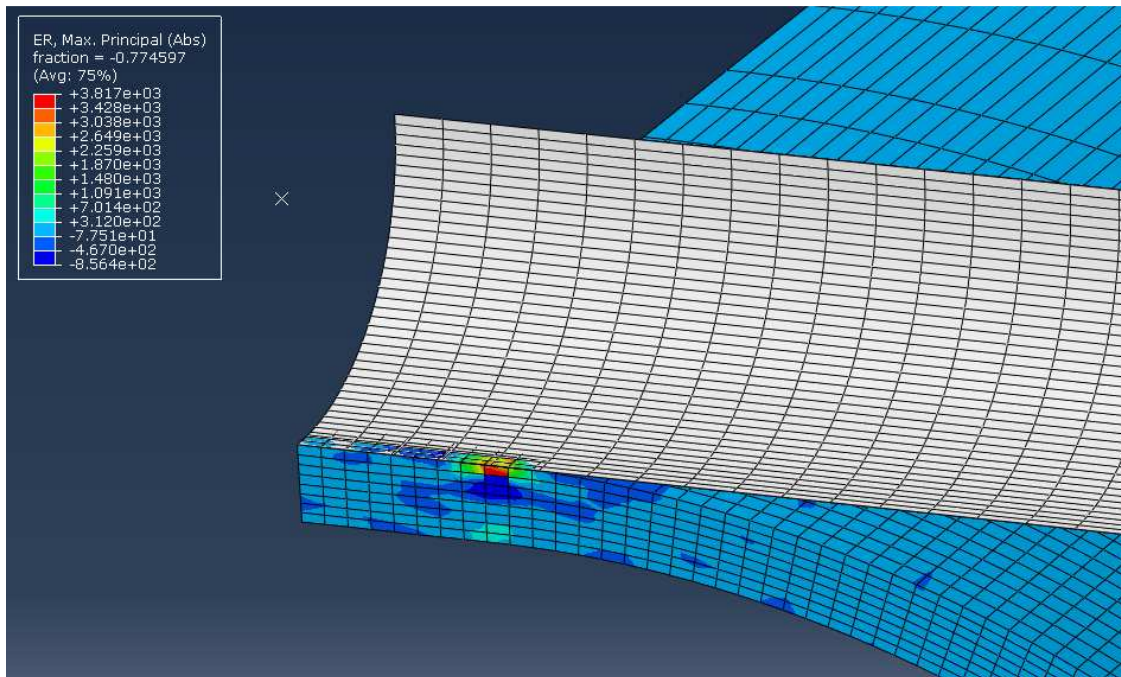


Figure 70: Maximum strain rate detected during the analysis with 12" $D/t=40$ bare steel pipe, i.e. 3817 s^{-1} .

9.5. Conclusions

From the performed parameter study it is concluded that both clad and liner contributes to structural integrity of the pipes, though, with the largest contribution from cladding. While comparing the plastic deformations from clad and lined pipes with bare steel pipes it is noted that the deformation curves converge as the wall thickness increases. Furthermore, the study shows non-conservative results for the bare steel pipes with small wall thicknesses while comparing the analytical solution from DNV-RP-F111 with the FE results.

While evaluating DNV-RP-F111, eq. 3.10, by comparing with FE results for bare steel pipes, it is recommended to implement the diameter D as the FE results shows that the maximum contact force is highly dependent on the diameter. Furthermore, on the basis of FE results, it is recommended to revise both DNV-RP-F111, eq. 3.10 and 3.9, in that order, as the both equations shows relatively large deviations compared with the FE results for

bare steel pipes. Finally, it is recommended to treat lined pipes as bare steel pipes, when evaluating the deformation of the pipe as the difference is relatively small.

Regarding clad pipes it is proposed to include the clad material in the wall thickness while calculating the pipe deformation. At the same time, the yield strength of the clad material should be accounted for by calculating an average yield strength representing both materials; see eq. 9.6.

Additionally, DNV-RP-F111, eq. 3.5, which estimates the relation between Contact force and deformation of the pipe, is evaluated by comparing with FE results. The conclusion supports, as previously stated, that the contact force and deformation of the pipe is highly dependent on the pipe diameter.

Finally, the contact between shell surfaces of all $D/t=40$ lined pipes induces a failure of the shell-to-solid coupling constraint. The failure could not be corrected by changing the contact definitions, wherefore the full circumference of these pipes is modelled with solid elements as illustrated in Figure 69.

10. Additional Studies of Lined Pipes

As the bond between liner and outer pipe is mechanical, trawl gear impact could cause delamination between the two pipes. This section studies the delamination of lined pipes, including the influence of internal pressure and the lined pipe residual stresses.

10.1. Delamination of Liner and Backing Material

One of the objectives of this project is to study possible delamination between liner and backing material. Thus, all 15 lined pipe analyses is examined for delamination, not only the directly visible delamination at the symmetry planes, but also the not visible delamination is examined by creating different section cuts in the geometry. The extent of the delamination is categorized in three categories, i.e. no or negligible, small or medium and severe delamination; see below for the quantification of the categories. The results of the examination are given in Table 13 and all pipe dimensions are given in Table 11 of section 9.1.

Table 13: The extent of delamination for the different pipe dimensions analysed. The colour specifications are given below the table.

<i>D</i>	<i>D/t</i>				
	15	20	25	30	40
12"					
16"					
24"					

No or negligible delamination, 0-0.1 mm
Small or medium delamination, 0.1-1 mm
Severe delamination, 1 mm<

As illustrated in Table 13, only the 12" pipe with $D/t=40$ shows severe delamination, and thus, the rest of this study focusses on this pipe dimension. Not surprisingly, with the smallest wall thickness of the analysed pipes, 7.92 mm, this pipe dimension shows the largest plastic deformation, i.e. 109.39 mm.

The severe delamination of the 12" $D/t=40$ pipe is located at three different locations as outlined in the following sections.

10.1.1. Location 1

Location 1 is located around or near the point at which the pipe folds, i.e. probably where the largest bending of the pipe wall is present. Location 1 is pointed out in Figure 71, left picture, with a close-up in the right picture. The maximum delamination at this location is approximately 2.5-3 mm. Furthermore, it is observed that severe damage of the pipe wall is present at this location.

The meshing of the region surrounding location 1 is relatively coarse as it is located some distance away from the impact area. Thus, it is recommended to refine the mesh of this region for more accurate evaluation of delamination at this location.

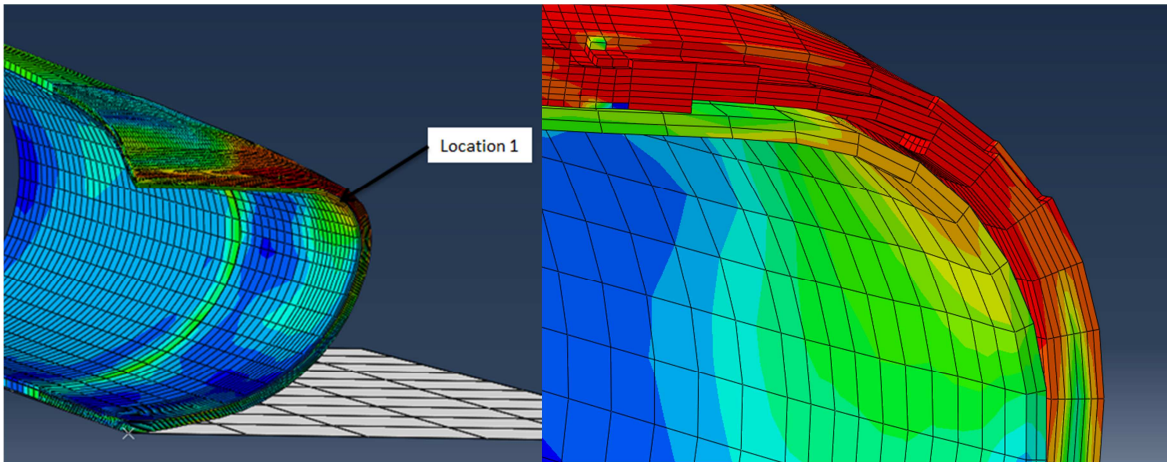


Figure 71: Location 1 is pointed out in the left picture, with a close-up in the right picture.

10.1.2. Location 2

Location 2 is located at the intersection between the two symmetry planes, opposite of the impact zone as illustrated in Figure 72, left picture, with a close-up in the right picture. The magnitude of the delamination is measured to approximately 2.5 mm. Though, some uncertainties are present at this location, as the outer pipe is pinned to the rigid surface at this location, which could lead to local deformations. Furthermore, the mesh is relatively coarse at this location which could lead to inaccurate results. Again it is recommended to refine the mesh in this region for a more accurate evaluation.

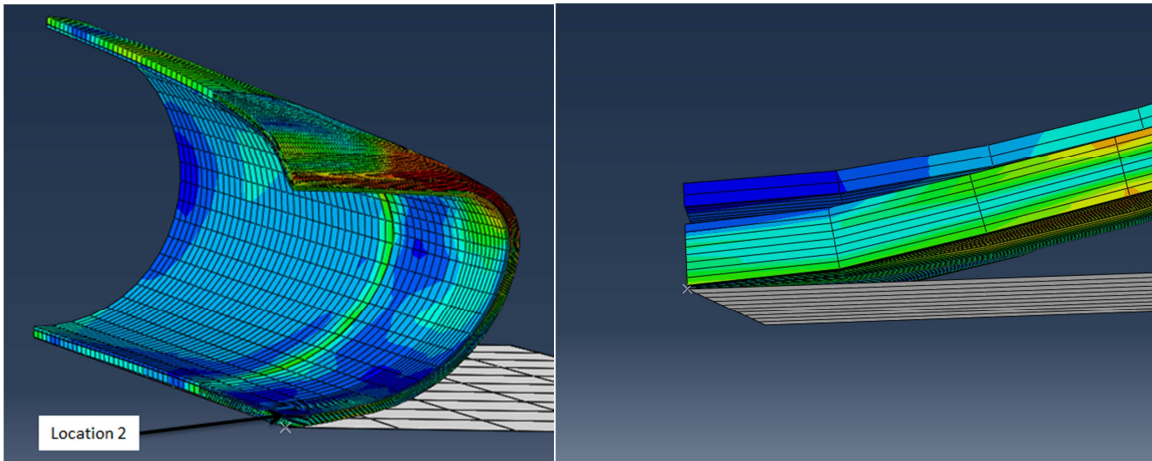


Figure 72: Location 2 is pointed out in the left picture, with a close-up in the right picture.

10.1.3. Location 3

Location 3 is not directly visible, wherefore a section cut is used to illustrate the delamination. The section cut plane is rotated with an angle of 48° from the symmetry plane measured at the un-deformed geometry as illustrated in Figure 73, left picture. The maximum delamination is located approximately 40 mm from the end symmetry plane as illustrated in Figure 73, right picture, with a close-up at the section cut. The maximum delamination at this location is approximately 3 mm.

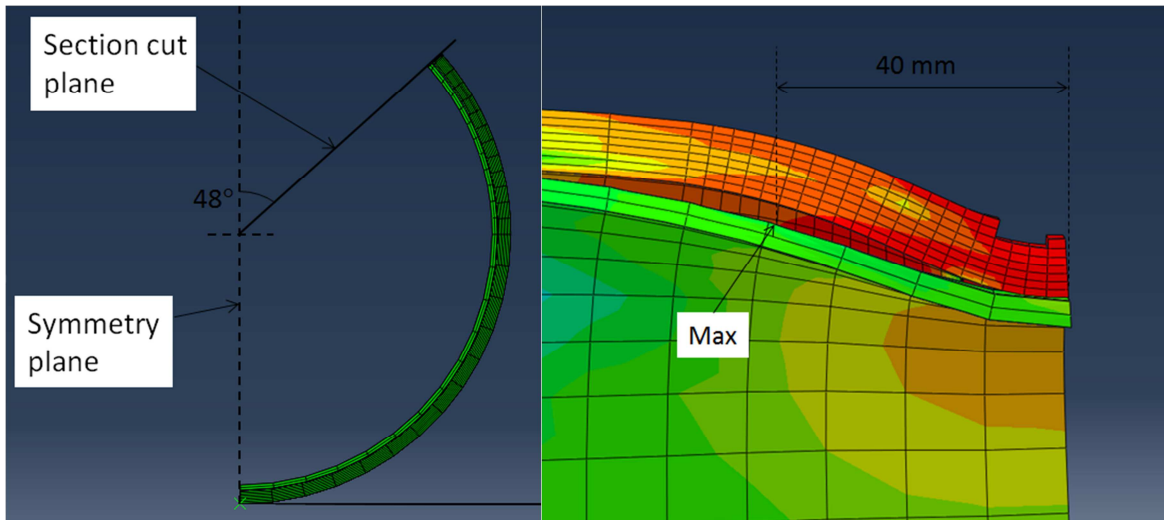


Figure 73: Left picture illustrates the rotation of the section cut plane. Right picture is a close-up at the section cut plane, where the maximum delamination is located approximately 40 mm from the end symmetry plane.

10.2. The Influence of Internal Pressure on Delamination and Plastic Deformation

Subsea pipelines are often subject to internal pressure of various magnitudes. Thus, this section studies the influence of internal pressure on the delamination of the 12" $D/t=40$ pipe described in the previous sections.

Two analyses are carried out with internal pressure magnitude of 50 bar and 100 bar, i.e. 5 MPa and 10 MPa. The results are given in Table 14, where plastic deformation and delamination from the two analyses with internal pressure are compared with the initial analysis without internal pressure. The influence of internal pressure is evident as both plastic deformation and delamination decreases significantly with increasing pressure.

Table 14: Results from the two analyses with internal pressure are compared with the initial analysis without internal pressure.

Internal pressure [bar]	Plastic deformation [mm]	Delamination loc. 1 [mm]	Delamination loc. 2 [mm]	Delamination loc. 3 [mm]
0	109.39	2.5-3.0	2.5	3.0
50	61.69	1.5	0.1	0.7
100	46.27	1.0	0.1	0.5

Regarding the delamination, the internal pressure have some effect, but not enough to re-establish full contact between liner and backing material. Though, these results should not be taken as fully trustworthy, as the mesh size and the fact that the geometries are represented by first order elements could induce inaccuracies and lack of compatibility in contact between liner and outer pipe.

The relatively large decrease of plastic deformation due to internal pressure is not considered as worth implementing in the analytical solutions, as internal pressure rarely is specified as a minimum value, and could not be present at all during shutdowns.

10.3. The Influence of Lined Pipe Residual Stresses

As outlined in section 3.3, test results shows significant variations in the magnitude of residual stresses in lined pipes. Thus, a study is made to investigate the influence of the magnitude of the residual stresses. One analysis is carried out with the 12” $D/t=40$ lined pipe, but with residual stresses increased to twice the magnitude of the initial analysis, i.e. -300 MPa and -40 MPa liner stresses, in the hoop and axial directions respectively. The results are given in Table 15.

Table 15: The results of the analyses with different magnitudes of the residual stresses.

Residual hoop stress (liner) [MPa]	Residual axial stress (liner) [MPa]	Plastic deformation [mm]	Delamination loc. 1 [mm]	Delamination loc. 2 [mm]	Delamination loc. 3 [mm]
-150	-20	109.39	2.5-3.0	2.5	3.0
-300	-40	108.87	3.5	2.5	4.0

The result of the analysis shows little and negligible change in plastic deformation, but a significant increase of the delamination in location 1 and 3. This could be explained by the magnitude of the increased residual stresses of the liner, which brings the material well into the plastic region, as the yield strength of the CRA is 170 MPa.

10.4. Conclusions

Only one of the 15 analysed lined pipe dimensions shows delamination exceeding 1 mm, namely the 12” $D/t=40$ pipe. The severe delamination of this pipe is located at three different locations, with a magnitude in the range of 2.5-3 mm.

By analysing the 12” $D/t=40$ lined pipe with internal pressure of 50 bar and 100 bar respectively, a significant decrease of the plastic deformation and delamination is noted. Though, fully contact between liner and outer pipe is not re-established. Due to relatively coarse mesh in some of the delaminated regions the results should not be taken as fully trustworthy. Thus, it is recommended to do further studies with refined mesh in the delaminated regions to achieve reliable results.

Finally, a study of an increase in residual stresses shows little impact on the plastic deformation, but a relatively large increase of the delamination in location 1 and 3.

11. Conclusions

This section summarises the main aspects of the project by giving general conclusions and recommendations on the basis of the project work. First, the conclusions made during the material and pipe modelling parts of the project are outlined. Finally, all conclusions made from the analyses results are presented with corresponding recommendations and an overall conclusion on the project as a whole.

11.1. Material Modelling Conclusions

Generally, the material modelling is based on the minimum specified requirements from the standards, i.e. no test data is available. This leads to a general conservative representation of the materials with a few exceptions as outlined below.

The materials selected to represent outer pipe and clad/liner are DNV SMYS 415 and Alloy 316L respectively. The stress-strain relations are represented by the Ramberg-Osgood material model and it is found to be well suited to the application as it is calibrated from the minimum specified yield strength and tensile strength.

The impact simulations are found to be highly rate dependent, why strain rate dependency is represented by the Cowper-Symonds relation and implemented by the scaling function. Though, some uncertainties are present regarding the Cowper-Symonds parameters used, as these vary significantly in the literature studied.

The ductile damage and failure option in Abaqus are used to implement an upper limit to the load bearing capacity of the material with satisfying results. The damage and failure parameters are calibrated to fit the minimum specified elongation of the materials by FE tensile test simulations. This approach is generally recommendable when no test results are available, as the minimum specified requirements from the standards are based on tensile testing.

The above described implementation of the material models is generally considered as conservative as it is based on the minimum specified requirements from the standards and test results are likely to show considerable larger yield strengths and tensile strengths, but a few non-conservative assumptions are made regarding the material models. The implementation of strain rates will decrease the straining limit of the material. Furthermore, the liner material undergoes some strain hardening during manufacturing, but both factors are neglected due to lack of quantification, which are non-conservative assumptions.

11.2. Pipe Modelling Conclusions

Generally, focus is on computational costs as a large number of analyses are needed to perform the parameter study. Thus, the pipes are modelled with double symmetry, i.e. only $\frac{1}{4}$ of the geometry is modelled. Furthermore, the geometry is represented by a combination of shell and solid elements to include local effects at the impact area without building a full solid model. These modelling selections are generally recommendable, with a few remarks as described below.

The clad pipes are modelled with mesh tie constraints to represent the metallurgical bond between cladding and backing material. Though, the implementation of the mesh tie constraint results in over-constrained DOFs at the shell-to-solid coupling, creating a slip in the constraint. The problem is solved by removing the mesh tie constraints at these DOFs and thereby creating another error, as the metallurgical bond is no longer present, right at the shell-to-solid coupling. This error is evaluated as negligible, as all clad pipes are examined for any delamination without any findings.

The mechanical bond between liner and backing material is represented by a friction coefficient and residual liner stresses which are set to have constant values for all lined pipe analyses. Though, one analysis is carried out with higher residual stresses showing a minimum influence of the indentation of the pipe, but a considerable increase in delamination between liner and backing material, i.e. the delamination depends on the magnitude of residual stresses.

A big issue in this project is the computational costs. The elements available in Abaqus Explicit are limited to mainly first order elements with the possibility to enhance with incompatible modes to improve bending behaviour. The first order and the incompatible brick elements are tested during pure bending and the results are compared with known analytical beam theory solutions. The regular first order element performs well with respect to the transverse deformation but shows deviations of the stresses. The incompatible element performs well with respect to both deformations and stresses. Though, the incompatible element is found to perform poorly during large deformations as an impact analysis with the incompatible element failed to converge. Thus, when performing large straining applications like the performed impact simulations, the element selection is limited to first order elements.

While settling for the first order element, it is evident that computational costs are a key factor. During the convergence study, the solution fails to fully converge with the mesh refined to 2x2 mm in the impact area, giving a calculation time of over eight hours. Thus, it is recommended to consider the available computational power before starting a parameter study with a large number of analyses. Though, it should be noted that the model is verified against test results with reasonable compliance, and to further establish reliable results during the parameter study, analyses are carried out with bare steel pipes for comparison.

11.3. Conclusions on the Results

The parameter study involves pipes with diameters of 12", 16" and 24" with D/t relations of 15, 20, 25, 30 and 40, giving a total of 15 analyses for each type of pipe, i.e. 45 total analyses when analysing bare steel, clad and lined pipes. Furthermore, a few extra lined pipe analyses are carried out to do additional studies, and the conclusions made are summarised below:

- The plastic deformations of both clad and lined pipes are smaller than for the bare steel pipes. Generally, clad pipes show the smallest plastic deformations. The plastic deformations of the three types of pipes analysed converges as the wall thickness is increased.
- All pipes generally shows smaller plastic deformation than estimated by DNV-RP-F111, except the bare steel pipes with $D/t=40$.
- Generally, the study shows that both plastic deformation and maximum contact force, as calculated by DNV-RP-F111, eq. 3.9 and 3.10, are highly dependent on the diameter, which is not included in the two equations.
- Delamination is present for most lined pipe dimensions analysed, but only the 12" $D/t=40$ shows severe delamination, i.e. larger than 1 mm. The severe delamination is located in three different locations.
- Internal pressure removes the delamination to some degree, but full contact is not re-established between liner and outer pipe.
- An increase of the lined pipe residual stresses has negligible effect on the plastic deformation but causes an increase in the delamination.

Generally, it is recommended to consider revising the analytical solutions stated by DNV-RP-F111 to include the diameter as both plastic deformation and maximum contact force are highly dependent on the diameter. Furthermore, the contribution from cladding could be implemented in the solutions by taking the thickness of the cladding into account.

The results should not be taken as fully trustworthy due to the mesh limitations as outlined in section 11.2, but they give a good indication of the influence of cladding and liner while subjected to trawl gear impact. Thus, the goal for this project is considered as fulfilled.

References

- /1/ DNV-RP-F111, Interference between Trawl Gear and Pipelines, October 2012
- /2/ H.Wathne et al., Interference between Trawl Gear and Pipelines, June 2007
- /3/ <http://www.maerskoil.com> , 2007
- /4/ DNV-OS-F101, Offshore Pipeline Systems, August 2012
- /5/ DNV-RP-F110, Global Buckling of Submarine Pipelines, October 2007
- /6/ API 5LD, Specification for CRA Clad or Lined Steel Pipe, March 2009
- /7/ ASME B36.10M-2004, Welded and Seamless Wrought Steel Pipe, October 2004
- /8/ ASTM A240/A240M – 12a, Standard Specification for Chromium and Chromium-Nickel Stainless Steel Plate, Sheet, and Strip for Pressure Vessels and for General Applications, February 2013
- /9/ B. Berg et al., A New Production Method for CRA Lined Steel Pipe Based on Sheet Metal, 4th Pipeline Technology Conference 2009
- /10/ A.C. de Koning et al., Kuroki T&P Co, TFP and TFT Back in Town, 2003
- /11/ A. Hilberink, Mechanical Behaviour of Lined Pipe, December 2011
- /12/ E. S. Focke, Reeling of Tight Fit Pipe, June 2007
- /13/ 3DS Simulia, Abaqus Documentation version 6.12
- /14/ R.R. Pedersen & L. Damkilde, Introduction to Structural Dynamics, February 2011
- /15/ R.D. Cook et al., Concepts and Applications of Finite Element Analysis, 4th edition, 2001
- /16/ S. Krenk, Continuum Mechanics of Solids, August 2005
- /17/ K. Krabbenhøft, Basic Computational Plasticity, June 2002
- /18/ <http://www.axelproducts.com/pages/highstrainrate.html>, 12/4-2013
- /19/ W. Ramberg & W.R. Osgood, Description of Stress-Strain Curves by Three Parameters, July 1943
- /20/ Internal Communication in DNV, Spring 2013
- /21/ C. Vogel, Metallurgi for Ingeniører, 9th edition, 2007
- /22/ L. Damkilde, En Introduktion til Beregning af Rammekonstruktioner med Lineært-Elastisk/Ideal-Plastisk Materialeopførsel, October 1993
- /23/ B.C. Jensen, Teknisk Ståbi, 22nd Edition, January 2013
- /24/ HSE Offshore Technology Report – The Behaviour of Carbon Steels at High Strain Rates and Strain Limits, June 2000
- /25/ G. Lu et al., Energy Absorption of Structures and Materials, 2003
- /26/ S.M Walley & J.E. Field, Elastic Wave Propagation in Materials, 2005